INTERNATIONAL VERSION

OCT-A Simplified

A step-by-step guide to image acquisition, analysis, and interpretation

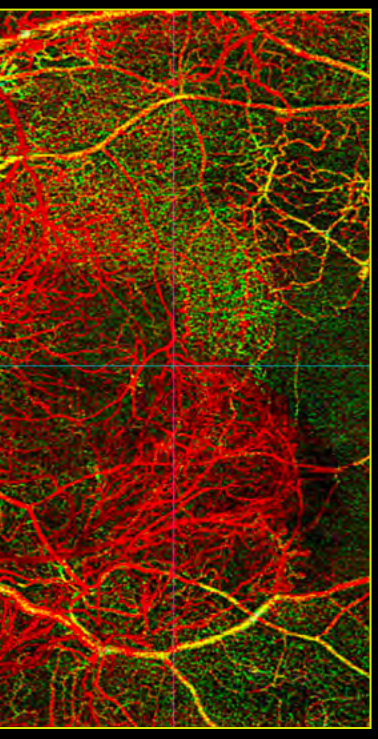

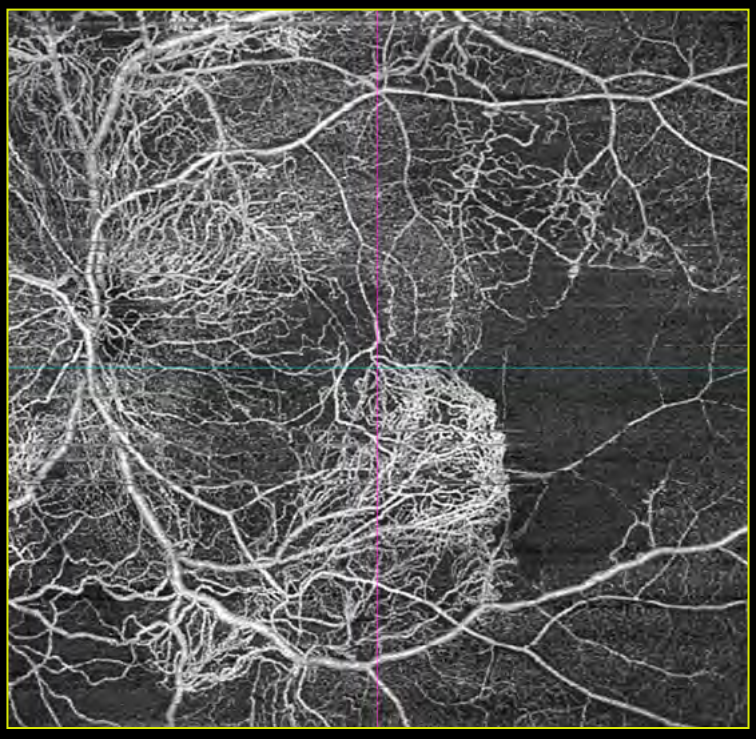

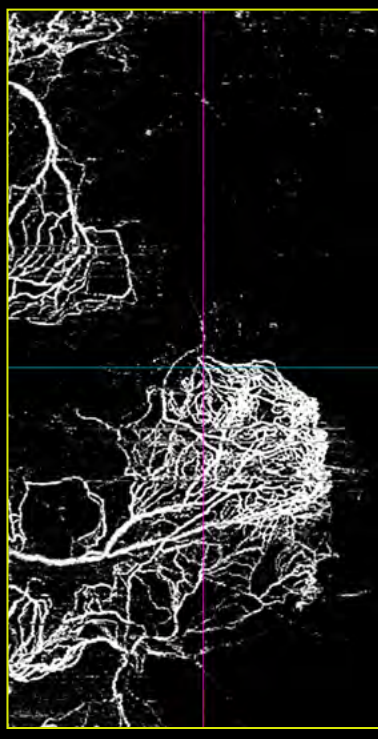

Content contributed by Ricardo Luz Leitão Guerra, MD, MSc, FICO
Leitão Guerra – Oftalmologia, Salvador, Brazil

ZEISS

Table of contents

1. Introduction to OCT-A and the need for an SOP ... 3
2. Basic concepts ... 4
2.1. Retinal and choroidal circulation ... 4
2.2. OCT-A imaging and layer-specific analysis ... 5
2.3. Clinical applications ... 6
3. OCT-A acquisition ... 7
3.1. Characteristics of the scanning method ... 7
3.2. Patient-related factors and artifacts ... 9
3.3. Optimizing acquisition with CIRRUS OCT ... 10
4. Segmentation and display modes ... 12
4.1. Vitreoretinal interface (VRI) ... 13
4.2. Superficial retinal layer (SRL) ... 13
4.3. Deep retinal layer (DRL) ... 14
4.4. Avascular layer ... 14
4.5. RPE-RPE fit ... 15
4.6. Sub-RPE ... 15
4.7. Outer retina and choriocapillaris ... 16
4.8. Choriocapillaris ... 16
4.9. Choroid ... 17
4.10. Retina ... 17
4.11. Whole eye ... 18
4.12. Depth-encoded map ... 18
4.13. Summary ... 19
5. OCT-A analysis ... 20
5.1. The role of analyzing angiographic and structural images ... 21
5.2. Qualitative analysis ... 23
5.2.1. En face angiographic maps ... 23
5.2.2. Flow overlay on B-scan in OCT-A ... 26
5.3. Quantitative analysis ... 27
5.3.1. Vessel density analysis ... 27
5.3.2. Perfusion density analysis ... 28
5.3.3. Foveal avascular zone analysis (FAZ) ... 28
5.3.4. Longitudinal analysis and change detection ... 29
5.3.5. Clinical applications and challenges ... 29
6. Structural en face OCT: Beyond OCT-A quality assessment ... 30
6.1. Vitreoretinal interface (VRI) segmentation ... 30
6.2. Mid retina ... 31
6.3. IS/OS–Ellipsoid zone segmentation ... 31
6.4. Choroid ... 32
6.5. Minimum intensity projection ... 33
7. Key components of the OCT-A report – CIRRUS reports ... 34
8. Enhancing sensitivity to OCT-A findings ... 36
8.1. Image processing ... 36
8.2. Refining segmentation ... 37
8.3. Multimodal imaging ... 37
9. Step-by-step SOP for OCT-A acquisition and analysis ... 38
9.1. Preparation ... 38
9.2. Acquisition ... 39
9.3. Analysis: Quality assessment ... 40
9.4. Analysis: Interpretation and report ... 40
10. Flowchart for rapid OCT-A interpretation ... 41
11. Training checklists ... 43
12. Case studies and practical examples ... 44
12.1. Diabetic macular edema (DME) ... 44
12.2. Diabetic retinopathy (DR) – FAZ abnormality ... 44
12.3. Diabetic ischemic maculopathy – Deep capillary plexus ischemia ... 45
12.4. Refractory proliferative diabetic retinopathy ... 45
12.5. Advanced proliferative diabetic retinopathy ... 46
12.6. Non-ischemic branch retinal vein occlusion (BRVO) ... 46
12.7. Ischemic branch retinal vein occlusion (BRVO) ... 47
12.8. Non-ischemic central retinal vein occlusion ... 47
12.9. AMD – Drusen ... 48
12.10. AMD – GA ... 48
12.11. AMD – Type 1 MNV + quiescent ... 49
12.12. AMD – Type 1 MNV + fluid ... 49
12.13. AMD – Macular neovascularization and RPE tear ... 50
12.14. AMD – Type 3 MNV ... 50
12.15. Polypoidal choroidal vasculopathy – Gilson 83445 ... 51
12.16. Macular telangiectasia (MacTel) Type 1 ... 51
12.17. Macular telangiectasia (MacTel) Type 2 ... 52
12.18. Central serous chorioretinopathy ... 52
12.19. Sickle cell ischemic maculopathy ... 53
12.20. Foveal hypoplasia ... 53
12.21. References ... 54

Section 1

Introduction to OCT-A and the need for an SOP

Optical coherence tomography angiography (OCT-A) is a noninvasive imaging technique that provides three-dimensional visualization of the chorioretinal microvasculature without requiring dye injection, marking a significant advancement in ophthalmic diagnostics. By capturing red blood cell movement through dynamic imaging, OCT-A integrates functional vascular data with the structural details obtained from conventional OCT. This capability makes OCT-A a powerful tool for assessing ocular conditions characterized by vascular abnormalities, including age-related macular degeneration (AMD) and diabetic retinopathy (DR).

Beyond its ability to visualize vascular changes at a microstructural level, OCT-A also offers a distinct advantage over traditional imaging modalities. Unlike fluorescein angiography, which relies on dye injection, OCT-A employs sequential imaging, allowing clinicians to distinguish between superficial and deep retinal vascular layers—an essential differentiation that conventional techniques often fail to achieve. As a result, OCT-A has gained prominence in clinical practice due to its key benefits, including rapid image acquisition, reduced patient discomfort, and the elimination of allergic reactions associated with dye-based techniques. Figure 1 shows a comparison between fluorescein angiography (FA) and an OCT-A image.

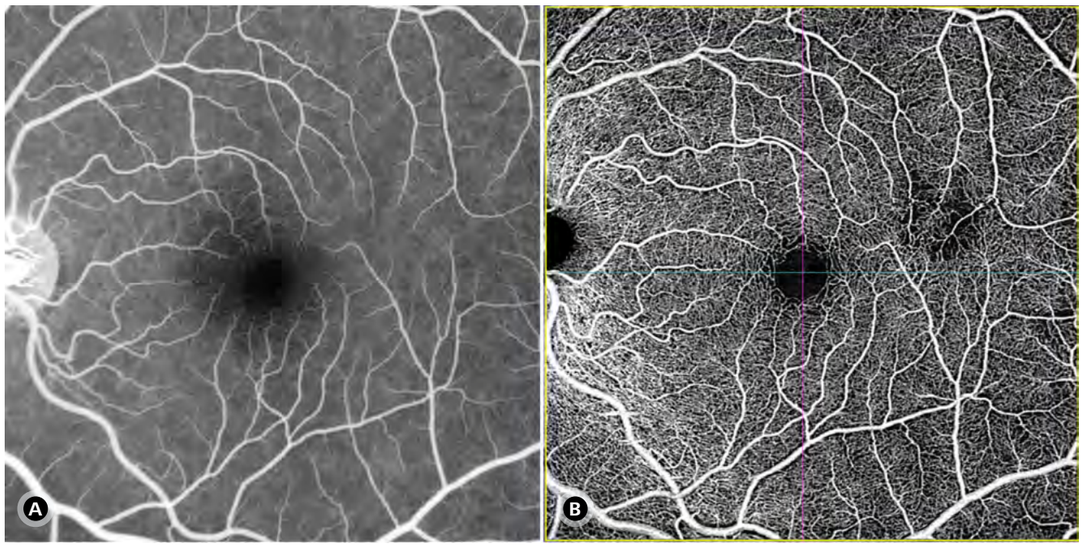

Figure 1: Comparison between FA (A) and OCT-A – Retina Map (B) in the same patient with sickle cell disease, showing a focal area of macular non-perfusion in the superior temporal quadrant. OCT-A demonstrates superior capability in detecting the lesion compared to FA in this case.

However, despite these advantages, the adoption of OCT-A has not been without challenges. Early technological limitations, such as motion artifacts, a narrower field of view compared to conventional methods, and depth-related signal loss, initially hindered image quality and clinical applicability. Nevertheless, continuous advancements in image acquisition and processing have addressed many of these concerns. These refinements have led to broader and more sensitive scanning areas, significantly improving the accuracy and reliability of OCT-A assessments. Even with these advancements, some challenges remain, particularly those related to image misinterpretation due to incomplete or inadequate acquisition and analysis.

To maximize the clinical utility of OCT-A, the implementation of best practices is essential. Optimizing image quality and ensuring accurate interpretation require careful patient preparation, including the use of dilating drops and effective management of common artifacts—both of which are critical for obtaining reliable results. Additionally, patient comfort and stability must be prioritized during the imaging process, as even minor movements can compromise scan quality.

While OCT-A continues to evolve, its role in retinal evaluation remains primarily complementary rather than standalone. Ongoing research aims to refine OCT-A by addressing its current limitations and broadening its diagnostic and therapeutic applications in ocular disease management. This e-book is designed to simplify the understanding and application of OCT-A, providing practical, immediately applicable insights that enhance clinical decision-making. By offering clear, useful guidance, this resource helps physicians improve their diagnostic accuracy and optimize patient treatment, making OCT-A a more effective tool in daily practice. As innovations continue to emerge, OCT-A is poised to further strengthen its clinical relevance, ultimately contributing to more precise and informed retinal disease evaluation.

Comparative benefits and limitations of OCT-A imaging

Pros	Cons
Noninvasive	Misinterpretation risk
Quick acquisition	Technical difficulties
No dye needed	Cannot assess leakage
Separate layers	Signal loss in depth
Reduces discomfort	

Section 2

Basic concepts

OCT-A is a noninvasive imaging modality that enables the assessment of retinal and choroidal microvasculature without the need for contrast dye injection. By detecting blood flow through motion contrast analysis, OCT-A provides depth-resolved visualization of vascular structures, offering significant advantages over traditional FA and indocyanine green angiography (ICGA).

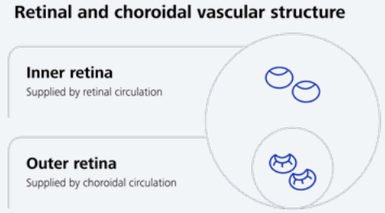

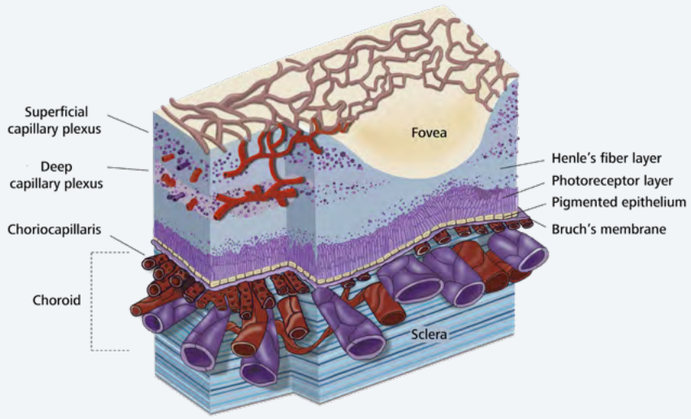

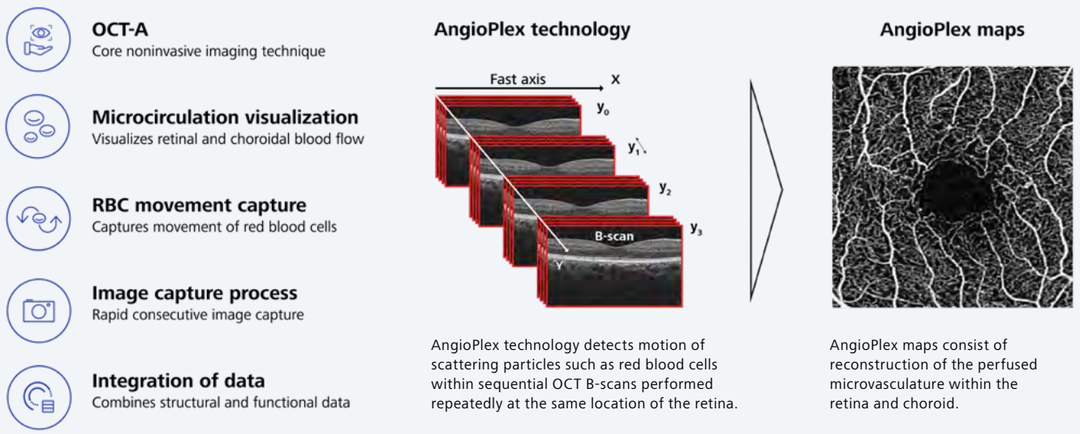

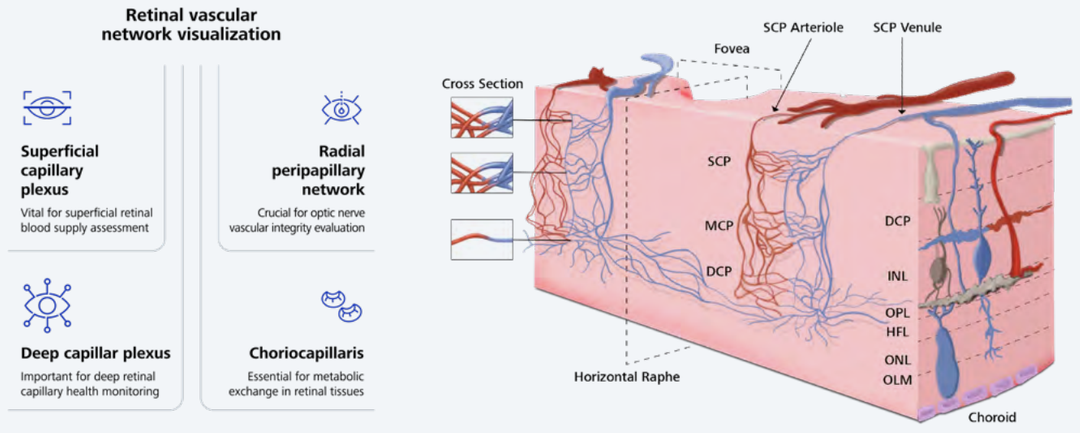

2.1. Retinal and choroidal circulation

To understand the significance of OCT-A, it is essential to first appreciate the distinct vascular systems of the retina and choroid, both crucial for maintaining visual function. The retinal circulation supplies oxygen and nutrients to the inner retina, while the choroidal circulation nourishes the outer retina, including the photoreceptors and retinal pigment epithelium (RPE). Given the retina's high oxygen demand and susceptibility to ischemic damage, evaluating vascular integrity is paramount for diagnosing and managing retinal diseases.

The retinal microvasculature is organized into distinct capillary plexuses: the superficial capillary plexus (SCP), intermediate capillary plexus, and deep capillary plexus (DCP). These plexuses, along with the radial peripapillary capillary network near the optic nerve, ensure efficient perfusion of the retina. Unlike traditional dye-based methods, which primarily visualize the superficial plexus, OCT-A offers the unique advantage of imaging each vascular layer separately. This layered approach enhances the ability to detect microvascular abnormalities specific to different retinal depths.

Similarly, the choroidal circulation, located beneath the retina, comprises three primary layers: the choriocapillaris, Sattler's layer (medium-caliber vessels), and Haller's layer (large-caliber vessels). The choriocapillaris, with its dense, mesh-like capillary network, plays a critical role in the metabolic exchange between the choroid and the outer retina. Although larger choroidal vessels are challenging to visualize due to signal attenuation by the overlying RPE, advanced imaging methods such as enhanced depth imaging (EDI) have significantly improved the ability to assess deeper choroidal structures.

Section 2: Basic concepts

2.2. OCT-A imaging and layer-specific analysis

Building upon these anatomical distinctions, OCT-A's imaging fundamental principle rely on the static nature of retinal tissue, with red blood cell movement within vessels serving as the dynamic component detected during scanning. By capturing consecutive images of the same region in rapid succession and evaluating the differences between them, OCT-A generates angiographic images that illustrate perfusion.

One of OCT-A's key strengths is its ability to eliminate the risks associated with contrast dye injections, making it safer for repeated imaging sessions. Furthermore, its superior depth resolution enables selective analysis of individual vascular layers, allowing clinicians to identify microvascular abnormalities and differentiate pathologies affecting specific retinal or choroidal layers. Complementing these angiographic images are structural OCT images, including cross-sectional B-scans and en face views, which provide anatomical context for vascular alterations (Figure 2). This integration facilitates the identification of associated retinal changes, such as vitreoretinal traction, macular edema, and subretinal fluid accumulation.

Segmentation, a pivotal feature of OCT-A, enhances the diagnostic precision by isolating specific vascular layers for analysis (Figure 3). By defining anterior and posterior boundaries, segmentation minimizes interference from overlapping structures, allowing for clearer interpretation of microvascular abnormalities. Accurate segmentation is especially critical for detecting pathological changes, as different plexuses are disproportionately affected by distinct diseases.

By combining qualitative and quantitative assessments, OCT-A enhances the ability to detect, monitor, and manage retinal and choroidal pathologies. An important consideration is that, unlike FA, OCT-A cannot assess vascular leakage or permeability, both of which are crucial in diseases involving blood-retinal barrier dysfunction. Thus, while OCT-A is a powerful diagnostic tool, it should be regarded as a complementary method rather than a standalone technique. It is most effective when integrated with other imaging modalities to ensure a comprehensive evaluation of retinal and choroidal diseases.

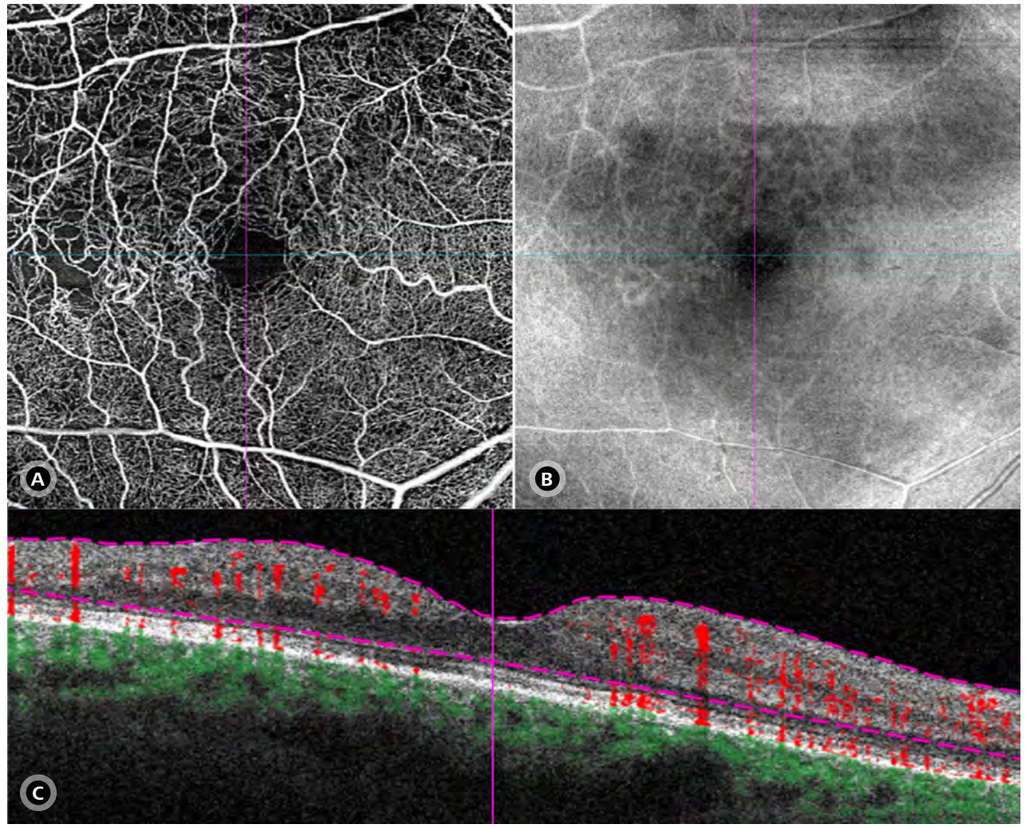

Figure 2: En face OCT angiographic image (A), en face structural OCT image (B), and B-scan with flow overlay in a case of branch retinal vein occlusion

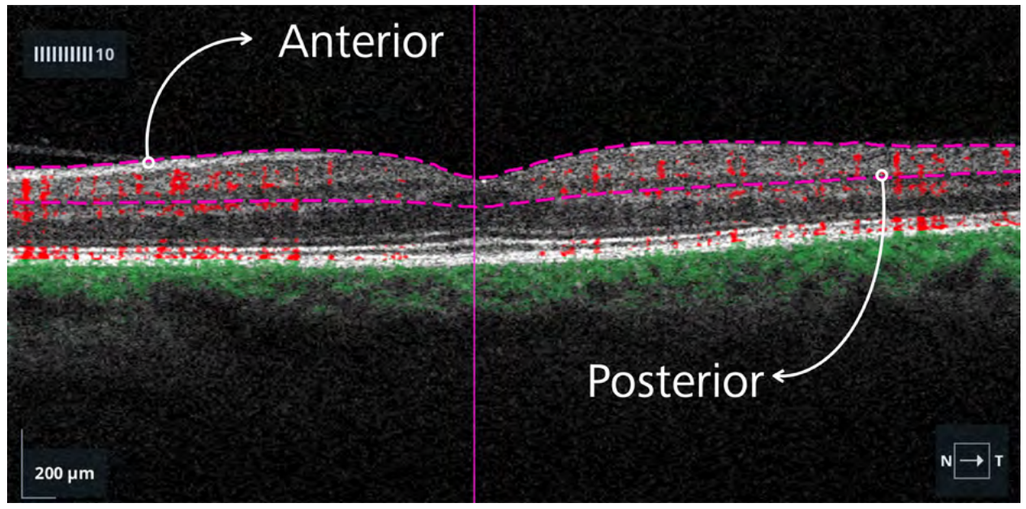

Figure 3: Segmentation – Anterior and posterior profile lines.

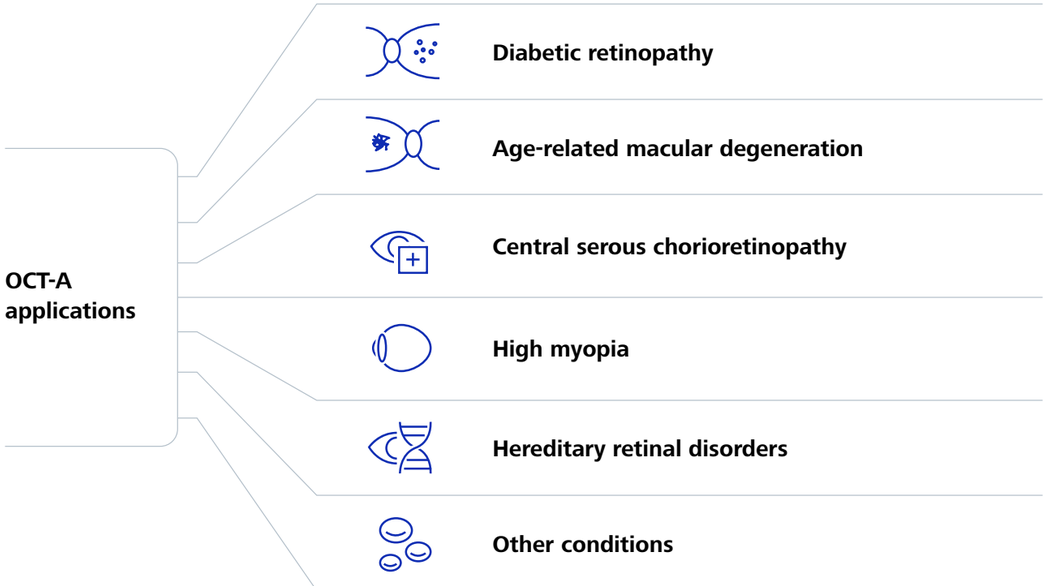

2.3 Clinical applications

OCT-A has proven invaluable across a broad spectrum of ophthalmologic and systemic diseases. In DR, for instance, it enables early detection of microvascular abnormalities such as microaneurysms, capillary nonperfusion, and neovascularization. By assessing changes in the SCP and DCP, OCT-A aids in disease staging and monitoring progression. It also provides insights into foveal avascular zone (FAZ) enlargement, a hallmark of macular ischemia in diabetic patients (Figure 4). Notably, OCT-A has demonstrated the ability to detect early neurovascular changes even in diabetic patients without clinically evident retinopathy, underscoring its potential role in preemptive disease management.

In AMD, OCT-A is instrumental in detecting and characterizing macular neovascularization (MNV), enabling MNV subtype differentiation and precise monitoring of anti-VEGF treatment response (Figure 5). Additionally, it allows for the evaluation of choriocapillaris alterations, which may contribute to AMD progression. Similarly, in retinal vein occlusion (RVO), OCT-A aids in assessing macular ischemia, capillary nonperfusion, and neovascularization, providing detailed analyses of vascular damage in both superficial and deep plexuses. This information is critical for guiding treatment decisions and educating patients about their prognosis.

The utility of OCT-A extends to conditions such as central serous chorioretinopathy (CSC), where it visualizes choroidal vascular abnormalities, and high myopia, where it evaluates MNV and FAZ alterations linked to myopic maculopathy. In hereditary retinal disorders like retinitis pigmentosa, OCT-A reveals reduced vessel density, reflecting progressive retinal degeneration. Additionally, glaucoma assessment benefits from OCT-A's ability to evaluate the peripapillary vasculature and the retinal nerve fiber layer, offering insights into disease progression.

Expanding beyond ophthalmic diseases, OCT-A has demonstrated promise in neurodegenerative and systemic conditions. In multiple sclerosis, it detects peripapillary vessel density loss, particularly following acute optic neuritis, and may serve as a biomarker for disease progression and treatment response. Similarly, in Parkinson's and Alzheimer's diseases, OCT-A identifies microvascular changes in the macular and peripapillary regions, offering valuable insights into neurovascular pathology.

OCT-A is also being explored in hypertensive retinopathy, rheumatoid arthritis, and systemic lupus erythematosus. It has shown potential for detecting retinal changes due to hydroxychloroquine toxicity and assessing retinal perfusion in retinal artery occlusion. Furthermore, OCT-A serves as a pivotal tool in clinical trials, offering objective, reproducible information that facilitates the assessment of novel therapies for retinal diseases.

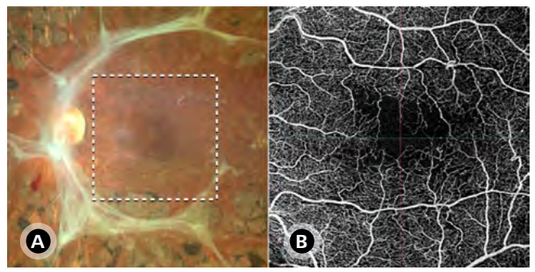

Figure 4: Severe macular ischemia in a case of proliferative diabetic retinopathy. (A) a clinical retinal image captured using the CLARUS 700, and (B) an en face OCT-A image demonstrating flow voids and enlargement and irregularity of the foveal avascular zone (FAZ).

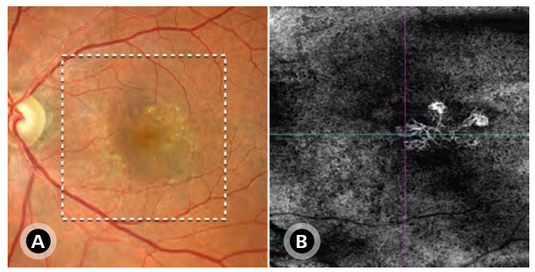

Figure 5: OCT-A enabling the differentiation of MNV subtypes with (A) a clinical retinal image captured using the CLARUS® 700, highlighting the OCT-A scan location, and (B) an en face OCT-A image with customized segmentation below the retinal pigment epithelium (RPE), confirming the presence of a Type 1 MNV with features suggestive of an aneurysmal variant.

Section 3

OCT-A acquisition

The excellence of an OCT-A image is defined by its ability to accurately depict vascular structures while minimizing artifacts—elements that do not correspond to the actual tissue or pathology being imaged. These artifacts can stem from a variety of factors, including patient-related conditions, device limitations, and environmental influences.

Given the direct impact of image quality on diagnostic accuracy, achieving high-resolution and artifact-free OCT-A imaging begins with a meticulous acquisition process. Proper image acquisition is crucial, as suboptimal scans can compromise both qualitative interpretation and quantitative assessments, leading to potential misdiagnoses or unreliable data.

To ensure optimal scan quality, attention must be given to both technical scanning parameters and patient-related variables. These elements directly influence the reliability of vascular assessments and the overall diagnostic value of the examination. By minimizing artifacts, optimizing imaging conditions, and implementing advanced acquisition techniques, clinicians can achieve clearer, more precise vascular representations. This, in turn, enhances clinical decision-making, facilitates disease monitoring, and improves patient outcomes.

Factors affecting OCT-A quality

Scanning techniques

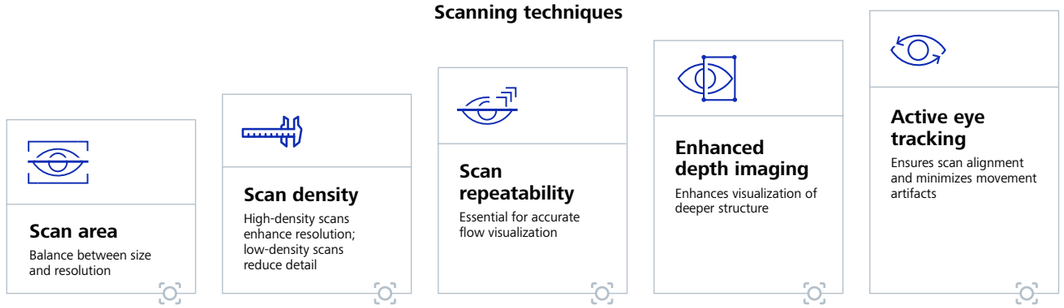

3.1. Characteristics of the scanning method

The integrity of OCT-A imaging hinges on the technical parameters of the scanning method, which determine resolution, sensitivity, and overall diagnostic efficacy. Key factors, such as scan area, A-scan and B-scan density, B-scan repeatability, EDI, and active eye tracking, play critical roles in image fidelity. Misaligned or suboptimal settings can compromise both qualitative and quantitative assessments, potentially leading to undetected vascular abnormalities and reducing the clinical utility of the examination.

A crucial consideration in scanning is the relationship between scan area and scan density. While larger scan areas provide a broader view of the retinal and choroidal vasculature, insufficient scan density may reduce resolution and obscure microvascular structures. Diseases such as AMD and DR, which demand high-resolution imaging for detecting neovascular complexes and capillary dropout, particularly benefit from optimized scanning settings. Conversely, smaller scan areas, such as 3×3 mm macular scans, provide higher spatial resolution, allowing for detailed visualization of fine vascular structures. Figure 6 compares FAZ visualization in a 3×3 mm central area using three different scanning approaches.

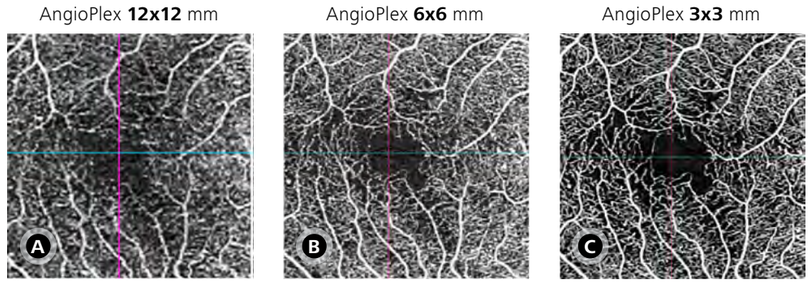

Figure 6: Comparison of FAZ visualization in a central 3×3 mm area using three different scanning methods: (A) obtained with an AngioPlex 12×12 mm scan, (B) with an AngioPlex 6×6 mm scan, and (C) with an AngioPlex 3×3 mm scan.

Section 3: OCT-A acquisition

To mitigate such issues, the CIRRUS OCT integrates advanced scanning technologies that enhance image acquisition and minimize errors. The device offers a versatile range of AngioPlex scanning options tailored to clinical applications. These include macular AngioPlex scans (3×3 mm, 6×6 mm, HD 6×6 mm, 8×8 mm, HD 8×8 mm, and 12×12 mm), 4.5×4.5 mm optic nerve head (ONH) AngioPlex scans (Figure 7), and montage AngioPlex scans, which are generated from six 6×6 mm scans or five 8×8 mm scans (Figure 8). Figure 9 shows the retinal area analyzed using different AngioPlex single scans in a patient with diabetic retinopathy.

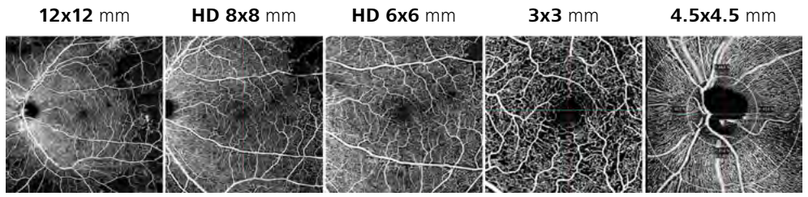

Figure 7: Types of AngioPlex single scans available on the CIRRUS 6000 device.

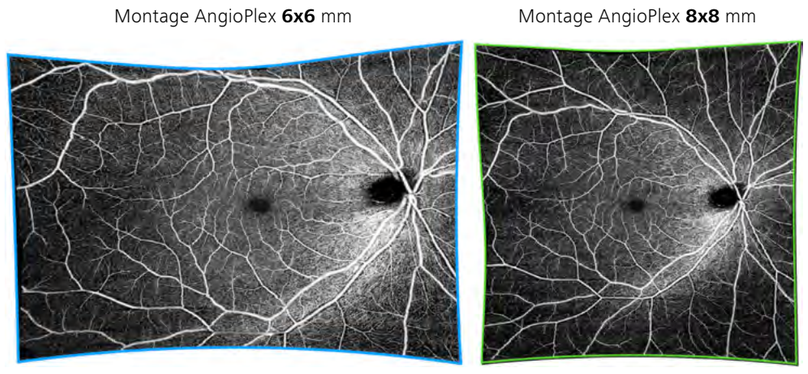

Figure 8: Types of AngioPlex montage scans available on the CIRRUS 6000 device.

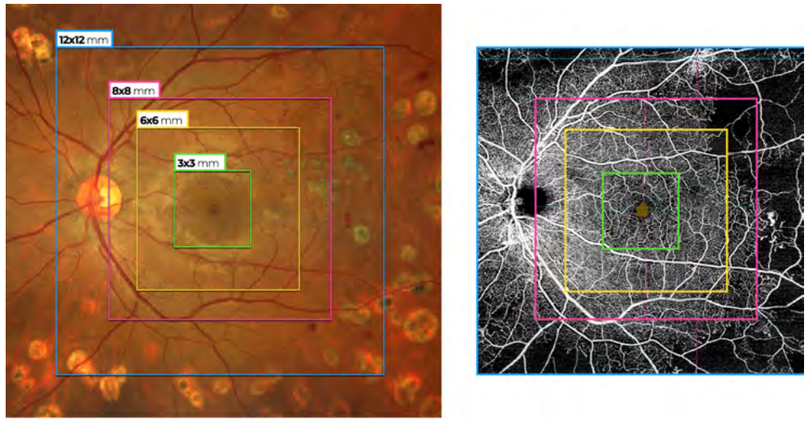

Figure 9 Retinal area analyzed using different AngioPlex single scans in a patient with diabetic retinopathy.

The montage scans, in particular, extend the field of view by merging smaller scans into a single composite image without sacrificing resolution, providing clinicians with a broader perspective of the retinal vasculature. Conversely, the HD 6×6 mm and 8×8 mm scans, due to their higher point density, allow for the analysis of larger fields with a resolution comparable to that of the 3×3 mm scan (Figure 10). Additionally, they offer the advantage of being a single scan, eliminating the need for image montage. A comparison of the analyzed area between AngioPlex 12×12 mm single scan and the images generated from montaged 6×6 mm and 8×8 mm scans is shown in Figure 11.

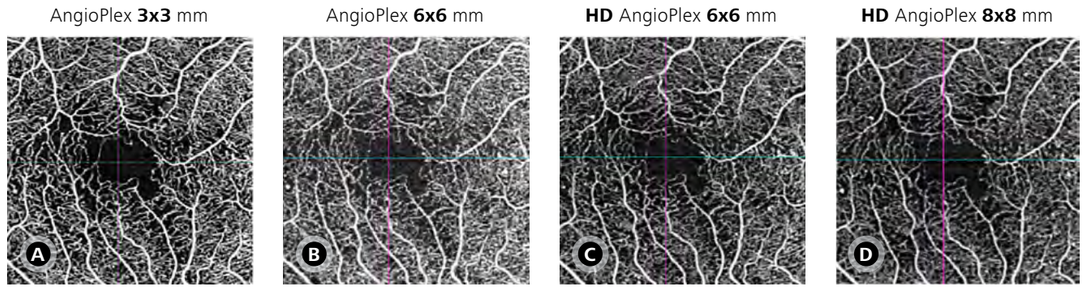

Figure 10: Comparison of FAZ visualization in a central 3×3 mm area using four different scanning methods. (A) AngioPlex 3×3 mm, (B) AngioPlex 6×6 mm, (C) HD AngioPlex 6×6 mm, and (D) HD AngioPlex 8×8 mm. The results demonstrate an excellent correlation between the HD scans and the standard 3×3 mm scan, combining high image quality with a larger field of view, while maintaining the advantage of single-scan acquisition.

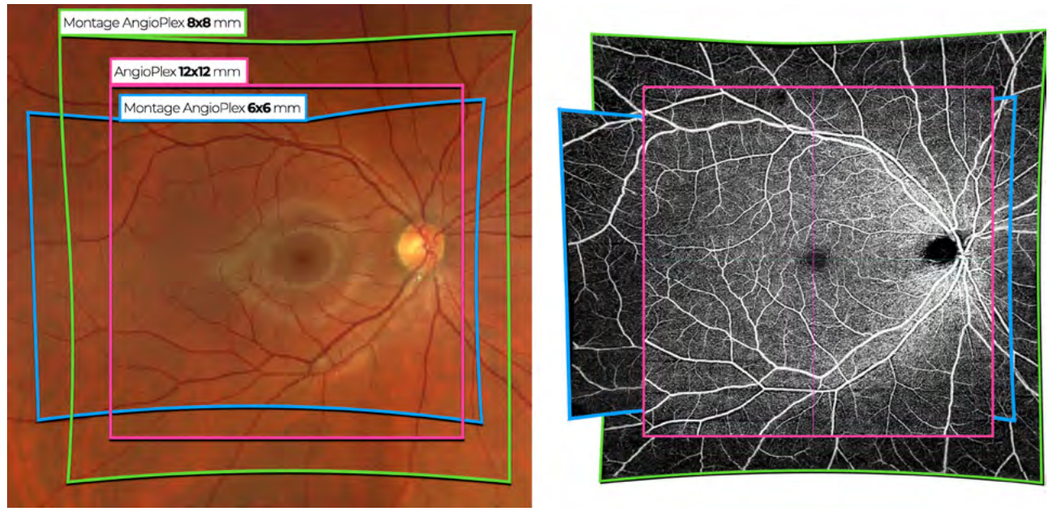

Figure 11: Comparison of the analyzed area between AngioPlex 12×12 mm single scan and 6×6 mm and 8×8 mm montage scans.

Section 3: OCT-A acquisition

Transitioning to the assessment of deeper ocular structures, the EDI mode stands out as an indispensable tool when the primary goal is to evaluate subretinal and choroidal structures, such as in cases of MNV. By optimizing focus and signal penetration, EDI enhances visualization of the choriocapillaris and choroidal vasculature, enabling the identification of choroidal thickness variations, vascular anomalies, and other pathological changes. These capabilities are particularly valuable for diagnosing and monitoring conditions such as AMD, as they provide clinicians with high-resolution imaging of deeper tissues that inform disease management and treatment planning (Figure 12).

Figure 12: Three examples of Type 1 MNV captured using the HD AngioPlex 6×6 mm scan with the EDI system.

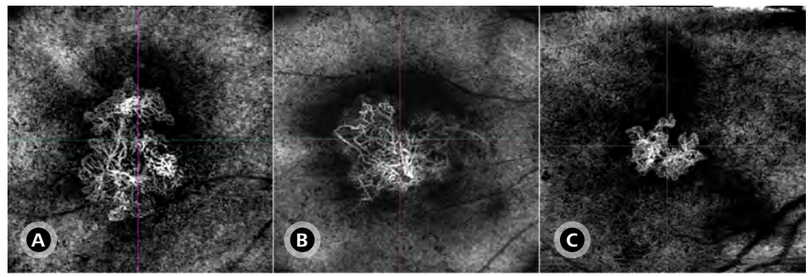

Figure 13: En face OCT-A image showing vessel discontinuities due to motion artifacts. The points of vascular discontinuity are marked with arrows.

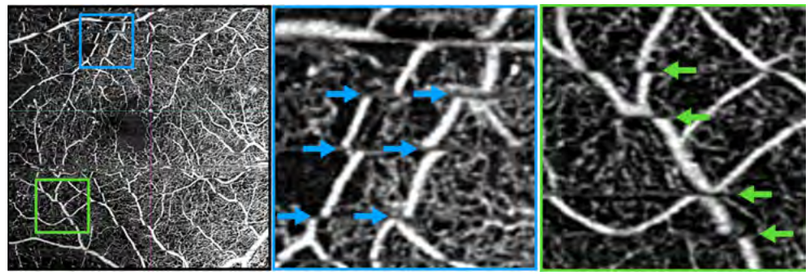

3.2. Patient-related factors and artifacts

The quality and diagnostic reliability of OCT-A are heavily influenced by patient-related factors, which can introduce artifacts that compromise image interpretation. These factors include patient positioning, ocular media opacities, fixation instability, and tear film alterations. Addressing these issues is crucial to optimizing image acquisition and ensuring accurate vascular analysis.

Motion artifacts are among the most significant challenges in OCT-A imaging, particularly in patients with poor fixation due to advanced retinal diseases. These artifacts manifest as vessel duplication, stretching, discontinuities, or white streaks, depending on the severity of movement and the acquisition method. Motion artifacts not only distort image interpretation but also affect quantitative metrics, reducing the reliability of disease monitoring.

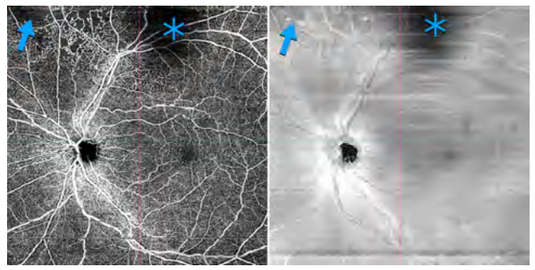

Figure 14: En face OCT-A image (left) and a corresponding structural en face map (right), showing two darker areas: one due to a flow void (arrow) and the other caused by a shadowing artifact (asterisk). Flow void areas maintain a similar appearance to adjacent tissue at the structural map, while shadowing artifacts exhibit marked hyporeflectivity, aiding in proper identification and diagnostic accuracy.

To mitigate these distortions, the CIRRUS OCT incorporates FastTrac™ real-time eye-tracking technology, which actively adjusts scan positioning in response to minor ocular movements. This system preserves spatial coherence across consecutive B-scans, ensuring proper alignment and reducing distortion. Additionally, FastTrac enhances vertical scan alignment monitoring, which is particularly relevant when analyzing capillary networks at different retinal depths.

When motion artifacts persist, the device's targeted re-scan functionality allows for the reacquisition of affected image segments without requiring a full scan repeat, optimizing both workflow efficiency and patient comfort. Furthermore, in longitudinal studies, FastTrac facilitates precise scan registration, ensuring that scans obtained at different time points align seamlessly. This feature improves disease monitoring and enhances clinical decision-making.

Beyond motion-related distortions, shadowing artifacts caused by signal blockage pose another critical challenge in OCT-A imaging. Signal attenuation—resulting from media opacities (e.g., cataracts, vitreous opacities) or overlying retinal structures—can obscure deeper layers, affecting vascular assessment (Figure 14).

To address these limitations, the CIRRUS OCT integrates EDI, which improves the visualization of deeper structures and reduces signal attenuation. This technology enhances subretinal assessments, particularly for pathologies affecting the choriocapillaris and choroidal vasculature.

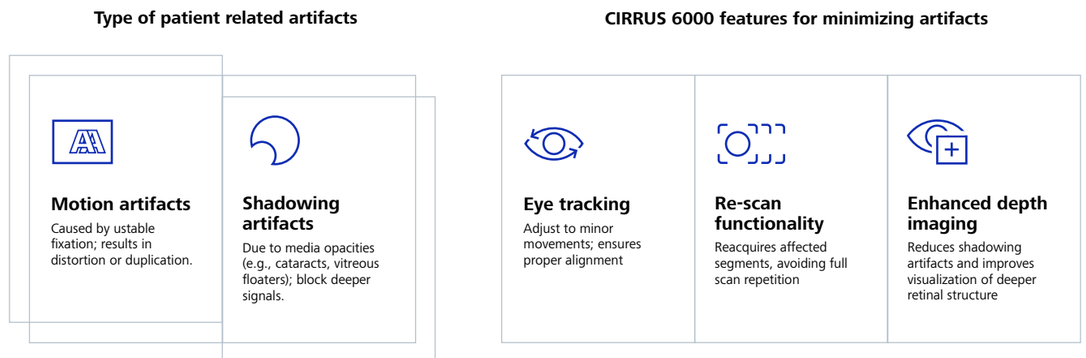

Section 3: OCT-A acquisition

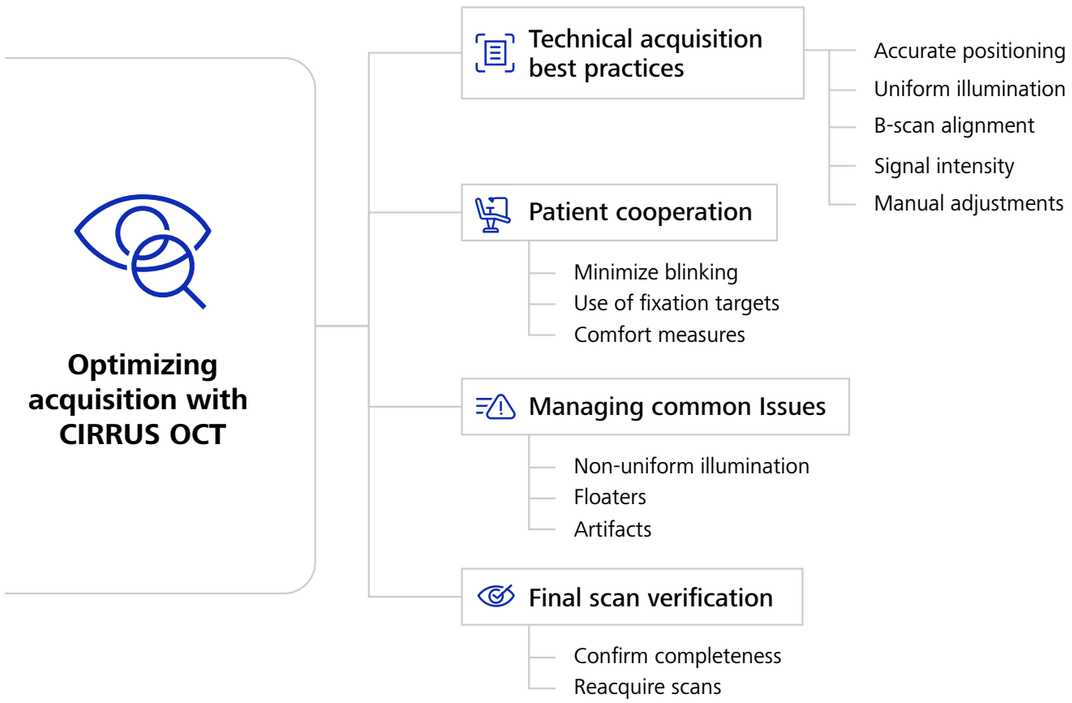

3.3. Optimizing acquisition with CIRRUS OCT

The CIRRUS OCT is equipped with advanced features that enhance scan acquisition, ensuring high-quality imaging and excellent reproducibility. Achieving optimal results, however, requires meticulous attention to detail and the proper application of these tools during the examination process. After selecting the most appropriate scanning method for the specific clinical case, the examiner must fully understand and effectively utilize these features to maximize image quality, diagnostic accuracy, and consistency.

Patient cooperation is fundamental to obtaining high-quality OCT-A images. Proper preparation and clear instructions can significantly impact the success of the scan. If tear film is poor it helps to ask the patient to blink occasionally to refresh the tear film, but patients should be advised to minimize blinking and eye movement while maintaining fixation on the designated target. The CIRRUS OCT facilitates this with 21 fixation points that can be strategically selected to optimize scanning of the area of interest. In cases where patients experience fixation difficulties, external illumination using the contralateral eye may improve stability. For those who blink excessively or struggle with fixation, the use of lubricating eye drops or mild topical anesthetics can enhance comfort and minimize involuntary movement during scanning.

Transitioning to the technical aspects of scan acquisition, accurate positioning plays a critical role in achieving a well-centered and properly aligned image. The iris target should be centered on the pupil to ensure that the scan captures the intended retinal region (Figure 15). For patients with corneal or lens opacities, slightly offsetting the pupillary alignment may help mitigate the impact of these opacities on image clarity. Additionally, uniform illumination across the entire scan area is essential to prevent dark corners or shadowing artifacts, which can obscure diagnostic details. Ensuring proper B-scan alignment, with the scan positioned approximately 100 µm below the top of the image window, further minimizes the risk of segmentation inaccuracies and misalignment errors.

Building upon the importance of scan alignment, signal intensity is a critical determinant of image quality in CIRRUS OCT. The device utilizes a color scale to indicate signal strength, with higher-quality scans displayed in green. A signal strength of at least 6 out of 10 is recommended for diagnostic-quality imaging 7 and above for OCT-A metrics. If signal intensity falls below this threshold, corrective measures should be implemented. These may include adjusting patient positioning to optimize alignment with the scanning target, instructing the patient to maintain steady fixation, or ensuring that eyelids are not obstructing the image. In cases where refractive errors compromise the signal, manual focus adjustments may be required. Additionally, reactivating the FastTrac function can address tracking errors that contribute to signal loss. If these adjustments prove insufficient, repeating the scan is advised to ensure a reliable image for diagnostic evaluation.

Non-uniform illumination is another common issue that can compromise image quality, resulting in areas of underexposure or excessive brightness (Figure 16). To achieve optimal illumination, the iris target should be centered on the pupil, and fine adjustments may be necessary to ensure even light distribution. For patients with corneal opacities, slight realignment can reduce shadowing effects. Moreover, the fundus image must be sharp and well-defined, with clearly visible branched blood vessels. When floaters interfere with imaging, instructing the patient to move their eyes from side to side can shift the floater's position, improving image clarity.

Figure 15: Representations of a well-centered iris target prior to OCT capture.

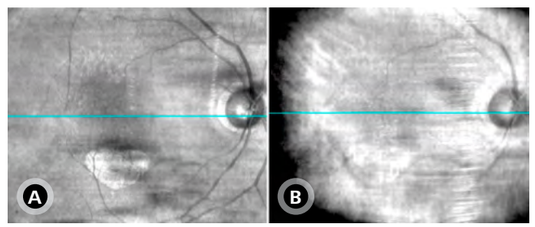

Figure 16: Examples of uniform (A) and non-uniform (B) illumination. Notice the iris margin silhouette is visible on the left edge, demonstrating how improper illumination can introduce artifacts and affect image interpretation.

Section 3: OCT-A acquisition

Artifacts related to scan acquisition can significantly degrade OCT-A image quality and should be actively minimized. Motion artifacts caused by patient movement can lead to signal displacement and image distortion. These artifacts can be mitigated by activating the FastTrac eye-tracking system, which adjusts scan positioning in real-time to maintain alignment. If tracking fails, as indicated by red progress bars, the scan should be reacquired after re-establishing proper patient fixation. Similarly, shadowing artifacts caused by improper illumination can obscure deeper retinal layers and must be addressed by ensuring uniform lighting during the scan.

Concluding the acquisition process, it is crucial to verify that all acceptance criteria are met before saving the scan. The scan should be complete, with no missing information in any imaging windows. If gaps or interruptions are detected, reacquiring the scan is essential to maintain data integrity. In cases of uncertainty regarding image quality, it is always preferable to repeat the scan rather than risk proceeding with an unreliable dataset. This ensures the diagnostic accuracy and reproducibility of the results.

- Ensure patient minimizes blinking and maintains fixation
- Position scan for accurate depth alignment
- Align and adjust equipment for optimal scan
- Ensure signal strength meets diagnostic standards
- Adjust light to prevent shadowing and underexposure
- Make necessary corrections to scan parameters
- Identify and minimize artifacts
- Check and confirm scan quality before saving
- Adjust light to prevent shadowing and underexposure

Section 4

Segmentation and display modes

OCT-A generates angiographic images by capturing vascular information from different planes of the retina and choroid. However, without proper segmentation, these images may display overlapping structures from multiple layers, complicating interpretation. The primary advantage of OCT-A is its ability to segment specific layers, isolating vascular structures and reducing interference from adjacent planes. This segmentation process, defined by anterior and posterior profile lines, enhances the visualization of microvascular networks at different depths, facilitating the identification of pathological changes and improving diagnostic accuracy.

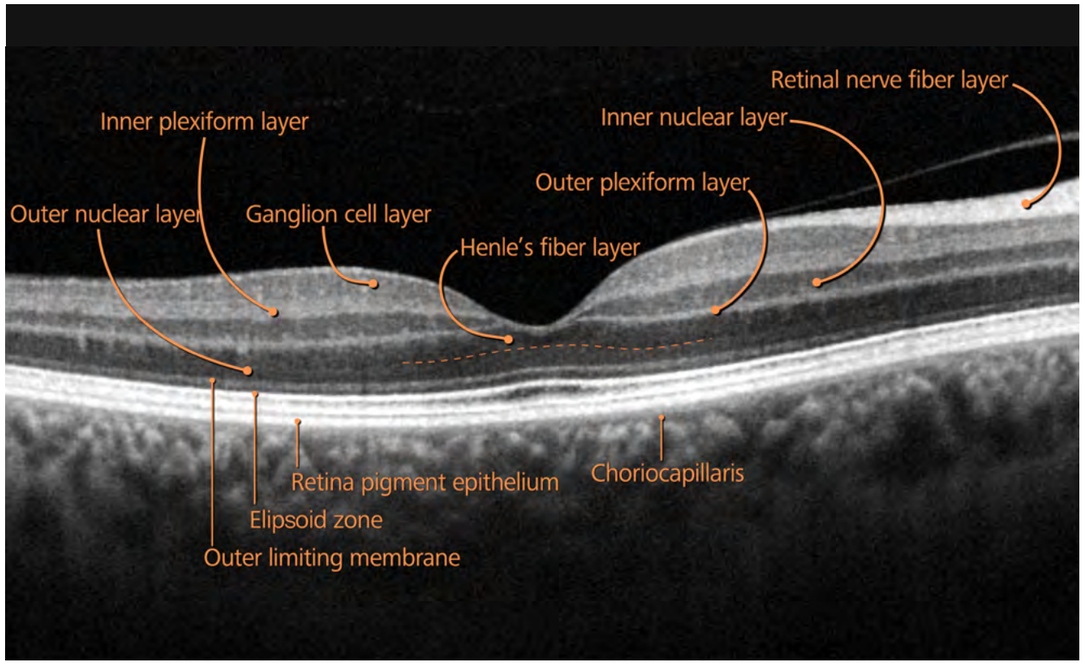

Figure 17: Main anatomical landmarks in an OCT B-scan.

Building on this foundation, segmentation is not only essential for improving image clarity but also plays a crucial role in generating high-quality en face angiographic images with precise anatomical and clinical relevance. While automated segmentation algorithms streamline this process, they are not infallible. In cases involving significant structural abnormalities or segmentation errors, manual adjustments may be required to refine the segmentation boundaries. The ability to manually correct segmentation enhances the accuracy of retinal and choroidal assessments, ultimately leading to more precise clinical interpretations and improved patient management.

To achieve this level of precision, the CIRRUS OCT employs advanced segmentation algorithms that automatically detect key anatomical landmarks, which serve as reference points for defining segmentation boundaries (Figure 17). These landmarks include the inner limiting membrane (ILM), inner plexiform layer (IPL), outer plexiform layer (OPL), RPE, and RPE-fit (a reference position corresponding to Bruch's membrane). Once these structures are identified, the software allows for precise adjustment of segmentation profile lines, shifting them anteriorly (toward more superficial layers) or posteriorly (toward deeper structures) using predefined distances measured in microns. For instance, to access the ellipsoid zone of the photoreceptors, the system positions the posterior profile line at RPE-fit minus 70 µm, effectively shifting the segmentation boundary 70 µm anterior to the detected RPE-fit position. This level of fine-tuned control ensures accurate visualization of retinal layers critical for diagnosing and monitoring various pathologies.

Expanding on this capability, the CIRRUS OCT provides 12 standard segmentation protocols, each with predefined anterior and posterior boundaries tailored for comprehensive vascular assessments. These segmentations are indispensable for detecting vascular abnormalities and guiding treatment decisions. However, beyond these standard presets, the system offers a crucial degree of flexibility—clinicians can modify existing segmentation settings or create entirely new segmentation boundaries customized to specific anatomical variations or pathological findings. This customization capability enhances diagnostic precision by enabling targeted analysis of retinal and choroidal structures beyond the constraints of standard segmentation protocols.

The following sections will provide a detailed exploration of the key characteristics of the standard segmentations and display modes available in CIRRUS OCT. By examining these features, we aim to highlight their role in OCT-A interpretation, disease monitoring, and clinical decision-making, demonstrating how segmentation advances both diagnostic accuracy and patient outcomes.

Section 4: Segmentation and display modes

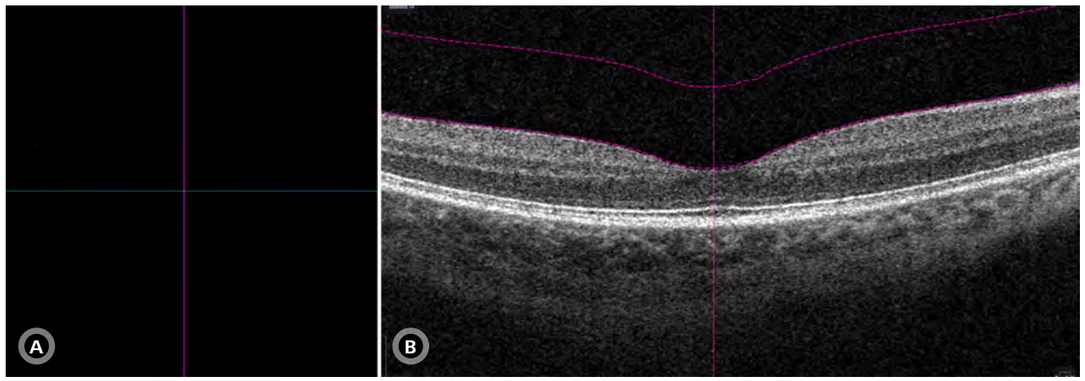

Figure 18: En face OCT-A image of the vitreoretinal interface (A) and B-scan showing segmentation lines (dashed pink line) of the analyzed area (B) in a normal patient. The en face image (A) appears markedly dark due to the absence of vessels in the vitreous cavity in normal individuals.

4.1. Vitreoretinal Interface

Boundaries

- Anterior Limit: ILM - 300 µm
- Posterior Limit: ILM

What it shows

The vitreoretinal interface (VRI) segmentation highlights disorders above the normal retinal plane, within the vitreous cavity (Figure 18). This segmentation is particularly useful for detecting abnormal vascular structures extending into the vitreous, as well as pathological alterations affecting the interface between the vitreous and the retina.

Clinical utility

VRI segmentation is essential for assessing the presence of vascular structures above the retinal plane, aiding in the identification of proliferative retinopathies, such as proliferative diabetic retinopathy and RVOs. Beyond angiographic imaging, the en face structural view enhances the detection of VRI diseases, including epiretinal membranes and vitreomacular traction. The integration of structural and angiographic analysis reinforces the importance of comprehensive evaluation, ensuring accurate diagnosis and improved clinical decision-making.

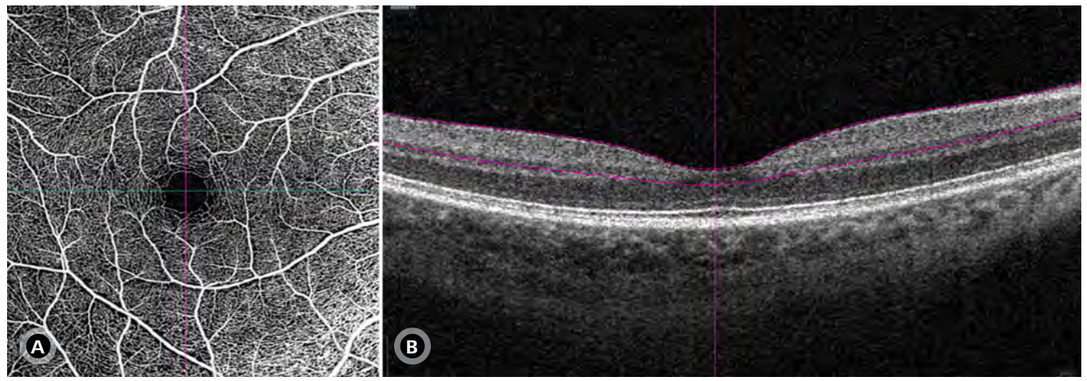

Figure 19: En face OCT-A image of the superficial retinal layer (A) and B-scan showing segmentation lines (dashed pink line) of the analyzed area (B) in a normal patient.

4.2. Superficial Retinal Layer

Boundaries

- Anterior Limit: ILM
- Posterior Limit: IPL

What it shows

The superficial retinal layer (SRL) segmentation highlights the SCP, which plays a critical role in retinal microcirculation (Figure 19). This layer is particularly relevant in vascular pathologies affecting the inner retina, as it provides detailed visualization of capillary networks essential for maintaining retinal perfusion.

Clinical utility

The SRL is crucial for diagnosing and monitoring DR, RVO, and hypertensive retinopathy, as these conditions frequently lead to capillary dropout, non-perfusion, microaneurysms, and vascular dilations within this layer. Moreover, this segmentation serves as the primary dataset for quantitative analysis, providing key metrics, such as vessel density, perfusion density, and FAZ measurements.

Section 4: Segmentation and display modes

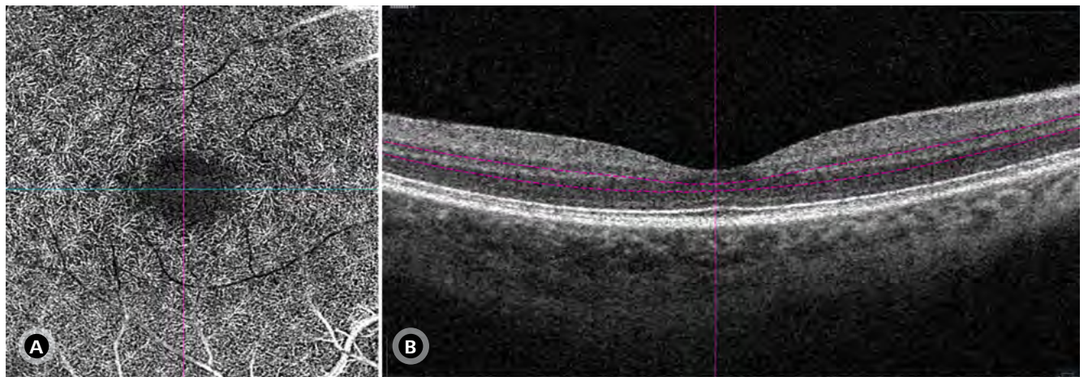

Figure 20: En face OCT-A image of the deep retinal layer (A) and B-scan showing segmentation lines (dashed pink line) of the analyzed area (B) in a normal patient.

4.3. Deep Retinal Layer

Boundaries

- Anterior Limit: IPL
- Posterior Limit: OPL

What it shows

The deep retinal layer (DRL) segmentation focuses on the DCP, allowing for the visualization of microvascular structures located in the deeper retinal layers (Figure 20). This layer is particularly important for evaluating retinal perfusion, as it is more prone to ischemic damage compared to the SRL.

Clinical utility

The deep retinal plexus is highly susceptible to ischemia, making this segmentation crucial for detecting diabetic macular ischemia, RVO, and sickle cell disease, as well as conditions associated with ischemic damage such as paracentral acute middle maculopathy (PAMM). The DRL also provides insight into capillary remodeling in retinal vascular diseases. Given its role in microvascular pathology, this segmentation is particularly valuable for assessing perfusion deficits that may not be evident in the superficial retinal plexus.

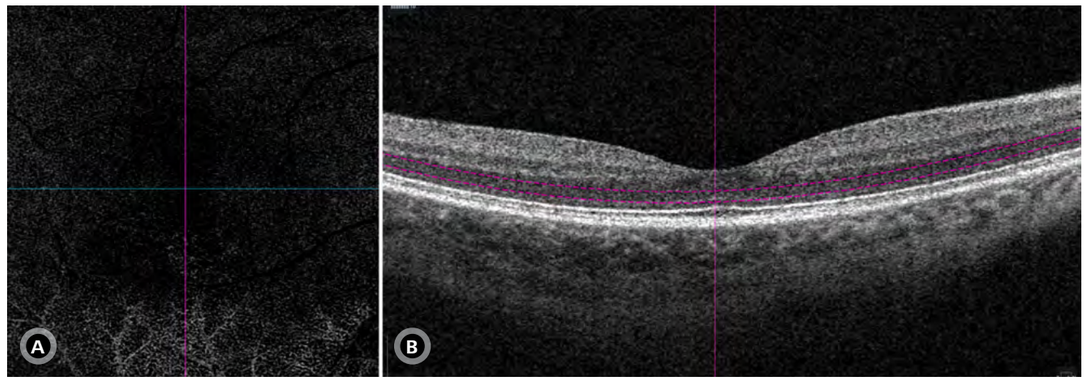

Figure 21: En face OCT-A image of the avascular layer (A) and B-scan showing segmentation lines (dashed pink line) of the analyzed area (B) in a normal patient.

4.4. Avascular layer

Boundaries

- Anterior Limit: OPL
- Posterior Limit: RPE-fit -70 µm

What it shows

This segmentation isolates retinal regions that should physiologically remain avascular, specifically the outer retina, where normal vascular structures are absent (Figure 21). Any vascular signals detected in this layer could indicate either pathological neovascularization or artifacts caused by segmentation errors or projection effects.

Clinical utility

The deep retinal plexus is highly susceptible to ischemia, making this segmentation crucial for detecting diabetic macular ischemia, RVO, and sickle cell disease, as well as conditions associated with ischemic damage such as paracentral acute middle maculopathy (PAMM). The DRL also provides insight into capillary remodeling in retinal vascular diseases. Given its role in microvascular pathology, this segmentation is particularly valuable for assessing perfusion deficits that may not be evident in the superficial retinal plexus.

Section 4: Segmentation and display modes

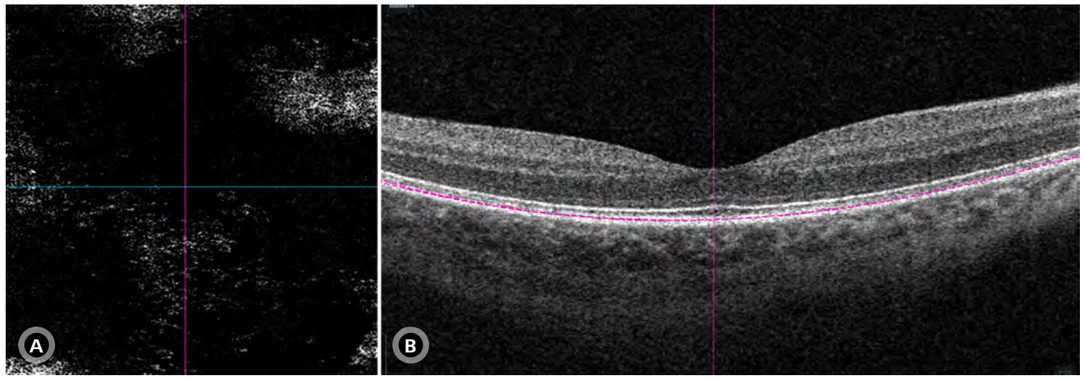

Figure 22: En face OCT-A image of the RPE-RPE fit layer (A) and B-scan showing segmentation lines (dashed pink line) of the analyzed area (B) in a normal patient.

4.5. RPE-RPE fit

Boundaries

- Anterior Limit: RPE
- Posterior Limit: RPE-fit

What it shows

This segmentation isolates vascular structures located between the RPE and Bruch's membrane, providing critical insight into sub-RPE pathology (Figure 22). It is particularly valuable for distinguishing fibrovascular pigment epithelial detachment (PED) from other PED subtypes by allowing detailed visualization of vascular components within this space.

Clinical utility

The RPE-RPE fit segmentation is essential for evaluating Type 1 MNV, commonly observed in conditions such as AMD and CSC. It facilitates differentiation between various PED subtypes, aids in detecting quiescent neovascularization, and enables a focused assessment of the subepithelial component of complex neovascular lesions.

By isolating neovascular structures confined beneath the RPE, this segmentation helps refine the diagnosis and characterization of multilayer neovascular processes, enhancing the precision of disease staging and treatment planning.

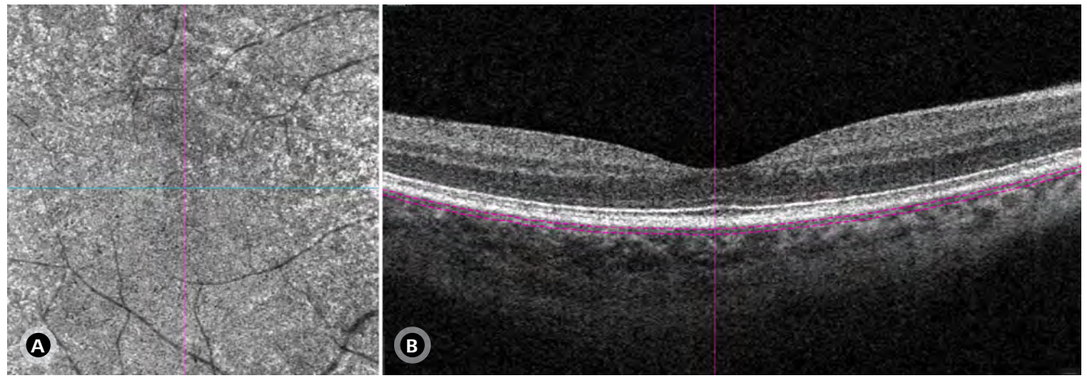

Figure 23: En face OCT-A image of the sub-RPE layer (A) and B-scan showing segmentation lines (dashed pink line) of the analyzed area (B) in a normal patient.

4.6. Sub-RPE

Boundaries

- Anterior Limit: RPE +29 µm
- Posterior Limit: RPE +49 µm

What it shows

This segmentation isolates a thin 20 µm layer beneath the RPE, capturing vascular structures located just below the retinal pigment epithelium (Figure 23). It is particularly useful for assessing the extent of Type 1 MNV and can aid in identifying superficial polypoidal lesions.

Clinical utility

The Sub-RPE segmentation plays a crucial role in the evaluation of Type 1 MNV across various retinal diseases, providing complementary data for characterizing PED subtypes and detecting superficial polypoidal lesions. This layer is also relevant in diseases that impact the choroidal vasculature, such as CSC and other conditions within the pachychoroid spectrum.

In cases of polypoidal choroidal vasculopathy (PCV), where polypoidal lesions may not be clearly visible on angiographic imaging due to irregular blood flow, the structural en face map provides additional information to enhance lesion identification.

Section 4: Segmentation and display modes

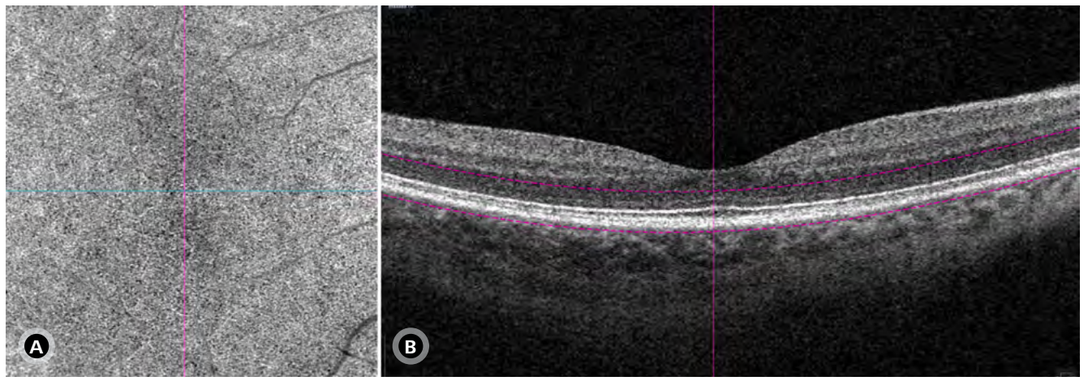

Figure 24: En face OCT-A image of the outer retina-choriocapillaris (A) and B-scan showing segmentation lines (dashed pink line) of the analyzed area (B) in a normal patient.

4.7. Outer Retina and Choriocapillaris

Boundaries

- Anterior Limit: OPL
- Posterior Limit: RPE-fit +38 µm

What it shows

The outer retina and choriocapillaris (ORCC) segmentation spans a larger thickness, covering the avascular portion of the outer retina up to the choriocapillaris (Figure 24). This broader range enhances its ability to detect and assess the full extent of different types of MNV, particularly Type 2 MNV. However, the increased segmentation thickness also makes it more susceptible to artifacts and noise, which can compromise image quality and interpretation.

Clinical utility

This segmentation is valuable for evaluating all types of MNV, especially Type 2 MNV, as the structural disorganization of the outer retina often affects the accuracy of automated segmentations in other layers. By capturing the vascular proliferation extending into the outer retina, this layer provides a more comprehensive view of neovascular lesions, assisting in diagnosis and monitoring disease progression and treatment response.

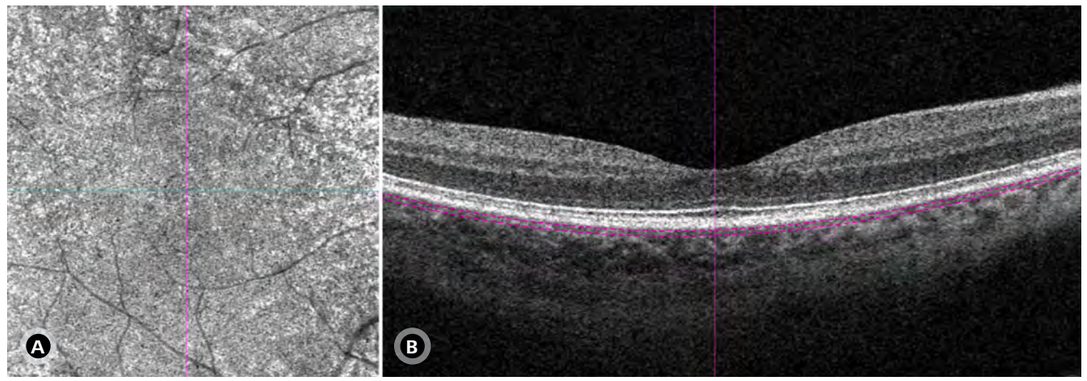

Figure 25: En face OCT-A image of the choriocapillaris (A) and B-scan showing segmentation lines (dashed pink line) of the analyzed area (B) in a normal patient.

4.8. Choriocapillaris

Boundaries

- Anterior Limit: RPE-fit +29 µm
- Posterior Limit: RPE-fit +49 µm

What it shows

This segmentation provides a detailed visualization of the choriocapillaris.

Clinical utility

The choriocapillaris segmentation is highly valuable for evaluating a range of diseases that affect this vascular layer, including AMD, CSC, and inflammatory chorioretinopathies (Figure 25). In these conditions, the normal relatively homogeneous grayish texture of the choriocapillaris appears disrupted by flow deficits, vascular density changes, and abnormal signal intensities.

In AMD, choriocapillaris impairment correlates with disease severity and serves as a potential biomarker for disease progression, aiding in both diagnosis and monitoring.

In CSC, OCT-A reveals distinct choriocapillaris flow abnormalities, reflecting localized ischemia and vascular hyperpermeability. High signal intensity and dilated choriocapillaris vessels often correlate with leakage points seen in FA.

In acute posterior multifocal placoid pigment epitheliopathy (APMPPE) and related inflammatory disorders, OCT-A identifies choriocapillaris flow voids, which aid in diagnosis and disease monitoring. Longitudinal OCT-A assessments help track perfusion changes over time, guiding treatment evaluation and response monitoring.

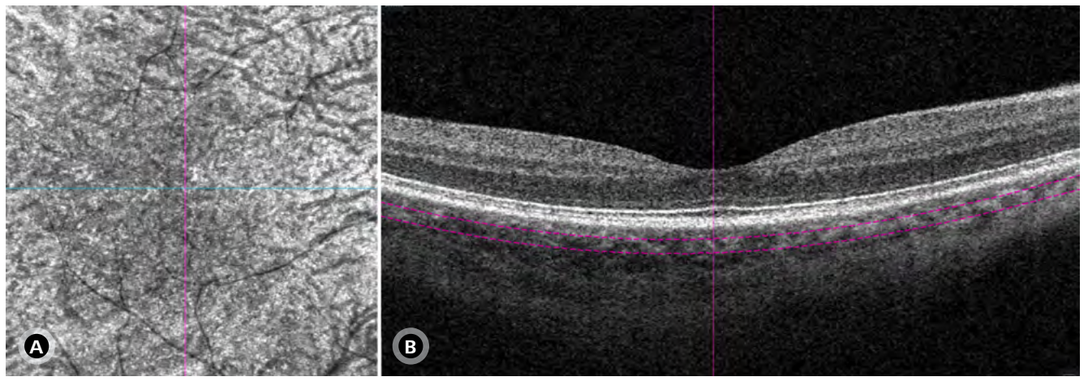

Figure 26: En face OCT-A image of the choroid (A) and B-scan showing segmentation lines (dashed pink line) of the analyzed area (B) in a normal patient.

4.9. Choroid

Boundaries

- Anterior Limit: RPE-fit + 64 µm
- Posterior Limit: RPE-fit +115 µm

What it shows

This segmentation highlights the choroidal vasculature, primarily focusing on the larger choroidal vessels in Haller's layer.

Clinical utility

The choroidal segmentation enables the evaluation of deeper choroidal structures, with the normal pattern displaying alternating areas of hypointense (black, tubular) and hyperintense (grayish, diffuse) signals, corresponding to the distribution of choroidal vessels (Figure 26). However, signal attenuation significantly affects this segmentation, primarily due to scattering caused by RPE pigmentation and the overlying choriocapillaris vessels, as well as projection artifacts from the choriocapillaris.

Typically, choroidal vessels appear as silhouettes, with progressive signal loss at greater depths. However, in cases of RPE loss or depigmentation, particularly in AMD, the absence of the choriocapillaris allows greater penetration of light into the choroid, facilitating the consistent visualization of medium and large-sized vessels in Sattler's and Haller's layers.

One critical consideration is the unblocking artifact, which can occur in patients with AMD and RPE loss. In these cases, enhanced visualization of deeper choroidal vessels may mimic MNV, potentially leading to false-positive interpretations.

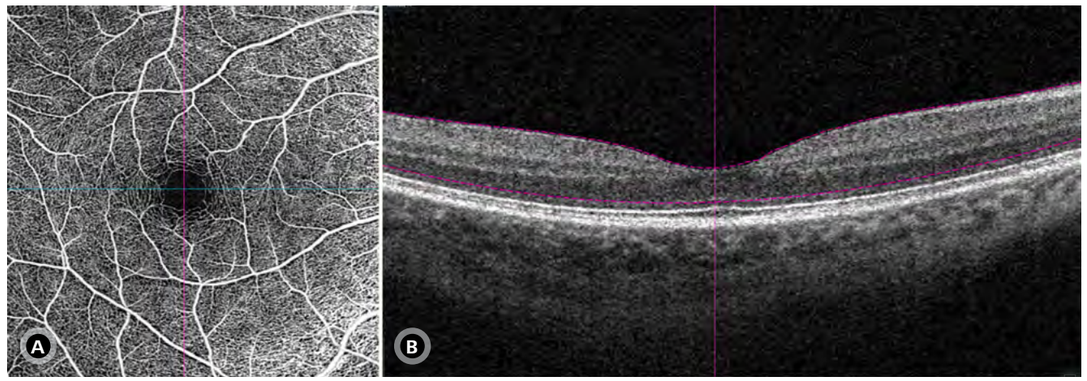

Figure 27: En face OCT-A image of the retina (A) and B-scan showing segmentation lines (dashed pink line) of the analyzed area (B) in a normal patient.

4.10. Retina

Boundaries

- Anterior Limit: ILM
- Posterior Limit: RPE-fit -70 µm

What it shows

This segmentation illustrates the entire retinal vasculature, integrating vascular information from multiple layers, including the SRL, DRL, and the avascular zone (Figure 27).

Clinical utility

The retina segmentation provides a global overview of retinal vasculature, making it particularly valuable for evaluating general vascular network integrity and detecting abnormalities across all retinal layers. It is particularly useful in retinal vascular diseases such as DR, RVO, and macular telangiectasia (MacTel), once it facilitates contextual analysis of microvascular alterations.

Section 4: Segmentation and display modes

4.11. Whole eye

Boundaries

- Anterior Limit: ILM
- Posterior Limit: RPE-fit -70

What it shows

This segmentation provides a broad, composite view of the entire posterior segment, integrating vascular and structural details from all retinal and choroidal layers, along with potential projections (Figure 28).

Clinical utility

The whole eye segmentation offers a global assessment of vascularization throughout the posterior segment, aiding in the identification of widespread vascular abnormalities. This is particularly useful in detecting large-scale perfusion deficits, ischemic changes, or structural alterations affecting multiple layers. However, due to the high degree of overlapping information, this segmentation is often challenging to interpret.

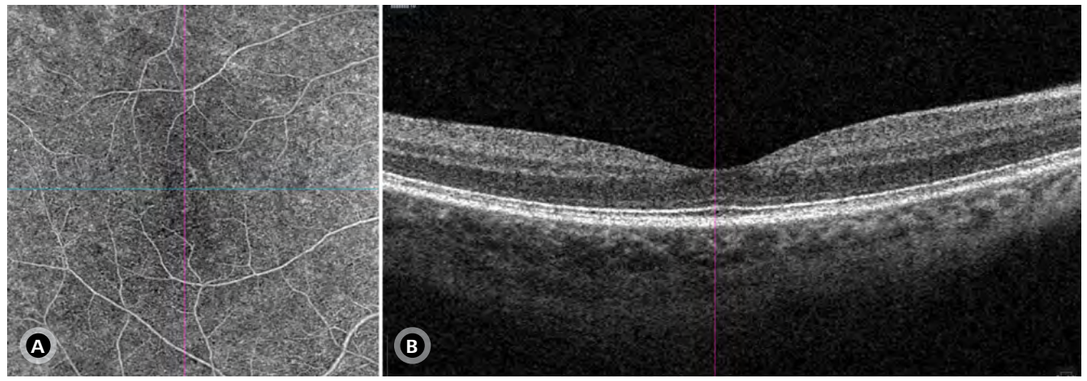

Figure 28: En face OCT-A image of the whole eye (A) and B-scan (B), which does not display segmentation lines, as this map includes all structures without layer-specific segmentation.

4.12. Depth-encoded map

Boundaries

- Anterior Limit: ILM
- Posterior Limit: RPE-fit -70

What it shows

The depth-encoded map is an intuitive color-coded tool that differentiates retinal layers by depth, enhancing vascular interpretation (Figure 29). It assigns red to the superficial layer, green to the DRL, and blue to the avascular zone (Figure 30). This cross-sectional visualization improves the distinction between vascular and avascular regions, enabling precise microvasculature analysis.

Clinical utility

This mapping technique is particularly useful in retinal vascular diseases, as it combines information from the SRL, DRL, and avascular segmentations into a single visualization. As a result, it enhances the ability to detect pathological changes across multiple layers simultaneously, improving diagnostic accuracy and efficiency.

Given its layer-by-layer differentiation, the depth-encoded map is especially valuable for assessing complex vascular abnormalities in conditions such as DR, RVO, and MacTel. It helps streamline diagnostic workflows by allowing faster interpretation of disease-related alterations across different retinal depths.

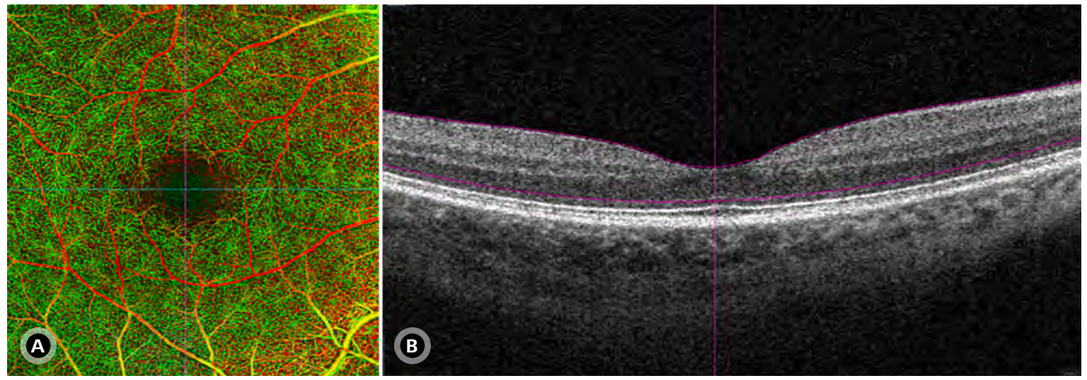

Figure 29: En face OCT-A image of the retina with depth-encoded presentation (A) and B-scan showing segmentation lines (dashed pink line) of the analyzed area (B) in a normal patient.

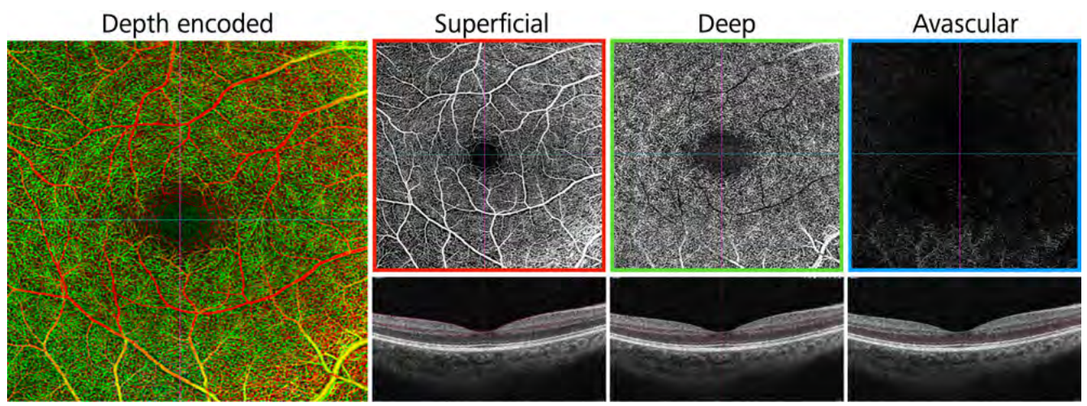

Figure 30: Illustration demonstrating that the color depth map combines superficial, deep, and avascular retina maps, allowing for depth visualization of retinal blood flow.

OCT-A layer segmentation and clinical applications

OCT-A map	Anterior limit	Posterior limit	Presented structure	Clinical applicability/indication
Vitreoretinal Interface	ILM - 300 µm	ILM	Highlights disorders above the normal retinal plane within the vitreous cavity.	Detecting abnormal vascular structures in the vitreous such as proliferative retinopathies like DR and RVO.
Superficial Retinal Layer	ILM	IPL	Emphasizes the superficial capillary plexus.	Monitoring of DR, RVO, hypertensive retinopathy. Allows quantitative analysis of vascular density and FAZ.
Deep Retinal Layer	IPL	OPL	Emphasizes the deep capillary plexus.	Identification of retinal ischemia (DR, RVO, PAMM), and capillary remodeling in retinal vascular diseases.
Avascular Layer	OPL	RPE-fit -70 µm	Isolates avascular retina region.	Detection of pathological neovascularization (Type 2 and 3 MNV), segmentation and projection artifacts.
RPE-RPE fit	RPE	RPE-fit	Isolates vascular structures between the RPE and Bruch's membrane.	Evaluation of Type 1 MNV in AMD and CSC, differentiation of fibrovascular PED.
Sub-RPE	RPE +29 µm	RPE +49 µm	Captures vascular structures just below the RPE.	Identification of Type 1 MNV, superficial polypoidal lesions in PCV, and assessment of pachychoroid spectrum diseases.
ORCC	OPL	RPE-fit +38 µm	Covers the external avascular retina and the choriocapillaris.	Evaluation of Type 2 MNV, improved visualization of neovascular proliferation in the outer retina.
Choriocapillaris	RPE-fit +29 µm	RPE-fit +49 µm	Emphasizes the choriocapillaris.	Monitoring of AMD, CSC, and inflammatory chorioretinopathies. Detects ischemia and perfusion abnormalities.
Choroid	RPE-fit +64 µm	RPE-fit +115 µm	Focus on the choroidal vasculature, especially the Haller layer.	Evaluation of choroidal changes in AMD, RPE depigmentation, neovascular analysis, and attenuated signal.
Retina	ILM	RPE-fit -70 µm	Displays the entire retinal vasculature, integrating information from multiple layers.	Global assessment of retinal vascular integrity, contextual analysis in vascular diseases such as DR, RVO, and MacTel.
Whole Eye	-	-	Integrates vascular and structural details of all retinal and choroidal layers.	Comprehensive assessment of perfusion and structural abnormalities. Detection of extensive ischemia.
Depth-Encoded Map	ILM	RPE-fit -70 µm	Color-coded map to differentiate retinal layers and improve vascular interpretation.	Useful for retinal vascular diseases. Enhances the detection of microvascular changes in DR, RVO, and MacTel.

Section 5

OCT-A analysis

Once a high-quality scan has been acquired, the next critical step is performing a detailed angiographic analysis to extract meaningful and reliable clinical information. However, before proceeding with the vascular assessment, it is essential to ensure the reliability and accuracy of the examination, particularly when the analysis is conducted by a clinician who was not responsible for acquiring the scan. The verification process involves several key elements that must be reviewed systematically to guarantee diagnostic accuracy.

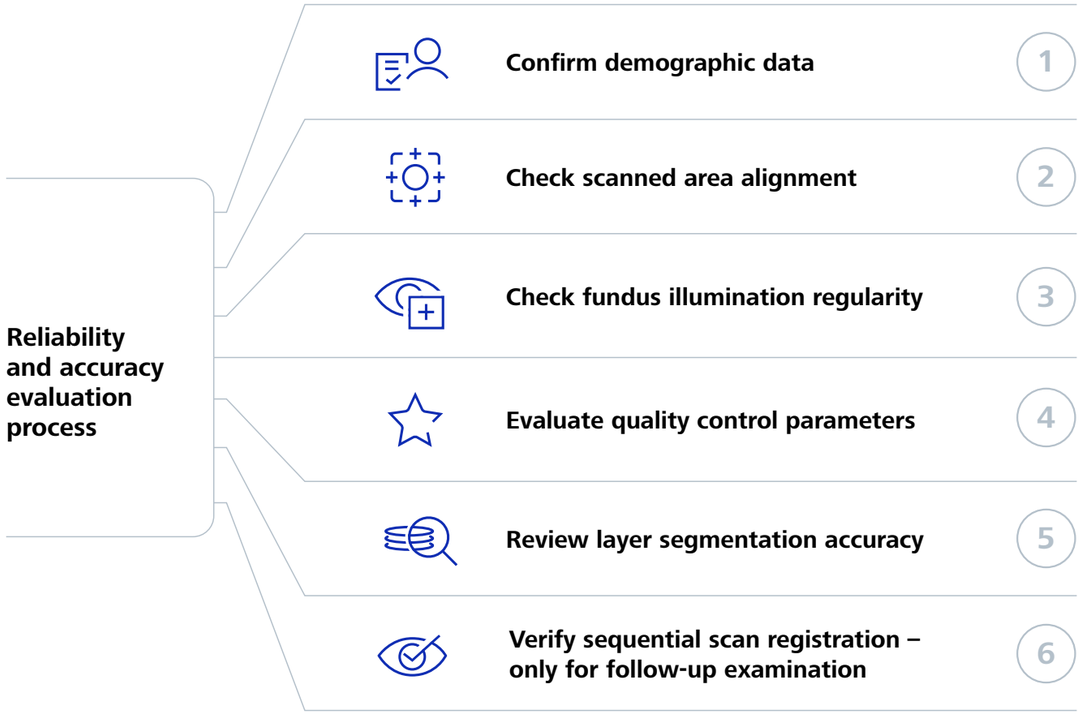

Verification steps for ensuring the reliability and accuracy of OCT-A scans

The first step in the analysis is confirming the patient's demographic data, including age and sex, as inaccuracies in these parameters can lead to improper comparisons with the device's normative database, ultimately resulting in misinterpretation of findings. Additionally, the examiner must verify that the scanned region is correctly aligned with the reference image, ensuring that the area of interest corresponds to the clinically relevant region. If a misalignment is detected, the examiner must determine whether it significantly affects the analysis and whether a new scan should be acquired.

Beyond these preliminary checks, it is crucial to evaluate the quality control parameters of the scan systematically. Signal intensity is a key determinant of image quality and should be assessed to confirm that it is sufficient for accurate vascular interpretation. A low signal intensity can compromise the visualization of vascular structures and reduce the sensitivity of the examination. Additionally, the presence of artifacts must be carefully examined, as they can distort angiographic data, potentially leading to misdiagnoses or limiting the examiner's ability to derive meaningful clinical insights.

Artifacts in OCT-A can originate from various sources, including patient-related factors, acquisition techniques, and software processing errors. These artifacts must be classified according to their origin and assessed for their impact on the reliability of the examination. Artifacts related to acquisition, such as motion artifacts and shadowing, were previously discussed in the acquisition section.

A major concern in OCT-A interpretation is segmentation artifacts, which result from errors in the automated segmentation algorithms that delineate retinal and choroidal layers. These errors can lead to both false-positive and false-negative findings, complicating the assessment of vascular alterations. Before conducting a detailed vascular analysis, it is imperative to review the accuracy of layer segmentation using B-scans. If segmentation errors are identified, they must be manually corrected to ensure that vascular signals are correctly assigned to their respective anatomical layers.

Additionally, projection artifacts are common in OCT-A due to the fundamental principles of angiographic imaging. These artifacts occur when light passing through the retina interacts with superficial vascular structures before being reflected by the RPE. This phenomenon causes residual vascular signals from the superficial layers to be erroneously projected onto deeper structures, creating misleading flow signals in the outer retina or subretinal space. The CIRRUS OCT software incorporates advanced features to mitigate projection artifacts in AngioPlex OCT scans; however, it is still necessary to verify their occurrence during image interpretation to avoid misdiagnoses.

For longitudinal studies and follow-up evaluations, proper registration of sequential scans is essential. If prior scans are available, the newly acquired scan must be correctly aligned with previous images to track vascular changes over time. If automatic registration fails, the device will display a "No Registration" warning, requiring manual alignment or the selection of an alternative scan series for comparison.

Section 5: OCT-A analysis

5.1. The role of analyzing angiographic and structural images

The simultaneous evaluation of en face angiographic and structural images is mandatory for accurately distinguishing true vascular structures from imaging artifacts, ensuring high-quality scan interpretation and improving diagnostic precision. Integrating these two imaging modalities enhances the assessment of vascular integrity, identifies segmentation errors, and aids in differentiating pathological findings from technical artifacts.

One of the primary objectives of comparing angiographic and structural en face images is to differentiate true vascularization from artifacts, particularly projection artifacts. These artifacts often appear as shadows of superficial vessels extending into posterior layers and may be identified during imaging as motion signals, referred to as decorrelation tails (Figure 31). They result from light passing through moving blood cells, combined with imprecise motion detection, leading to a weaker secondary signal below the original vessel location. While decorrelation tails may diminish in the outer nuclear layer, they tend to be more pronounced at the RPE.

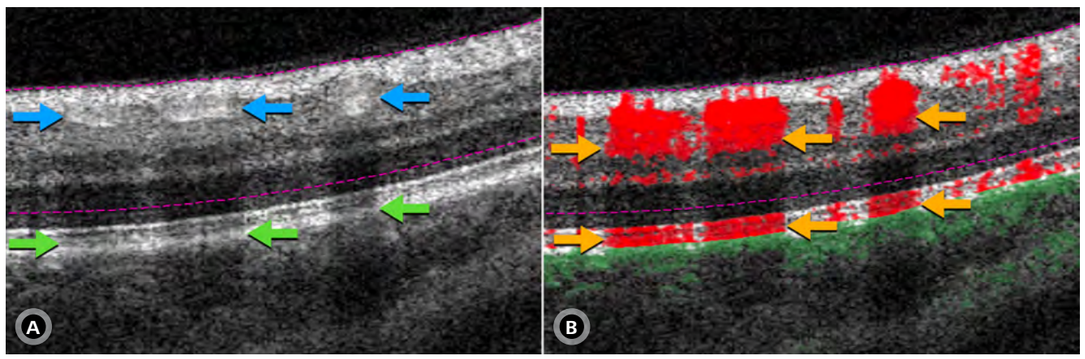

Figure 31: Structural OCT Image (A) and flow overlay on B-Scan (B) demonstrating projection artifacts caused by shadows of superficial vessels extending into posterior layers. In image A, blue arrows indicate the location of the vessels, while green arrows highlight the shadows cast on posterior structures, primarily on the RPE. In image B, yellow arrows emphasize the decorrelation tails occurring in areas that do not correspond to blood vessels.

Large vessels are visible in the SRL but anatomically should not be seen in the DRL, confirming that they are decorrelation artifacts rather than true vasculature if present during imaging. The RPE normally lacks vascular structures, so any apparent vascularization in this layer strongly suggests decorrelation tails rather than actual pathological neovascularization. Comparing the en face angiographic image with the corresponding structural B-scan allows for precise differentiation between real vascular networks and imaging artifacts, thereby reducing the likelihood of misinterpretation. To mitigate this artifact, the CIRRUS AngioPlex incorporates advanced software that identifies and eliminates most projection artifacts from the en face angiographic image (Figures 32 and 33).

Assessing signal quality in both angiographic and structural en face images is essential for ensuring reliable vascular evaluation. Low signal intensity in the angiographic map can appear as darkened or blurred areas, potentially affecting the visibility of capillary networks. Evaluating the structural en face image alongside the B-scan can help determine whether low signal intensity is due to technical factors—such as suboptimal image acquisition—or if it reflects an underlying pathological condition. If the angiographic image appears dark, but the structural image and B-scan show normal retinal architecture, it may indicate a vascular pathology rather than an imaging artifact (Figure 14, page 9).

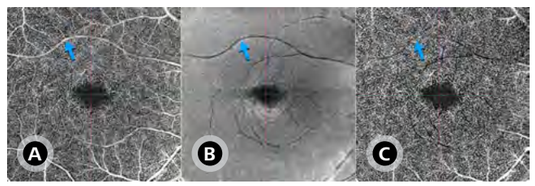

Figure 32: Comparison of en face angiographic imaging of the DRL segmentation (A), structural en face imaging (B), and en face angiographic imaging of the DRL segmentation after applying projection artifact removal software (C). In image (A), projection artifacts are indicated by a blue arrow, corresponding to a hyporeflective shadow in the structural image (B). These artifacts are entirely eliminated by the AngioPlex software, as demonstrated in image (C).

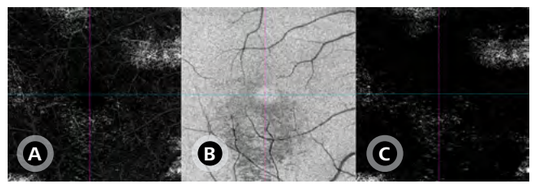

Figure 33: Comparison of en face angiographic imaging of the RPE-RPE fit segmentation (A), structural en face imaging (B), and en face angiographic imaging of the RPE-RPE fit segmentation after applying projection artifact removal software (C).

Section 5: OCT-A analysis

Structural en face imaging is also a valuable tool for identifying segmentation artifacts in OCT-A, which occur when the software inaccurately delineates retinal layer boundaries. These errors can result in the inclusion of signals from adjacent layers or the omission of relevant vascular structures, potentially leading to misinterpretation (Figure 34). A common situation that often leads to misinterpretation of the OCT-A exam involves patients with diabetic retinopathy (DR) or retinal vein occlusion (RVO) who present with macular edema containing large cystoid spaces. In these cases, there is a false impression of flow void, as the segmentation boundaries pass through the cystoid spaces, which exert mechanical displacement on the vessels, dislocating them from their normal anatomical positions. The structural en face image typically shows marked hyporeflectivity in the areas corresponding to the cystoid spaces, which deviates from the expected morphological pattern (Figure 35).

By providing a detailed panoramic view of retinal morphology, structural en face imaging complements traditional cross-sectional B-scans, improving artifact detection and ensuring more precise segmentation analysis.

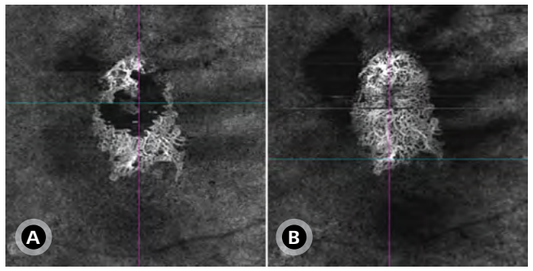

Figure 34: Visualization of Type 1 MNV in a scan with segmentation artifact (A) and after segmentation correction (B).

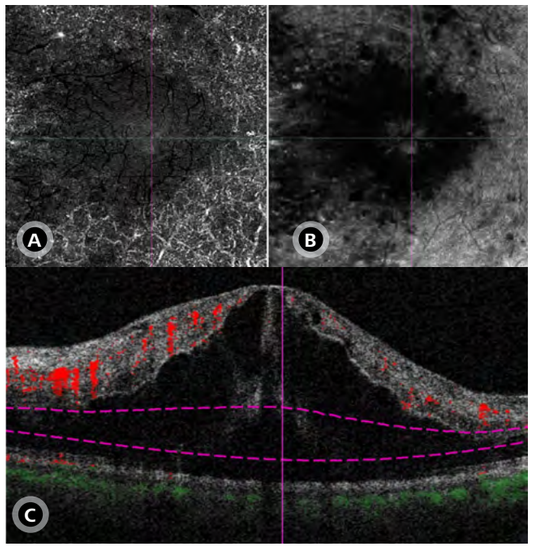

Figure 35: Segmentation artifacts in a case of severe macular edema due to CRVO. (A) Angiographic en face image showing absence of decorrelation signal in the foveal and parafoveal regions. (B) Structural en face image demonstrates marked hyporeflectivity at the same area, corresponding to cystoid spaces. (C) Segmentation lines over a flow-overlay B-scan confirm the presence of segmentation artifact.

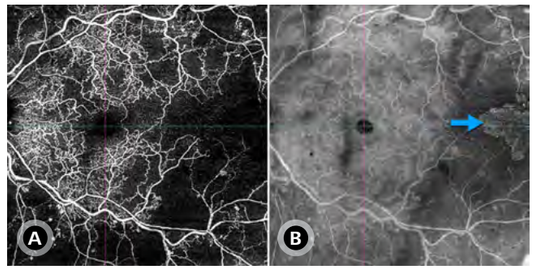

Figure 36: En face angiographic image (A) and structural image (B) in a case with segmentation artifact leading to the omission of relevant vascular structures. Note the loss of the expected retinal layer morphology in the structural image, highlighted by the blue arrow.

A key advantage of structural en face imaging is its ability to verify the expected morphology of retinal layers (Figure 36). By analyzing the segmented depth in relation to normal anatomy or known pathological patterns, deviations from the expected structure can indicate segmentation errors. This is particularly useful in cases where retinal alterations, such as geographic atrophy, complicate automated layer identification.

In addition to morphological assessment, structural en face imaging allows for the evaluation of layer continuity. Segmentation artifacts often present as irregularities or discontinuities in retinal layers, which can be more easily detected when viewed from a broader perspective. These artifacts, if unrecognized, may distort OCT-A findings by falsely indicating vascular abnormalities.

While B-scans remain essential for confirming segmentation accuracy, structural en face imaging provides a complementary approach by revealing large-scale artifacts and subtle misalignments that might be overlooked in cross-sectional views. The integration of both imaging methods enhances the reliability of OCT-A analysis, facilitating the distinction between true vascular structures and artifacts caused by segmentation errors.

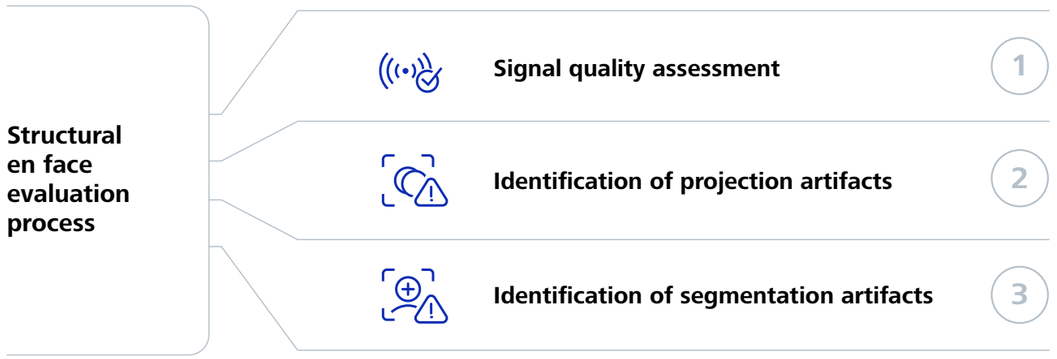

Angiographic and structural en face evaluation process.

5.2. Qualitative analysis

Qualitative analysis of OCT-A can be performed using en face angiographic maps or the flow overlay on B-scans, each providing distinct yet complementary perspectives on vascular integrity and pathology. En face angiographic maps offer a top-down view of the retinal and choroidal vasculature, facilitating the assessment of vessel density, capillary dropout, and neovascularization patterns across different layers. In contrast, the flow overlay on B-scans integrates vascular information with cross-sectional structural OCT imaging, allowing for a more precise evaluation of blood flow within specific retinal and choroidal layers. This combined approach enhances diagnostic accuracy by enabling the correlation of microvascular abnormalities with underlying morphological changes, contributing to a more comprehensive assessment of retinal diseases.

5.2.1. En face angiographic maps

The qualitative analysis of en face angiographic maps follows a systematic approach, starting with automated segmentation of the most anterior (internal) layers and progressively advancing to deeper layers. This sequential analysis is essential as it mirrors the path of light through retinal tissue, meaning that alterations in internal structures, such as shadowing from intraretinal hemorrhage, first appear at their site of origin and are subsequently replicated in deeper layers, aiding in exam interpretation. Similarly, vessels in the SCP are identified before the visualization of their projection artifacts.

The first stage of OCT-A analysis focuses on the VRI, which, under normal conditions, appears completely black due to the absence of vasculature. This layer is particularly valuable for detecting proliferative vascular abnormalities extending into the vitreous, such as neovascular fronds in proliferative diabetic retinopathy and vascular extensions in RVO (Figures 37, 38 and 39).

Following the VRI, analysis proceeds to the SRL, which highlights the SCP. This layer is crucial for detecting capillary dropout, microaneurysms, and vascular tortuosity—hallmarks of DR, hypertensive retinopathy, and RVO (Figure 40). Vessel and perfusion density measurements within this layer provide quantitative metrics for disease monitoring. Notably, the assessment of the FAZ in this segmentation serves as a key indicator of macular perfusion, where FAZ enlargement and irregularity suggest microvascular compromise in ischemic conditions.

Deeper vascular assessment involves the DRL, encompassing the DCP. The DCP is highly susceptible to ischemic damage, making this segmentation essential for detecting diabetic macular ischemia, PAMM, and microvascular remodeling in various retinal vascular diseases (Figure 41). Flow voids and nonperfusion areas in the DRL strongly correlate with disease severity and progression, providing critical insights into ischemic pathology beyond the superficial layer.

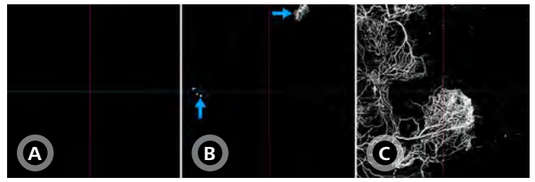

Figure 37: OCT-A images of the VRI in a normal patient (A) and in a patient with proliferative diabetic retinopathy (B and C), showing fibrovascular proliferations.

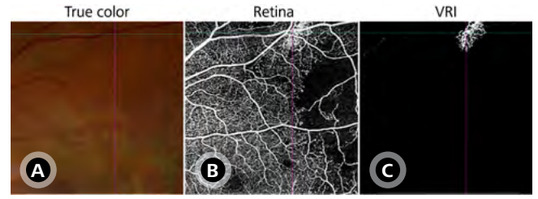

Figure 38: True color fundus image (A), OCT-A retina segmentation (B), and OCT-A VRI segmentation (C) in a patient with proliferative diabetic retinopathy, demonstrating the difficulty in identifying neovascularization in the clinical image and the enhanced detection using OCT-A, particularly with VRI segmentation.

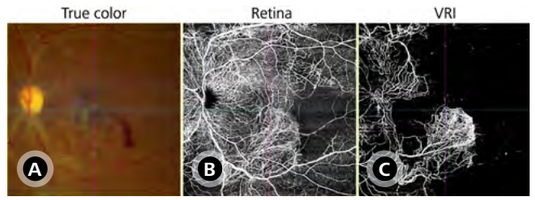

Figure 39: True color fundus image (A), OCT-A retina segmentation (B), and OCT-A VRI segmentation (C) in a patient with proliferative diabetic retinopathy, showing the clinical appearance of extensive neovascularization and its full extent as revealed through VRI segmentation.

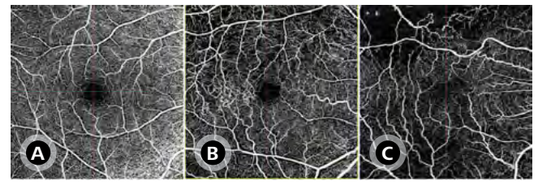

Figure 40: OCT-A images of the SRL in a normal patient (A) and in two cases of BRVO. The first case (B) shows flow voids and secondary telangiectasia in the temporal region involving the FAZ, while the second case (C) presents significant flow voids in the superficial capillary plexus without FAZ involvement.

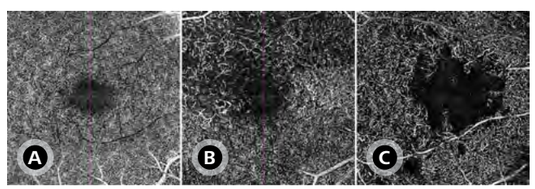

Figure 41: OCT-A images of the DRL in a normal patient (A), in a patient with superior temporal BRVO (B) showing flow voids in the affected region of the deep capillary plexus, and in a diabetic patient (C) demonstrating diffuse deep plexus impairment involving the FAZ.

Section 5: OCT-A analysis

The next stage of analysis examines the avascular layer, which should remain devoid of vascular structures under normal conditions. Any detected signal in this segmentation suggests either pathological neovascularization or projection/segmentation artifacts. This assessment is particularly relevant in neovascular AMD, where Type 2 and Type 3 MNV may extend into this layer (Figure 42). Additionally, this segmentation is particularly useful in MacTel.

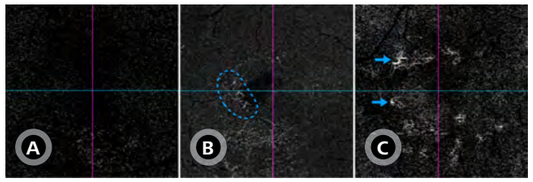

Figure 42: OCT-A images of the avascular layer segmentation in a normal patient (A), a patient with MacTel (B), and a case of AMD with Type 3 MNV (C). In image B, subtle vascularization is observed within the avascular zone (highlighted by the blue dashed line). In image C, despite some projection and segmentation artifacts, two sites confirmed on the structural B-scan and marked with blue arrows correspond to Type 3 MNV.

Moving posteriorly, the RPE-RPE fit segmentation isolates potential vascular structures confined between the RPE and Bruch's membrane. Under normal conditions, no vasculature exists in this region, resulting in a uniformly black angiographic map. This segmentation is critical for detecting quiescent Type 1 MNV, commonly observed in AMD and other diseases (Figure 43). In CSC, it helps differentiate fibrovascular PED from other PED subtypes, enhancing diagnostic precision in complex neovascular processes. Despite its utility, this map is highly susceptible to projection artifacts and must be interpreted with caution.

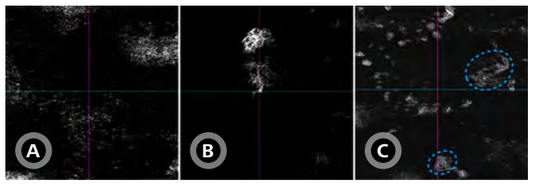

Figure 43: OCT-A images of the RPE-RPE fit segmentation in a normal patient (A), in a patient with quiescent Type 1 MNV (B), and in a patient with multiple projection artifacts and two regions of quiescent Type 1 MNV (highlighted by blue dashed lines) (C).

Further posteriorly, the choriocapillaris is the next structure evaluated. Under normal conditions, it can be visualized in three distinct yet complementary segmentation maps: Sub-RPE, choriocapillaris, and ORCC. Normal eyes should display similar images across these three segmentations (Figure 44); discrepancies warrant further investigation.

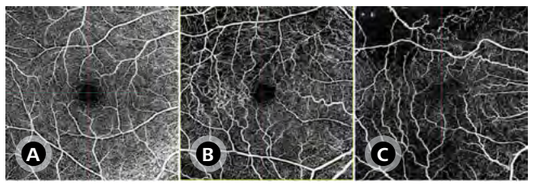

Figure 44: Appearance of the choriocapillaris in a normal patient, presented using three different segmentations: Sub-RPE (A), ORCC (B), and choriocapillaris (C), all demonstrating a similar vascular pattern.

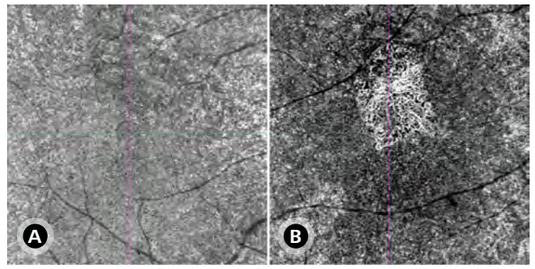

Figure 45: OCT-A images of the sub-RPE segmentation in a normal patient (A) and in a patient with polypoidal variant of AMD (B), showing a Type 1 MNV with a neovascular complex located in the choriocapillaris.

The sub-RPE segmentation normally corresponds to the choriocapillaris. However, anatomical alterations, such as PEDs, can disrupt this analysis. This layer is particularly valuable for assessing Type 1 MNV and detecting superficial polypoidal lesions associated with PCV. The presence of abnormal vascular structures within this segmentation supports the diagnosis of exudative AMD and pachychoroid spectrum disorders (Figure 45).

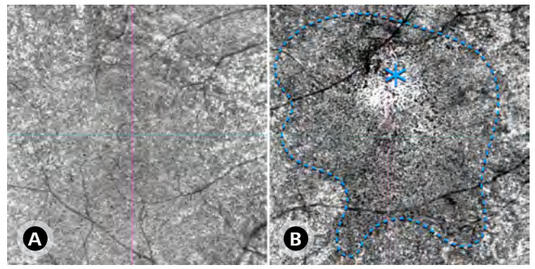

Figure 46: OCT-A images of the choriocapillaris in a normal patient (A) and in a patient with polypoidal variant of AMD (B), showing a Type 1 macular neovascular complex located in the choriocapillaris (blue asterisk) and an adjacent area of reduced choriocapillaris perfusion (blue dashed line).

The choriocapillaris segmentation provides a detailed visualization of choriocapillaris flow patterns, typically appearing as a relatively homogeneous gray texture in normal cases. In AMD, this layer offers crucial insights into disease severity and progression, with areas of decreased perfusion correlating with atrophic changes (Figure 46). In CSC, choriocapillaris flow alterations reflect vascular hyperpermeability and ischemic damage, aiding in the identification of leakage points. Furthermore, in inflammatory conditions such as APMPPE, choriocapillaris flow voids serve as biomarkers for disease activity.

Section 5: OCT-A analysis

The ORCC segmentation extends from the OPL to the choriocapillaris. Under normal conditions, the only vascular structure expected to generate a decorrelation signal in this segmentation is the choriocapillaris. This segmentation is useful for detecting Type 2 MNV, where neovascular proliferation extends into the outer retina (Figure 47). However, its increased thickness makes it more prone to artifacts and noise, necessitating multimodal correlation for accurate interpretation.

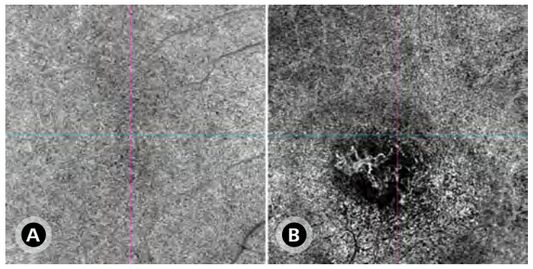

Figure 47: OCT-A images of the ORCC segmentation in a normal patient (A) and in a patient with AMD (B) showing Type 2 MNV.

The choroidal segmentation focuses on larger choroidal vessels within Haller's layer. This segmentation is particularly useful for evaluating choroidal circulation in diseases such as CSC and AMD (Figure 48). However, signal attenuation limits visualization at greater depths, requiring careful interpretation.

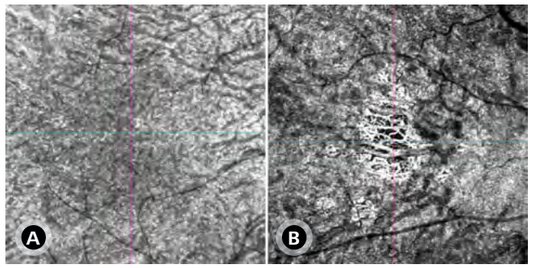

Figure 48: OCT-A images of the choroid in a normal patient (A) and in a patient with AMD and geographic atrophy (B).

Additional maps with thicker segmentations may be used for a more dynamic and targeted examination but are often noisier and more challenging to interpret. A broader assessment of retinal vasculature is achieved through retina segmentation, which provides an overview of general retinal perfusion status and can be visualized as a depth-encoded map, enabling the simultaneous assessment of distinct retinal layers (Figure 49). Meanwhile, the whole-eye segmentation offers a holistic view of the posterior segment, though its interpretation is complicated by overlapping information and projection artifacts (Figure 50).

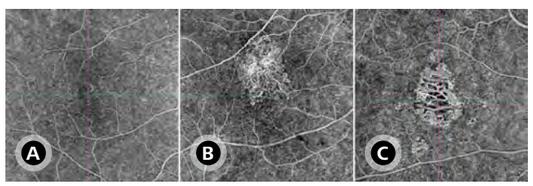

Figure 50: Whole eye OCT-A images in a normal patient (A) and in two patients with AMD—one with macular neovascularization (B) and another with geographic atrophy (C). In the latter, choroidal vasculature becomes visible due to the unmasking effect in the area of geographic atrophy.

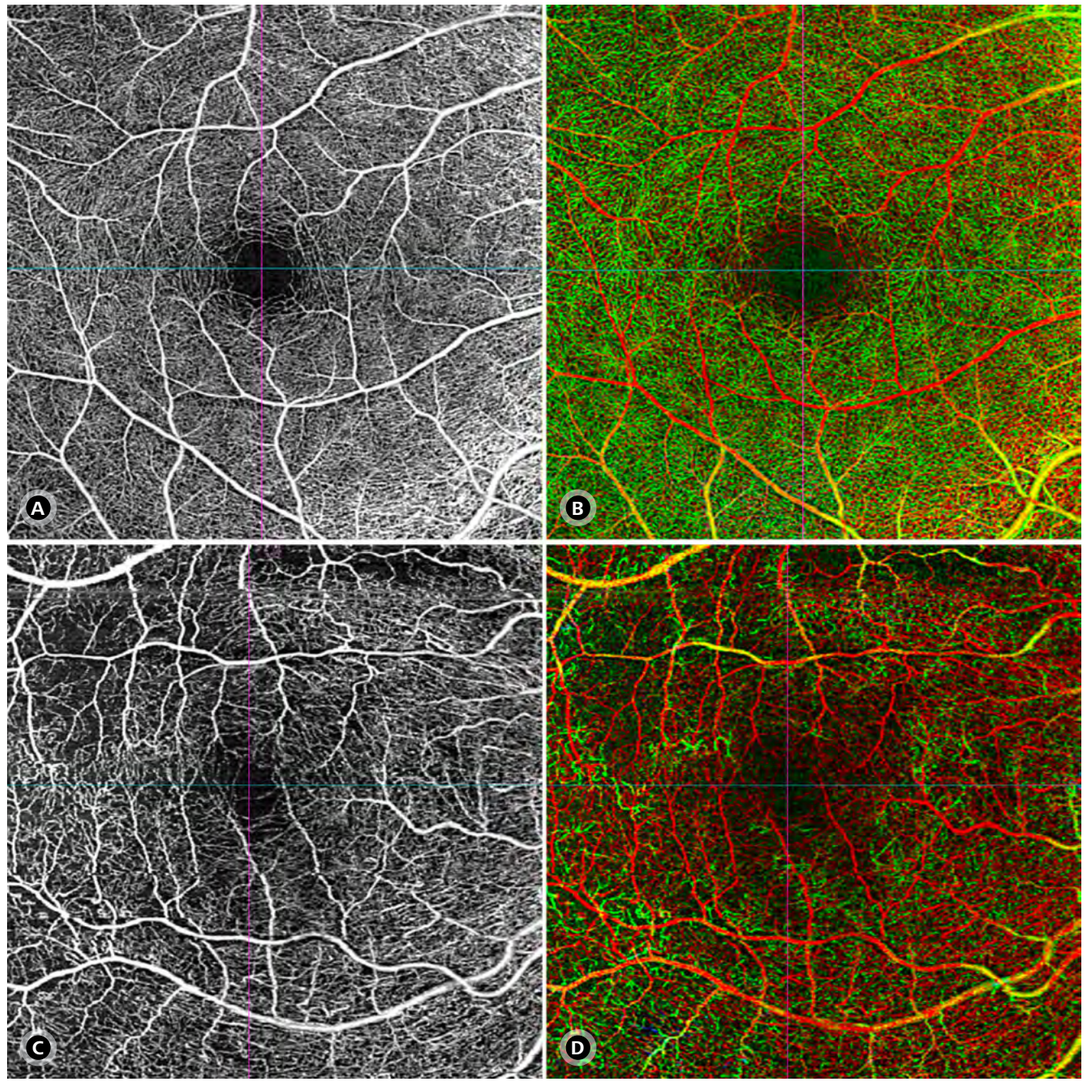

Figure 49: OCT-A images of the retina (left column) and depth-encoded representation (right column) in a normal patient (top row) and in a case of diabetic retinopathy with predominant deep plexus ischemia (bottom row), identified by the reduction of green coloration in the depth-encoded image.

Section 5: OCT-A analysis

5.2.2. Flow overlay on B-Scan in OCT-A

The flow overlay on a B-scan represents an additional qualitative approach to OCT-A analysis, enabling the simultaneous evaluation of structural and vascular features within ocular tissues. By integrating grayscale structural OCT imaging with color-coded blood flow data, this technique enhances diagnostic accuracy, facilitates disease monitoring, and informs clinical decision-making. The qualitative assessment of flow overlays focuses on tissue morphology, vascular patterns, lesion characteristics, and artifacts, making it an indispensable component of OCT-A interpretation.

A fundamental aspect of flow overlay analysis is the comprehensive evaluation of lesions, allowing for the correlation between tissue structure and microvascular changes. In this approach, the structural OCT B-scan is first examined to characterize hyperreflective or hyporeflective regions, which may indicate alterations in tissue integrity, fluid accumulation, or morphological abnormalities. The flow overlay, derived from OCT-A, then highlights blood movement within vessels, with color-coded signals marking perfused areas.

A key advantage of the CIRRUS OCT flow overlay is its dual-color display options, which optimize vascular layer differentiation (Figure 51). In Color 1 mode, all flow information is presented in light red, providing a straightforward representation of perfused areas. In Color 2 mode, flow above the RPE is displayed in light red, while flow below the RPE appears in green, facilitating the identification of choroidal vasculature and sub-RPE neovascularization. This distinction is particularly valuable in conditions such as diabetic retinopathy, RVO, and MNV, where precise localization of abnormal blood flow is crucial for accurate diagnosis and treatment planning.

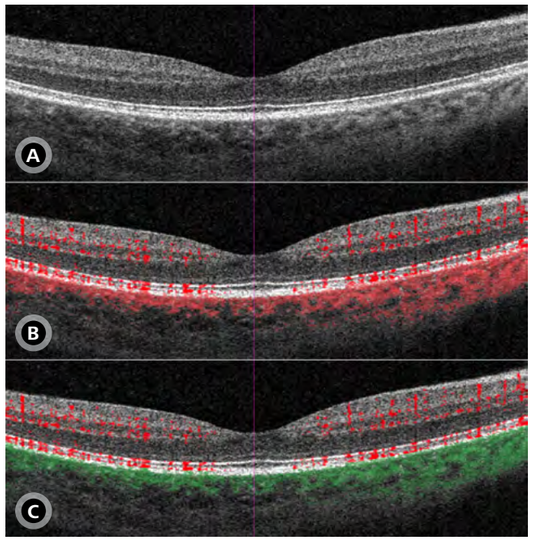

Figure 51: OCT B-scan of a normal patient shown in its structural aspect without flow overlay (A), with flow overlay using CIRRUS Color 1 mode (B), and with flow overlay using Color 2 mode (C).

By integrating structural and flow information, the flow overlay significantly enhances the detection of vascular changes and abnormalities. In diabetic retinopathy, for instance, microaneurysms can be identified more effectively by correlating structural OCT findings, such as focal fluid accumulation, with flow signals in the overlay (Figure 52). This tool also allows clinicians to evaluate vascularization in typically avascular planes, aiding in the detection of fibrovascular proliferations and Type 3 MNV (Figure 53 and 54). Additionally, it assists in identifying decorrelation tails, which appear as bright shadows of superficial vessels in deeper layers due to light transmission through moving blood cells. Recognizing these artifacts is essential to prevent misinterpretation of OCT-A findings (Figure 31, page 21).

The adjustability of flow overlay transparency in the CIRRUS OCT provides further flexibility in visualization, allowing for optimized contrast between vascular and structural elements. Segmentation lines, marking the upper and lower boundaries of the selected layer, can also be overlaid on the B-scan, ensuring accurate localization of vessels within specific retinal or choroidal layers. This feature is particularly beneficial for conditions requiring precise layer differentiation, such as MNV and subclinical vascular changes.

Beyond its diagnostic applications, the flow overlay on B-scans plays a critical role in disease progression monitoring and treatment response assessment. By visualizing changes in blood flow and vascular remodeling over time, this tool aids in tracking the efficacy of treatments such as anti-VEGF therapy and laser photocoagulation. Furthermore, its capacity to correlate vascular alterations with structural OCT features provides a comprehensive understanding of disease pathology.

In addition to its diagnostic and monitoring applications, flow overlay analysis is essential for artifact identification and correction. Segmentation errors, projection artifacts, and motion-related distortions can significantly affect OCT-A interpretation, leading to misclassification of vascular structures. By carefully examining B-scan overlays, clinicians can differentiate true vascular signals from artifacts, thereby improving the accuracy and reliability of the assessment.

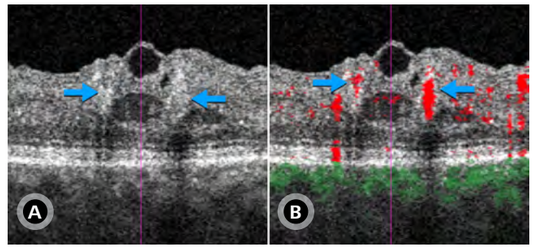

Figure 52: Structural OCT B-scan (A) and B-scan with flow overlay (B) in a diabetic patient showing microaneurysms (blue arrow).

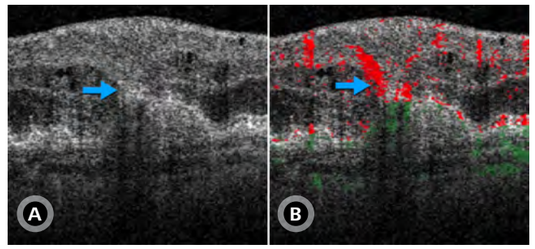

Figure 53: Structural OCT B-scan (A) and B-scan with flow overlay (B) in a patient with AMD presenting Type 3 MNV, with the communication point between retinal and choroidal vasculature identified (blue arrow).

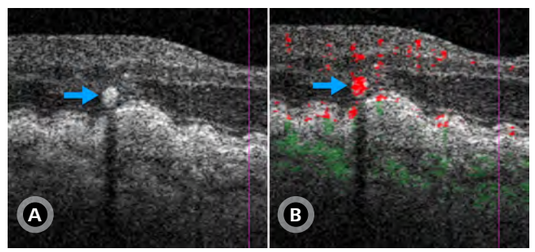

Figure 54: Structural OCT B-scan (A) and B-scan with flow overlay (B) of the contralateral eye from the previous patient, also presenting Type 3 MNV. The scan reveals flow within the hyperreflective lesion (blue arrow).

5.3. Quantitative analysis

OCT-A has significantly enhanced the evaluation of retinal and choroidal microvasculature, enabling the noninvasive quantification of vascular parameters essential for disease diagnosis, monitoring, and treatment assessment. The CIRRUS OCT incorporates the AngioPlex Metrix system, a robust tool designed for automated and standardized quantitative analysis of retinal vasculature. By providing key metrics, such as vessel density, perfusion density, and FAZ measurements, it facilitates a detailed assessment of microvascular integrity, enabling precise detection of ischemic changes and vascular remodeling.

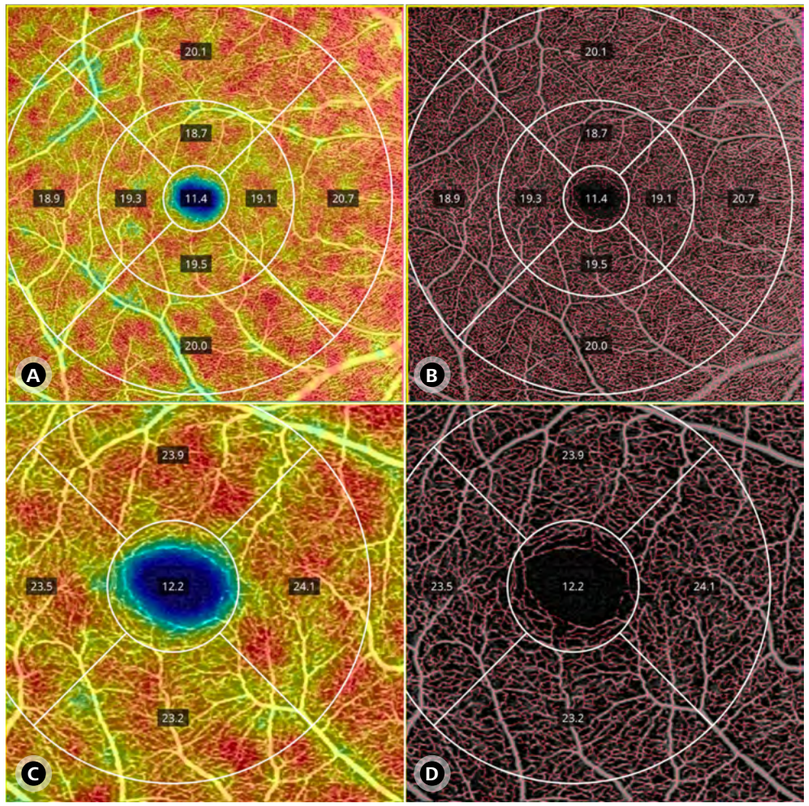

Figure 55: Vessel density maps from 6 mm scans (A and B) and 3 mm scans (C and D) in a normal patient. Images A and C display vessel density using a heat map, where warmer colors indicate higher vascular density, while images B and D show vessel tracings overlaid on the en face angiographic image. Quadrant-specific values are displayed on the corresponding analyzed regions.

5.3.1. Vessel density analysis

Vessel density is a fundamental metric in OCT-A analysis, quantifying the total length of perfused vasculature per unit area, expressed in mm/mm². This measurement is determined by binarizing the OCT-A image and calculating the proportion of white pixels (representing vessels) relative to the total pixel count within a specific measurement region (Figure 55). Vessel density is widely used in the assessment of retinal diseases, including diabetic retinopathy, glaucoma, AMD, and RVO. A reduction in vessel density may indicate capillary dropout, vascular rarefaction, or ischemia, serving as a key marker of disease progression (Figure 56). However, vessel density alone does not differentiate hypoperfusion from nonperfusion, necessitating correlation with perfusion density and structural OCT findings.

The accuracy of vessel density measurements depends on precise segmentation, artifact-free imaging, and the binarization method employed. The AngioPlex Metrix system in CIRRUS OCT automatically calculates vessel density for various scan types, including 3×3 mm and 6×6 mm macular angiography cubes and the 4.5×4.5 mm ONH angiography cube. These vascular maps facilitate the identification of progressive capillary loss, particularly in conditions such as diabetic retinopathy and glaucoma.

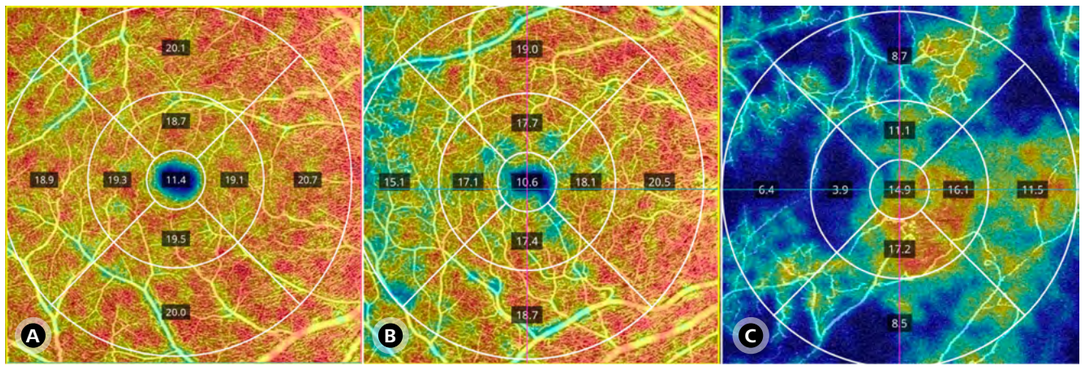

Figure 56: Comparison of vessel density in a normal patient (A), a patient with diabetic retinopathy (B), and a patient with severe macular ischemia due to CRVO (C).

5.3.2 Perfusion density analysis

Perfusion density is another critical quantitative OCT-A metric, representing the total percentage of perfused vasculature within a given region. Unlike vessel density, which quantifies only the length of vasculature, perfusion density accounts for both vessel length and caliber, making it a more stable parameter for evaluating retinal perfusion status (Figure 57). A reduction in perfusion density suggests compromised blood flow, which is particularly relevant in ischemic retinal conditions such as diabetic macular ischemia, hypertensive retinopathy, and retinal artery occlusion (Figure 58).

The CIRRUS OCT AngioPlex Metrix system generates automated perfusion density maps, displayed in Early Treatment Diabetic Retinopathy Study (ETDRS) grid regions, ensuring standardized comparisons across clinical studies and follow-up examinations. The ability to toggle between vessel density and perfusion density provides a comprehensive evaluation of retinal perfusion, supporting early disease detection and monitoring of disease progression.

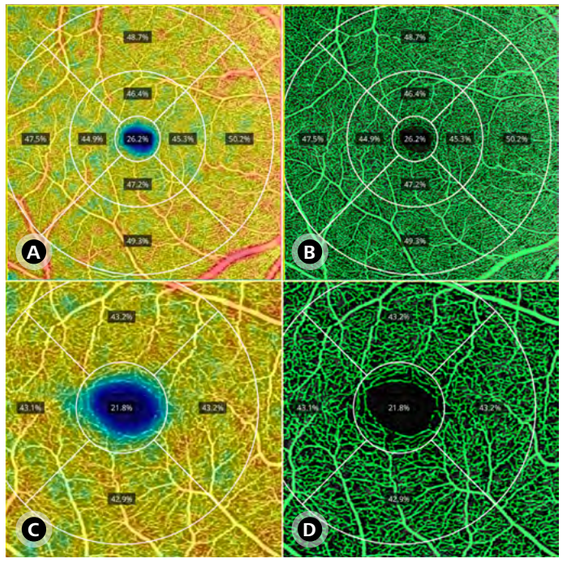

Figure 57: Perfusion density maps from 6 mm scans (A and B) and 3 mm scans (C and D) in a normal patient. Images A and C present perfusion density as heat maps, where warmer colors indicate higher vascular perfusion. Images B and D show vessel tracings overlaid on the en face angiographic images. Perfusion values for each quadrant are displayed directly on the respective regions.

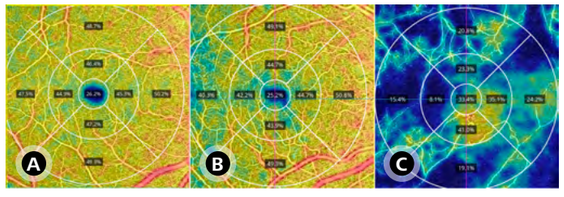

Figure 58: Comparison of perfusion density in a normal patient (A), a patient with diabetic retinopathy (B), and a patient with a history of CRVO and severe macular ischemia (C).

5.3.3. Foveal avascular zone analysis

The FAZ is a crucial quantitative metric in OCT-A imaging, offering insights into macular perfusion and ischemic damage. The FAZ, a capillary-free region in the foveal center, is automatically detected and segmented by the CIRRUS OCT AngioPlex Metrix system. The system calculates FAZ area (mm²), FAZ perimeter (mm), and FAZ circularity—a measure of FAZ roundness ranging from 0 to 1, where 1 represents a perfect circle (Figure 59).

FAZ enlargement strongly correlates with capillary dropout and ischemia, while reduced circularity suggests vascular remodeling or perifoveal capillary loss (Figure 60). FAZ parameters have been shown to correlate with visual acuity and serve as prognostic markers in conditions such as diabetic retinopathy, RVO, and hypertensive retinopathy. The AngioPlex Metrix system provides standardized FAZ measurements for 3×3 mm and 6×6 mm macular angiography scans for longitudinal disease monitoring.

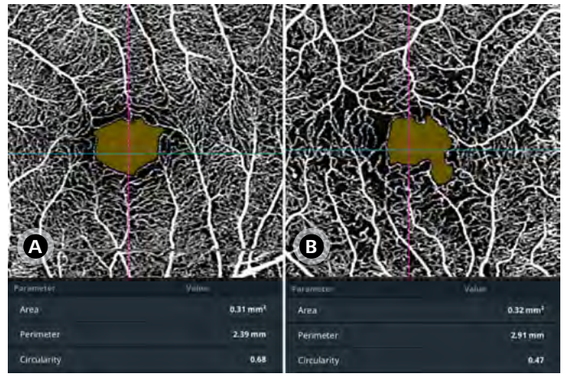

Figure 59: Measurements of the FAZ area, perimeter, and circularity in a normal patient (A) and in a patient with diabetic retinopathy (B).

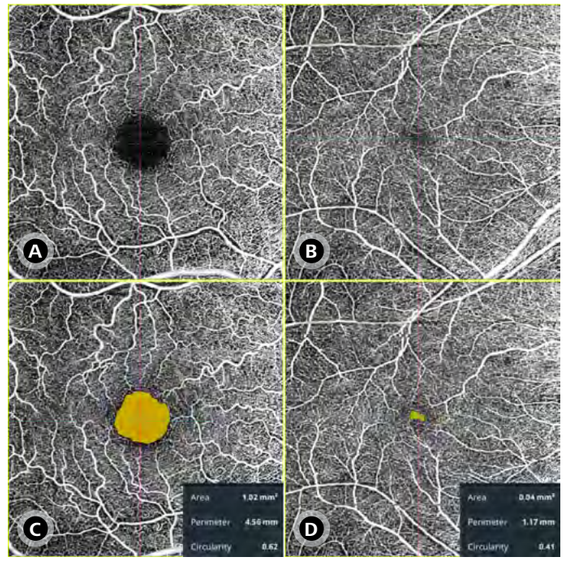

Figure 60: Measurements of the FAZ area, perimeter, and circularity in a patient with hypertensive retinopathy (A), showing an increased FAZ area and perimeter, and in a case of foveal hypoplasia (B), where the FAZ is nearly absent due to persistent vascularization in the typically avascular region.

5.3.4. Longitudinal analysis and change detection

Beyond individual metrics, the CIRRUS OCT includes a change analysis feature, allowing direct comparisons of angiography scans over time. This function is particularly valuable for tracking disease progression in conditions such as diabetic retinopathy, MacTel, and RVO. By aligning and registering sequential angiography scans, the system generates angiographic difference maps, which highlight areas of capillary loss, neovascularization, or perfusion recovery. This capability is useful for evaluating treatment response to anti-VEGF therapy, laser photocoagulation, or surgical interventions.

5.3.5. Clinical applications and challenges

Quantitative OCT-A metrics have broad clinical applications, including early detection of microvascular abnormalities, disease progression monitoring through vessel density and FAZ alterations, and treatment efficacy assessment in patients undergoing anti-VEGF therapy or laser treatment. Despite these advantages, quantitative OCT-A analysis is subject to variability, primarily due to artifacts and inter-device differences. The lack of universal binarization methods and the impact of image quality on measurements must be carefully considered during clinical interpretation.

To ensure data reliability and prevent inaccurate comparisons, the CIRRUS OCT restricts quantitative assessments to specific scan types. By employing standardized acquisition settings, the system enhances reproducibility across serial examinations, minimizing variability and ensuring that vascular measurements remain clinically meaningful and comparable.

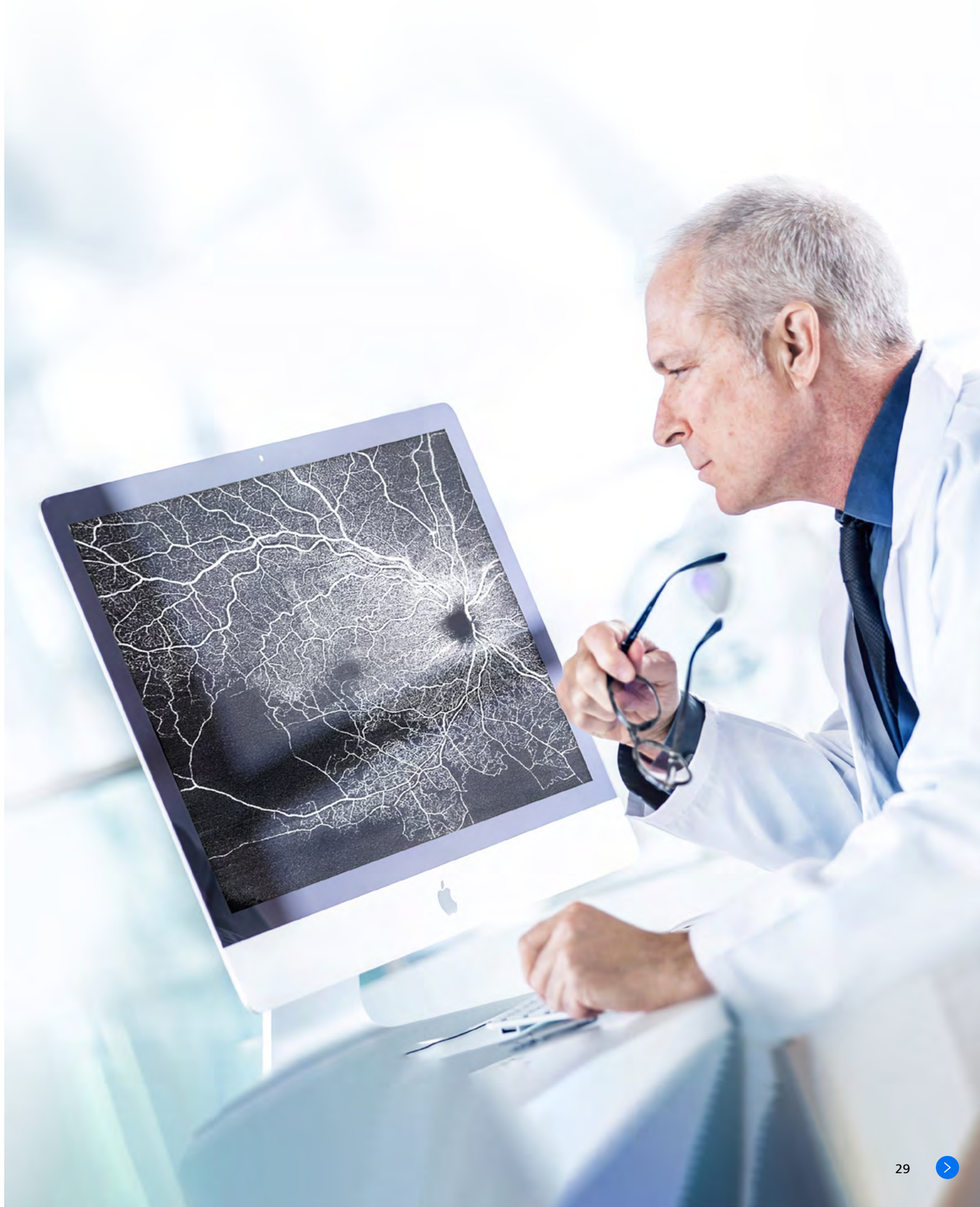

Section 6

Structural en face OCT: Beyond OCT-A quality assessment

The clinical utility of structural en face OCT imaging extends far beyond evaluating the reliability of OCT-A. It plays a pivotal role in the diagnosis and monitoring of a wide spectrum of retinal and choroidal diseases.

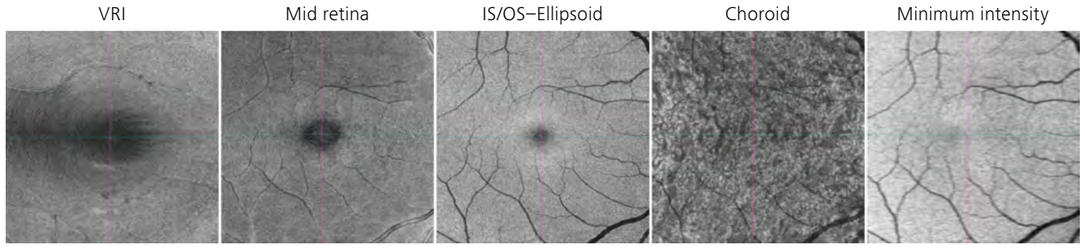

Figure 61: Structural en face OCT images with standard segmentations from the CIRRUS 6000 device in a normal patient.

By enabling layer-specific segmentation, structural en face OCT provides unique insights into the pathoanatomy of these conditions. The analysis of different segmentation slabs adds critical and complementary information that supports diagnosis, guides management decisions, aids surgical planning, and informs prognostic expectations. To achieve this, selecting the appropriate segmentation for each clinical scenario is essential.

In this context, the CIRRUS OCT stands out by enabling structural analysis directly from the same scans acquired for OCT-A. In addition to standard en face segmentations, it offers a practical and intuitive interface for editing and adjusting these layers, as well as creating custom segmentations tailored to specific clinical needs. The device allows precise evaluation through distinct segmentation of the vitreoretinal interface (VRI), mid retina, ellipsoid zone (IS/OS), choroid, and minimum intensity projection—each with specific clinical applications (Figure 61). In the following sections, we will discuss in detail the practical applicability of each of these segmentations across distinct retinal and choroidal diseases.

6.1. Vitreoretinal interface (VRI) segmentation

VRI segmentation allows detailed evaluation of the retinal surface and vitreoretinal interface, proving especially useful in tractional conditions such as epiretinal membrane (ERM), vitreomacular traction (VMT), and macular hole (MH), by highlighting membrane morphology, retinal folds, opercula, and tangential distortions. It also aids in postoperative assessment, including the detection of dissociated optic nerve fiber layer (DONFL) and resolution of surface folds after retinal detachment surgery.

Additionally, it contributes to the identification of fibrovascular proliferations, often secondary to vascular diseases, and arcuate retinal nerve fiber layer (RNFL) (Figures 62 and 63).

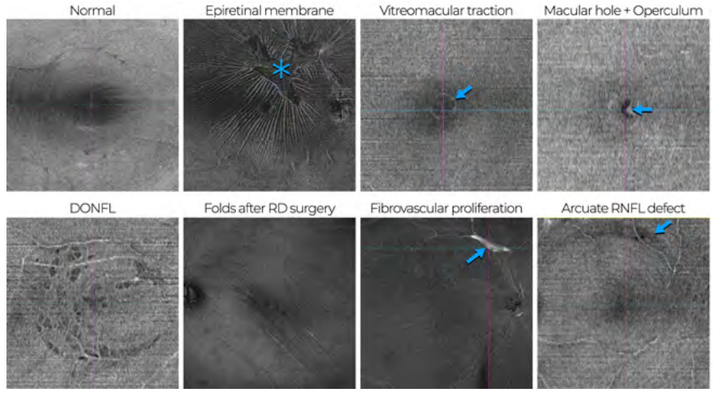

Figure 62: Structural en face OCT images (vitreoretinal interface – VRI – segmentation) in a normal patient and in distinct vitreoretinal diseases. In the case of epiretinal membrane, the membrane is marked with an asterisk, and multiple retinal surface folds are seen as alternating hyper- and hyporeflective radial lines originating from the membrane. In vitreomacular traction, a circular hyperreflective line (blue arrow) indicates vitreous adhesion. In macular hole, a hyporeflective C-shaped area corresponding to the full thickness macular hole is observed, along with a hyperreflective focus (blue arrow) representing an operculum partially attached to the inner retina. In dissociated optic nerve fiber layer (DONFL), wedge-shaped hyporeflective dimples appear in the area where the ILM was removed. Surface folds after retinal detachment surgery show an alternating hyper/hyporeflective pattern in the transition zone between attached and previously detached retina. Fibrovascular proliferation, secondary to BRVO in this case, appears as a hyperreflective lesion. Lastly, an arcuate RNFL defect, seen as a hyporeflective area, is noted following inadvertent RNFL injury during ERM peeling.

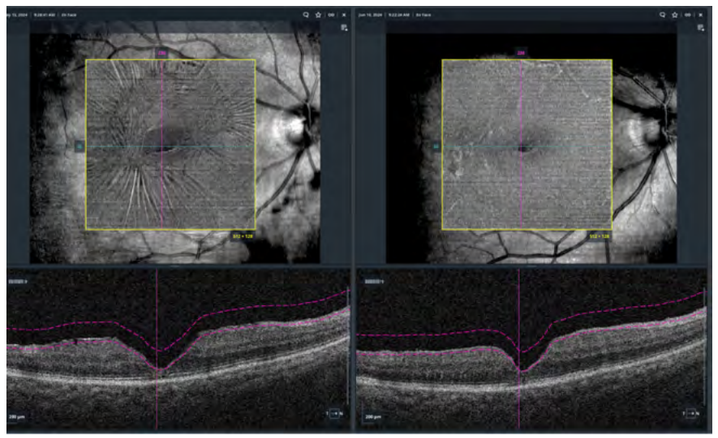

Figure 63: Structural en face OCT images (vitreoretinal interface – VRI – segmentation), along with structural B-scan and segmentation lines, evaluated using the Retina Workplace module of the FORUM® software, illustrating the follow-up evaluation of a patient undergoing vitreoretinal surgery. The left image shows the presence of an epiretinal membrane (ERM) and retinal surface folds prior to surgery, while the right image demonstrates a smooth retinal surface with resolution of folds and absence of ERM 22 days postoperatively.

6.2. Mid retina

Mid-retina segmentation provides a distinct view of retinal cytoarchitecture and is clinically useful across a wide spectrum of posterior segment diseases. In vascular conditions, such as paracentral acute middle maculopathy (PAMM), diabetic retinopathy (DR), retinal vein occlusion (RVO), and branch retinal artery occlusion (BRAO), it reveals ischemic lesions, microaneurysms, telangiectatic capillaries, and perivascular changes. In exudative and inflammatory diseases, including diabetic macular edema (DME), cystoid macular edema (CME), and uveitis, it enables visualization of intraretinal fluid and hard exudates. In tractional and degenerative disorders, such as epiretinal membranes (ERM), macular holes, degenerative myopia, and intraretinal cystoid degeneration, it highlights features such as retinal folds, foveoschisis, and cystoid spaces (Figure 64). By capturing characteristic patterns of reflectivity in each scenario, mid-retina en face imaging supports diagnosis, guides management, and informs prognosis.

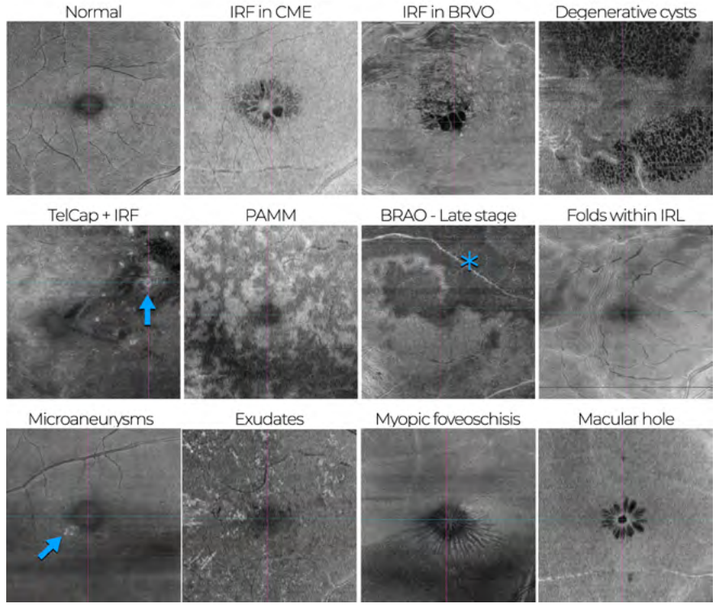

Figure 64: Structural en face OCT images (mid retina segmentation) in a normal patient and in distinct vitreoretinal diseases. Regardless of the underlying condition, intraretinal fluid (IRF) appears as hyporeflective lesions. Degenerative cystoid spaces, such as those observed after ERM removal, also appear hyporeflective. Telangiectatic capillaries typically present as circular lesions with a hyporeflective center and a hyperreflective halo, though they may exhibit marked hyperreflectivity depending on their depth and segmentation boundaries. Acute macular neuroretinopathy, a marker of ischemia, is seen as hyperreflective fern-like areas indicating ischemia in the mid-retina. Advanced ischemia, as in late-stage BRVO, results in hyporeflective zones, highlighted by an asterisk. Epiretinal membranes may cause folds extending into the mid-retinal layers, suggesting significant traction. Microaneurysms and exudates appear as hyperreflective foci. In degenerative myopia, foveoschisis lesions present as radially oriented hyporeflective spaces, and this segmentation aids in assessing their extent. In macular hole cases, the smallest diameter often occurs in the mid-retina, making this analysis valuable for prognosis. Cystoid spaces at the hole margins, also visible in this layer, are linked to postoperative anatomical outcomes.

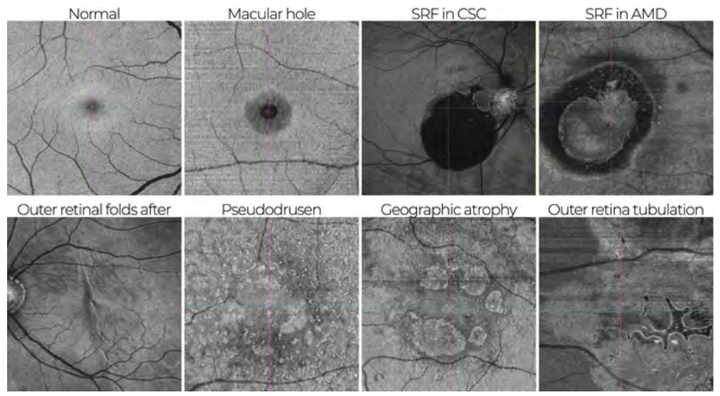

Figure 65: Structural en face OCT images (IS/OS-Ellipsoid segmentation) in a normal patient and in distinct vitreoretinal diseases. In cases of full-thickness macular hole, the largest diameter can be identified as a markedly hyporeflective area, allowing detailed assessment of its size, shape, and possible alterations of the RPE in the central region. Additionally, the spatial extent of ellipsoid zone (EZ) disruption at the hole margins can be visualized as a moderately hyporeflective border compared to adjacent tissue. Regardless of the underlying condition, SRF appears as a hyporeflective area, enabling comprehensive visualization of serous detachments associated with CSC and serving as a practical tool for SRF evaluation in neovascular AMD. Postsurgical EZ irregularities following retinal detachment (RD) repair can be observed as alternating hypo- and hyperreflective lines. The previously detached area can also be assessed for the restoration of normal reflectivity in conditions such as RD and CSC. In AMD, pseudodrusen appear as hyperreflective lesions with either punctate or reticular patterns, depending on the clinical presentation. Geographic atrophy (GA) areas may appear hyperreflective, while disruptions of the EZ adjacent to GA present as hyporeflective regions, indicating the extent and configuration of EZ loss. Outer retinal tubulations (ORTs) can also be visualized, often appearing as complex tubular networks with hyporeflective centers and hyperreflective borders.

6.3. IS/OS–Ellipsoid zone segmentation

Ellipsoid zone (EZ) segmentation provides high-resolution assessment of photoreceptor integrity and is a key tool in the diagnosis and prognosis of numerous retinal diseases. It is especially useful in degenerative conditions, such as AMD, retinitis pigmentosa, Stargardt disease, rod-cone dystrophies, and occult macular dystrophy, by revealing EZ loss, geographic atrophy, pseudodrusen, and outer retinal tubulations. In fluid-associated disorders such as diabetic retinopathy and CSC, it allows detection of subretinal fluid and subtle EZ abnormalities. In tractional and postsurgical scenarios including macular holes and retinal detachment repair it enables evaluation of EZ defects, outer retinal folds, and healing patterns (Figure 65). EZ imaging is also valuable in drug-related toxicity, such as hydroxychloroquine retinopathy, and in developmental anomalies like foveal hypoplasia.

Section 6: Structural en face OCT: Beyond OCT-A quality assessment

6.4. Choroid

Segmenting en face OCT to analyze the choroid provides valuable insights into the pathoanatomy of various retinal and chorioretinal diseases. It is particularly useful in degenerative conditions such as AMD, where it enables the detection and quantification of hypertransmission defects (hyperTDs), GA, nascent GA, and refringent drusen, often forming characteristic "donut" patterns. In chronic and acute CSC, it highlights focal leakage points and chronic RPE dysfunction through hyperreflective dots. This segmentation is also valuable for identifying lesions with variable choroidal reflectivity, such as choroidal nevi and RPE tears, and for detecting rare findings like Yasunari nodules in neurofibromatosis type 1 (Figure 66). By capturing distinct transmission patterns and structural alterations, choroidal en face imaging supports accurate diagnosis and enhances understanding of disease progression.

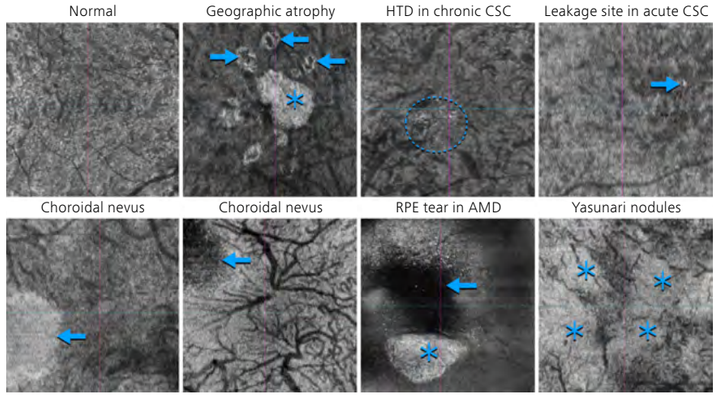

Figure 66: Structural en face OCT images (choroid segmentation) in a normal patient and in distinct vitreoretinal diseases. In AMD, this segmentation is particularly valuable for evaluating choroidal vascular patterns and identifying hypertransmission defects (HTDs), which are commonly seen in areas of RPE atrophy, such as geographic atrophy (GA) — highlighted with an asterisk — enabling spatial analysis of RPE involvement. HTDs may present a "donut" pattern when RPE pigment migration accumulates centrally, forming an image with a hyperreflective rim and hyporeflective center (arrow). HTDs can also be observed in chronic CSC as small hyperreflective dots (highlighted by the dashed line), indicating chronic RPE dysfunction. In acute CSC, the leakage point can be identified as a focal area of increased reflectivity within an otherwise homogeneous image (arrow). Choroidal nevi may appear with either marked hyporeflectivity or hyperreflectivity (arrow), depending on lesion depth and segmentation plane. Areas of RPE tear are visualized as markedly hyporeflective regions (asterisk), often accompanied by an adjacent hyporeflective area corresponding to the rolled RPE (arrow). The spatial distribution and extent of Yasunari nodules — pathognomonic of neurofibromatosis type 1 — are also visible as plaque-like hyperreflective lesions (asterisk).

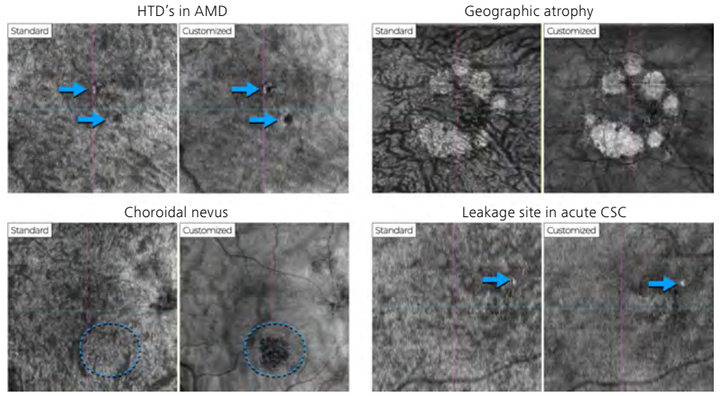

Figure 67. Comparison of structural en face OCT images using standard and customized choroid segmentation. In age-related macular degeneration (AMD), hypertransmission defects—even those of very small size—are more clearly visualized with the customized segmentation (arrow). The same applies to larger lesions, such as those found in geographic atrophy, improving longitudinal follow-up. In cases of choroidal nevus, even deeper lesions that are not visible with standard segmentation are easily detected using the customized settings. In CSC, small RPE defects responsible for subretinal fluid accumulation are also better highlighted through segmentation customization.

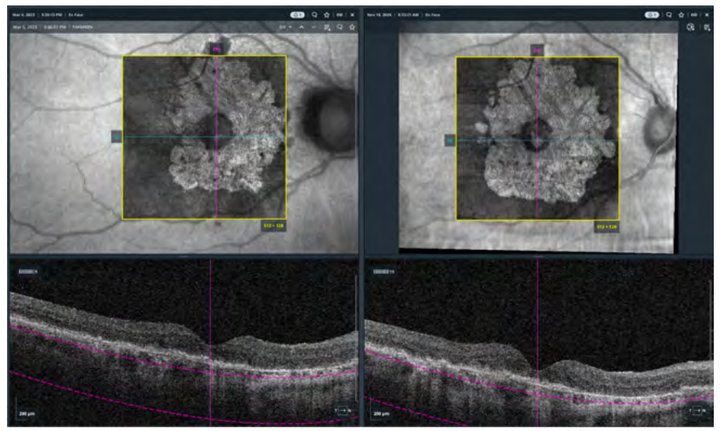

Figure 68: Structural en face OCT images (customized choroid segmentation), along with structural B-scan and segmentation lines, evaluated using the Retina Workplace module of the FORUM software, illustrating the baseline (left) and 20 months follow-up evaluation (right) in a case of geographic atrophy progression.

Choroid segmentation can be easily customized in the CIRRUS software to enhance the visualization of choroidal hypertransmission defects. This is accomplished by adjusting the segmentation boundaries—specifically, setting the offset to 64 µm and the thickness to 400 µm. The resulting map displays a more homogeneous pattern, minimizing interference from large-caliber choroidal vessels and enabling the detection of hypertransmission defects smaller than 125 µm. This facilitates the identification of lesions such as incomplete RPE and outer retinal atrophy (iRORA), complete RPE and outer retinal atrophy (cRORA), and the leakage point in CSC. In addition, this adjustment standardizes the appearance of choroidal nevi, which consistently appear hyporeflective regardless of lesion depth (Figure 67). This customized analysis is particularly valuable for monitoring the progression of geographic atrophy in patients with non-neovascular AMD (Figure 68).

Section 6: Structural en face OCT: Beyond OCT-A quality assessment

6.5. Minimum intensity projection

Structural en face OCT using minimum intensity (MI) segmentation is a noninvasive technique that enhances retinal assessment by displaying the darkest pixel along each A-scan within a selected retinal depth. The MI projection generates an en face image by identifying the minimum intensity pixel between the ILM and the RPE. In healthy retina, this minimum intensity typically lies within the outer nuclear layer (ONL) or Henle fiber layer (HFL). This method is particularly useful for highlighting subtle changes in these inherently low-reflective layers, which contain photoreceptor cell bodies and axons.

MI segmentation is especially valuable in degenerative conditions such as non-neovascular AMD, where increased MI signal at the margins of geographic atrophy (GA) may predict lesion enlargement and indicate widespread photoreceptor disruption. It also facilitates the detection and monitoring of fluid-related disorders—including neovascular AMD, diabetic retinopathy (DR), RVO, CME, and CSC—by clearly delineating intra- and subretinal fluid.

In addition, MI maps enhance the visualization of structural abnormalities, such as myopic foveoschisis, degenerative cystoid spaces, pseudodrusen, and photoreceptor layer involvement in Type 3 MNV, providing a sensitive tool for evaluating disease burden and therapeutic response (Figure 69). When combined with en face images from other structural OCT segmentations—available through the CIRRUS software or the Retina Workplace module of the FORUM® platform—MI analysis helps optimize workflow and increases diagnostic efficiency in routine ophthalmic practice (Figure 70).

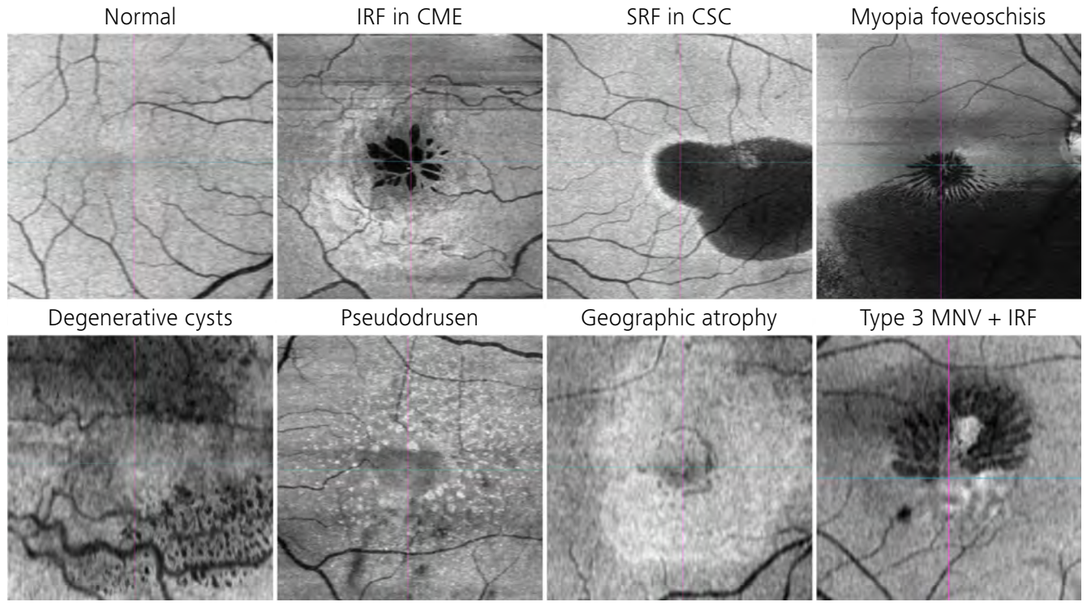

Figure 69: Structural en face OCT images (minimum intensity segmentation) in a normal patient and in various vitreoretinal diseases. In this map, hyporeflective lesions, such as intraretinal fluid, subretinal fluid, myopic foveoschisis, and degenerative cystoid spaces, appear as markedly hyporeflective areas. Conversely, conditions that alter normally hyporeflective layers—such as the outer nuclear layer (ONL) and Henle fiber layer (HFL)—including non-neovascular AMD, tend to exhibit increased reflectivity, with distinct patterns depending on the underlying pathology. Pseudodrusen, for instance, when extending beyond the external limiting membrane (grade 4), appear as small hyperreflective punctate or circular lesions. In geographic atrophy, an increased minimum intensity (MI) signal has been associated with GA enlargement and is considered a marker of widespread photoreceptor disruption. In neovascular AMD with active Type 3 MNV, both hyporeflective areas (representing intra- or subretinal fluid) and hyperreflective areas (indicating ONL and HFL involvement by the neovascular complex) can be observed.

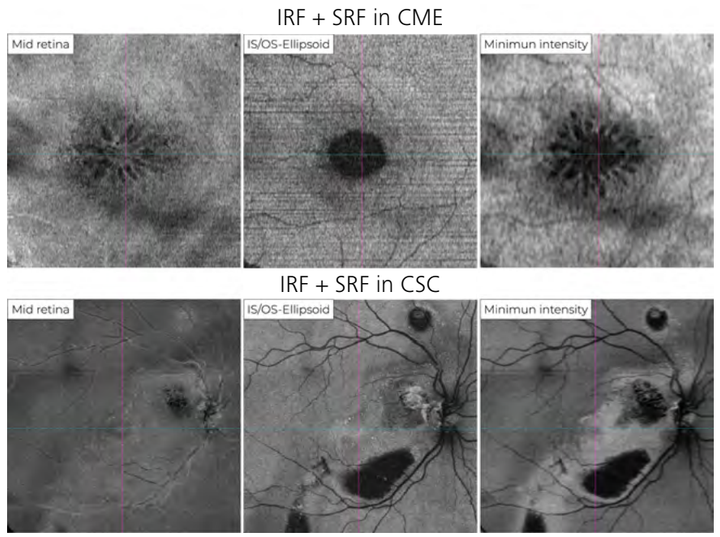

Figure 70: Structural en face OCT images of the mid retina, IS/OS–Ellipsoid, and minimum intensity segmentations, demonstrating the potential for optimized and intuitive assessment of intra- and subretinal fluid distribution in two distinct clinical scenarios: CME and CSC. This figure highlights the clinical relevance and practicality of combining en face images from different segmentations in the routine evaluation by ophthalmologists.

Section 7

Key Components of the OCT-A report – CIRRUS reports

The purpose of the OCT-A report is to highlight the key findings from the examination that led the examiner to the final conclusion and subsequent decision-making for the case, whether for confirming the diagnosis, follow-up, or defining the course of treatment. To address these points, the report must contain the key elements that should be analyzed in the OCT-A exam, as extensively discussed and detailed in the previous section, including information regarding the exam's reliability, the type of scan used, and the angiographic images (en face and flow overlay B-scan).

The CIRRUS OCT device generates comprehensive OCT-A reports that integrate multiple key components into a structured and intuitive layout, allowing for a thorough and efficient analysis of the scan results. These reports provide detailed examination parameters, ensuring an objective assessment of image quality and reliability, alongside both qualitative and quantitative data derived from the scan.

The standard report (Figure 71) includes an area describing the examination details and technical parameters, located in the header of the report. This section presents the fundamental patient and examination information, ensuring standardization and reproducibility. The main components include Patient Demographics (name, ID, date of birth, and gender), Examination Details (scan date and time, laterality, and operator), and Scan Parameters (scan type and area size). The signal intensity index, a metric for image quality, is also located in the report's header.

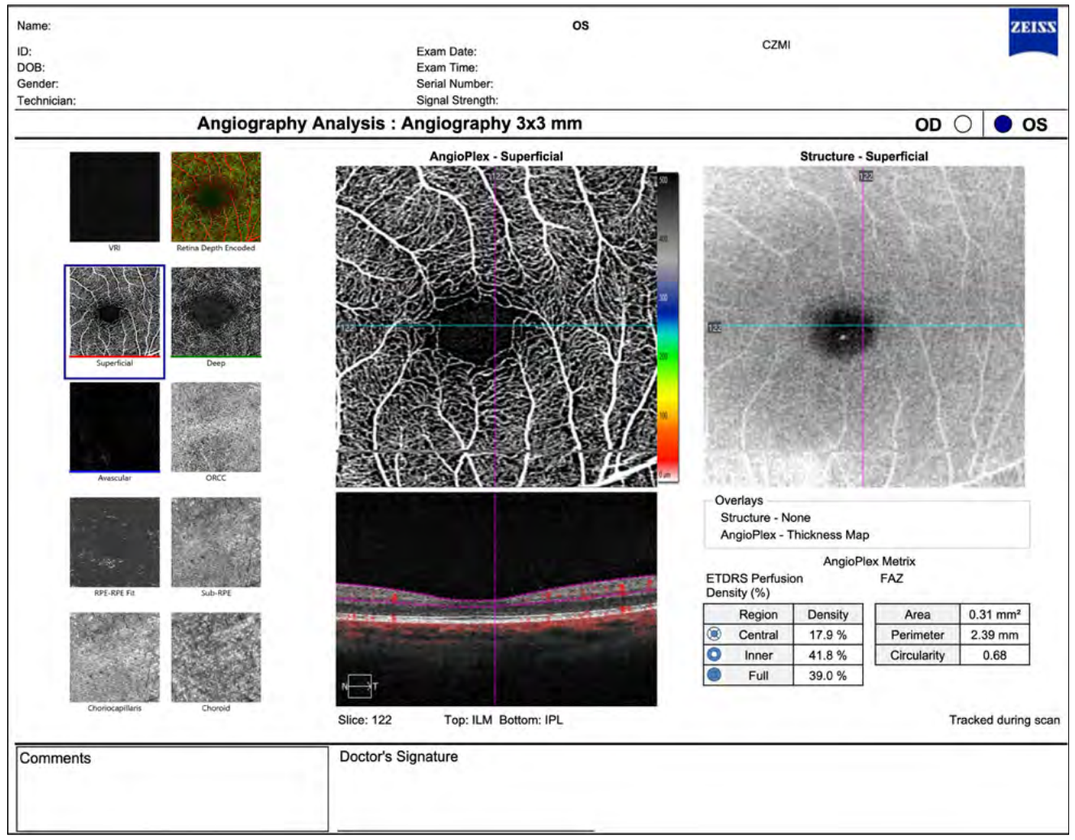

Figure 71: Standard CIRRUS OCT-A Report.

The use of EDI and FastTrac—two optional features related to the scanning process—are also highlighted in the report if utilized. Examinations performed using EDI display the description "Acquired using enhanced depth mode" in the "Comments" section, located in the bottom-left corner of the report. The notification of FastTrac usage is displayed in the bottom-right corner of the report, immediately above the device and software version information.

At the center of the report, the angiographic en face image is presented in a larger size, alongside its corresponding structural en face image. Immediately below the angiographic en face image, the flow overlay B-scan image can be observed. Quantitative analysis data, when available, are presented below the structural en face image. The report also includes images of all segmentations in smaller size, located on the left-hand side of the page. Figure 72 highlights the key components of the CIRRUS OCT-A report.

Section 7: Key components of the OCT-A report – CIRRUS reports

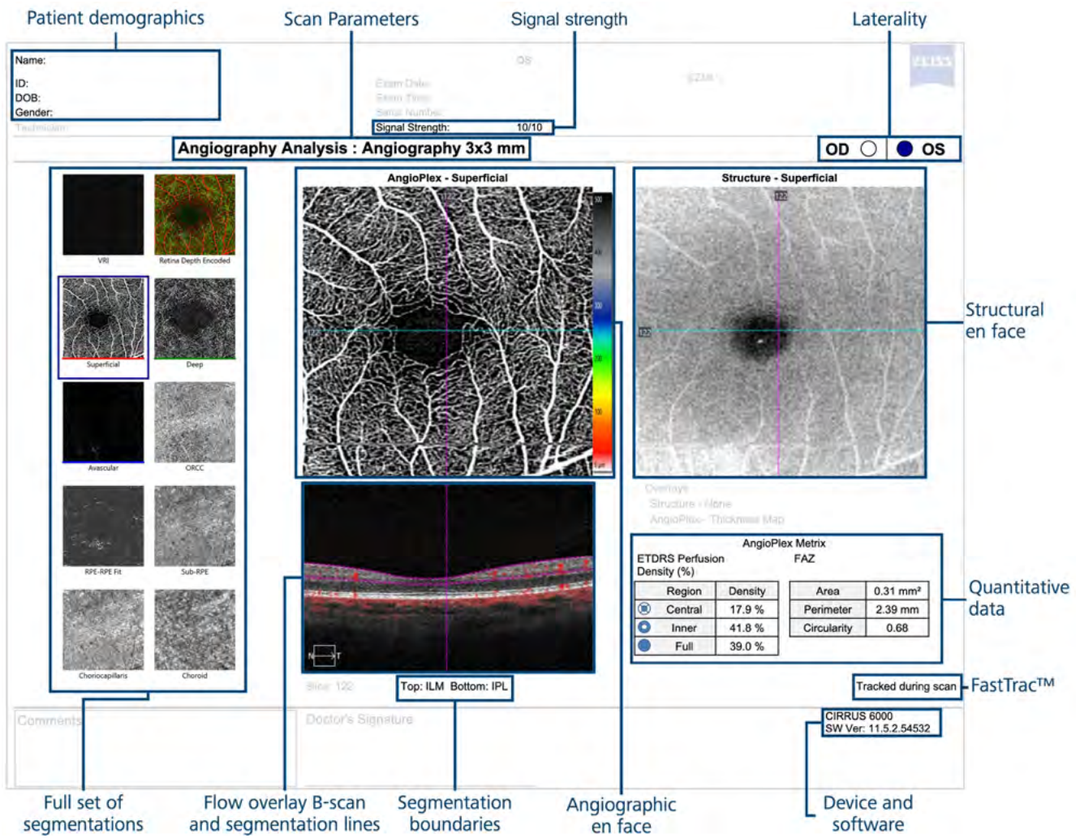

Figure 72: Standard CIRRUS OCT-A report with OS key components highlighted.

To achieve the highest standards of quality and effectiveness, the report should be customized for each case, illustrating and supporting the examiner's conclusions. To this end, the CIRRUS allows customization of the OCT-A report, enabling the personalization of findings and preventing the generation of multiple unnecessary documents. This optimizes data storage and reduces printing costs.

The report's presentation format can be customized to emphasize specific structures or findings, showcasing distinct angiographic maps, vascular network enhancements, color-coded maps, ETDRS grid overlays with corresponding quantitative analysis values, and delineation of the FAZ area. Additionally, it is possible to select the B-scan to be displayed and choose the visualization format, either structural or with flow overlay in one or two colors (Figure 73).

An additional advantage of the CIRRUS is its ability to create and generate a specific report for the structural OCT examination, enabling quantitative analysis via retinal thickness maps as well as qualitative analysis of en face structural images across different segmentations, including the possibility of creating customized segmentations (Figure 74). As described in the previous section, these images play a crucial complementary role in diagnosing various retinal and choroidal diseases and serve as an important supplementary tool in patient care.

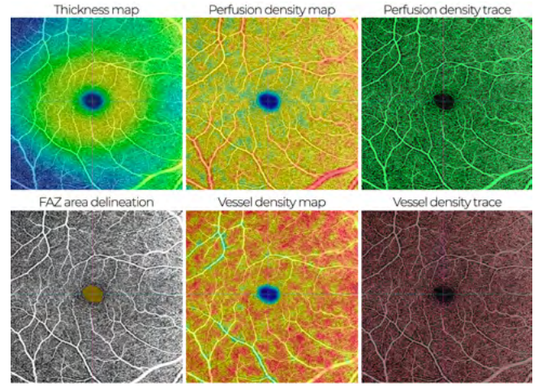

Figure 73: Customizable maps in the CIRRUS OCT-A Report. In addition to these maps, users can overlay the ETDRS grid and display quantitative metrics for each parameter.

The CIRRUS reports for structural OCT en face images follow a format similar to that of the OCT-A reports. Examination details and technical parameters are displayed in the header of the report. The selected en face image appears prominently in the central area, shown at higher magnification, with the corresponding structural B-scan and segmentation boundaries presented directly below. On the right-hand side, the remaining en face analyses are displayed, including any customized segmentations that were generated.

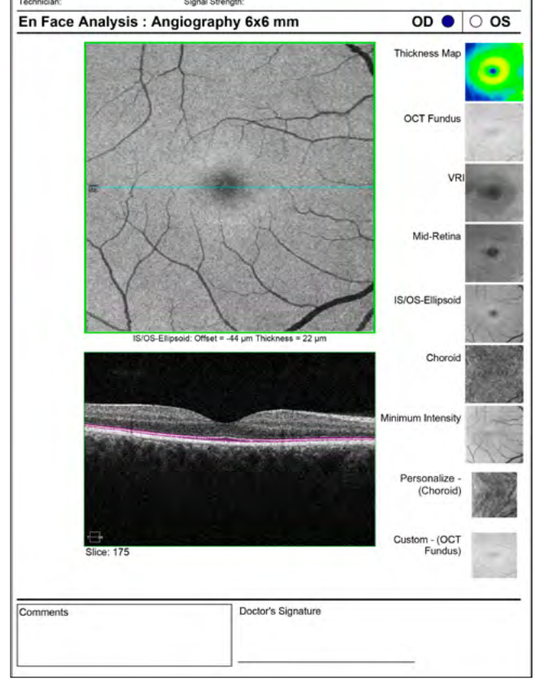

Figure 74: CIRRUS structural OCT en face report.

Section 8

Enhancing sensitivity to OCT-A findings

Despite being highly sensitive and reproducible, a comprehensive evaluation of OCT-A extends beyond a multi-map and multi-parameter approach. Achieving optimal diagnostic accuracy with OCT-A requires meticulous post-processing and integration of multimodal imaging techniques. This process is facilitated by specialized yet user-friendly software tools that enhance image quality, optimize segmentation accuracy, and enable precise quantitative measurements.

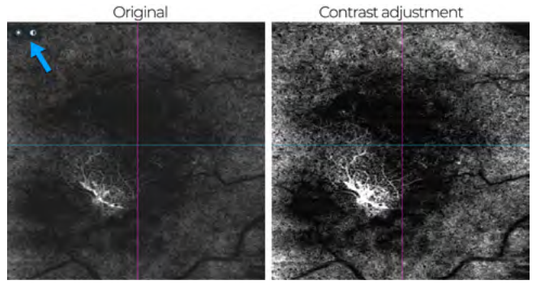

Figure 75: Contrast and brightness adjustment enhancing the identification of vascular abnormalities in a case of Type 1 macular neovascularization. Image adjustment tools are easily accessible—located in the upper left corner when using the FORUM software (blue arrow), or in the upper right corner in the CIRRUS software interface.

8.1. Image processing

To achieve reliable diagnostic outcomes, OCT-A image processing tools play a critical role in refining visualization and ensuring accurate assessments. Image processing features, such as brightness and contrast adjustments, improve the detection of subtle vascular abnormalities (Figure 75), particularly in low-perfusion regions. Additionally, annotation and calibration tools support precise measurement of vascular alterations, further contributing to diagnostic precision. The integration of three-dimensional visualization enhances the ability to identify deep retinal and choroidal vascular structures, an essential aspect of evaluating complex pathologies. Furthermore, navigation and registration tools help standardize scan alignment across multiple visits, minimizing inter-session variability and improving the reliability of follow-up assessments.

In clinical practice, these tools are essential not only for diagnosis but also for monitoring disease progression and guiding treatment decisions regarding indication and safety. For instance, the ability to measure the area of a quiescent macular neovascularization across follow-up visits allows clinicians to assess the lesion's progression and tailor treatment accordingly (Figure 76). Another highly practical application is the use of OCT-A to identify telangiectatic capillaries associated with focal macular edema. Linear measurements from the foveal center to the lesion enable a safe and precise decision regarding focal laser treatment (Figure 77).

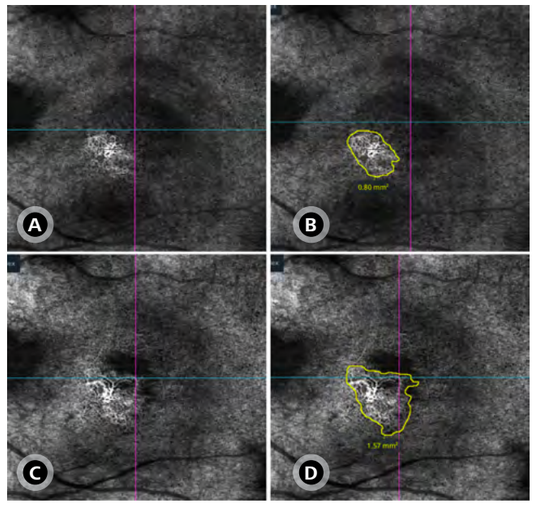

Figure 76: OCT-A area measurement tool from the CIRRUS platform allowing precise quantification of a quiescent Type 1 MNV at different visits (A and B at baseline; C and D at 15 months), confirming lesion growth to nearly double the area observed at the initial visit.

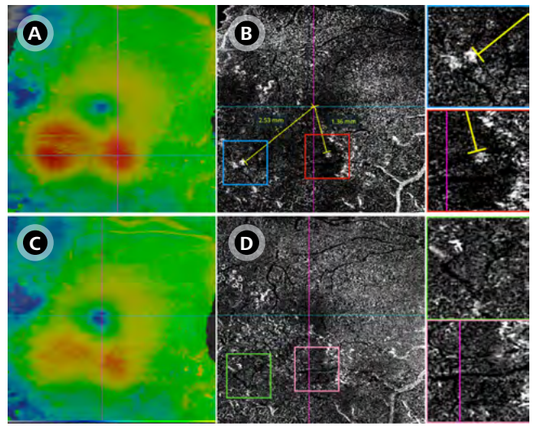

Figure 77: OCT-A linear measurement tool supporting the decision to perform focal laser treatment of a telangiectatic capillary by measuring the distance from the lesion to the foveal center, confirming a safe treatment margin. The examination also enables post-treatment comparison to assess therapeutic response. (A) Retinal thickness map showing two focal areas of edema. (B) Angiographic en face image of the deep retinal layers segmentation identifying two prominent lesions in the edematous region (highlighted in magnified views). (C) Macular thickness map one week after focal laser treatment showing partial resolution of the edema. (D) Angiographic en face image of the deep retinal layers seven days post-treatment demonstrating absence of flow signal at the site of the treated lesions (highlighted in magnified views).

Section 8: Enhancing sensitivity to OCT-A findings

8.2. Refining segmentation

Even with advanced image processing capabilities, the reliability of OCT-A assessments is largely dependent on accurate retinal layer segmentation. Automated segmentation algorithms, while efficient, may introduce errors—especially in eyes with significant pathology such as macular edema or retinal atrophy. In these cases, manual refinement is necessary to ensure the correct anatomical delineation of vascular layers. This is particularly important when distinguishing between the SCP, DCP, outer retina, and choriocapillaris, as segmentation errors can lead to misinterpretation of vascular findings.

Building upon this need for precise segmentation, standard presets provide a useful starting point but often require further customization to improve diagnostic sensitivity, particularly in complex cases. For example, in diabetic retinopathy or MNV, modifying segmentation profiles can significantly enhance the visualization of vascular abnormalities that may be difficult to distinguish using default settings.

A particularly effective refinement strategy for detecting Type 1 MNV involves adjusting the segmentation boundaries of the RPE–RPE fit layer. By setting the anterior segmentation line (top offset) to +29 µm and the posterior segmentation line (bottom offset) to +49 µm, clinicians can reduce projection artifacts that affect the RPE, thereby improving visualization of vascular structures located between the RPE and Bruch's membrane. This adjustment also includes a small portion of the underlying choriocapillaris, which may contain relevant features of the neovascular complex. These segmentation refinements not only enhance diagnostic accuracy but also increase confidence in clinical decision-making (Figure 78).

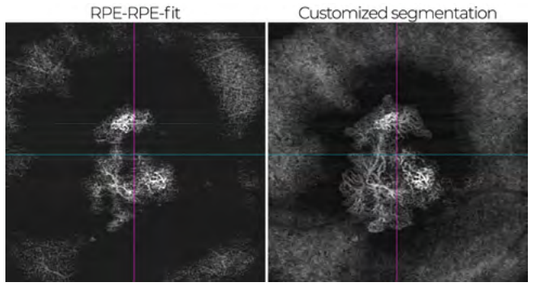

Figure 78: Comparison between standard RPE-RPE fit segmentation and customized segmentation to enhance the evaluation of a Type 1 MNV.

8.3. Multimodal imaging

OCT angiography (OCT-A) achieves its full clinical utility when interpreted alongside complementary imaging modalities. Structural OCT, color fundus photography (CFP), fundus autofluorescence (FAF), fluorescein angiography (FA), and near-infrared reflectance provide additional anatomical, functional, and metabolic context that enhances diagnostic interpretation and therapeutic planning.

The ZEISS FORUM software (Version 4.4) facilitates seamless multimodal integration within the Zeiss Retina Workflow Solutions. Its modern, intuitive interface allows for rapid navigation between imaging modalities through thumbnail previews and enables precise overlay of en face OCT or OCT-A images onto CFP, FAF, or FA (Figure 79). The ability to adjust image transparency and scroll through OCT slabs directly over corresponding clinical images offers powerful spatial correlation between structural and vascular data, supporting more comprehensive retinal evaluation.

This integration proves particularly valuable in several clinical scenarios. For example, FAF can assess retinal pigment epithelium (RPE) metabolism at the site of macular neovascularization (MNV), while FA helps localize leakage in central serous chorioretinopathy (CSC), which can then be correlated with choriocapillaris changes seen on OCT-A. In retinal vein occlusion (RVO), OCT-A can identify ischemic areas, and their comparison with previous laser treatment zones seen on FAF helps guide more precise therapy. Moreover, the combined use of CFP, near-infrared reflectance, and FAF allows clinicians to better delineate regions of interest and resolve ambiguities in OCT-A interpretation.

By leveraging the strengths of multimodal imaging, clinicians gain a deeper understanding of retinal and choroidal pathology, leading to more accurate diagnoses, improved monitoring, and more individualized treatment strategies.

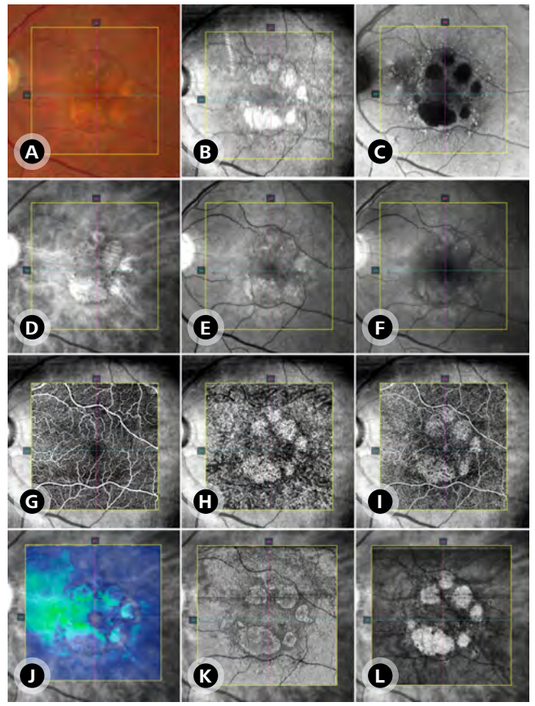

Figure 79: Examples of the various OCT-A en face image integrations with multimodal retinal imaging available through the FORUM software, illustrated in a case of non-neovascular AMD with geographic atrophy. A) True color image. B) Near infrared reflectance. C) Fundus autofluorescence. D) Red light reflectance. E) Green light reflectance. F) Blue light reflectance. G) En face angiographic image – Retina segmentation. H) En face angiographic image – Choroid segmentation. I) En face angiographic image – Whole eye segmentation. J) Retinal thickness map. K) En face structural image – IS/OS-Ellipsoid segmentation. L) En face structural image – Choroid (customized) segmentation.

Section 9

Step-by-step SOP for OCT-A acquisition and analysis

The acquisition and interpretation of high-quality OCT angiography (OCT-A) images require a systematic, standardized approach that integrates technical precision, operator expertise, and rigorous post-processing analysis. This section outlines the essential steps involved in the OCT-A workflow using the CIRRUS OCT platform, encompassing preparation, image acquisition, quality assessment, and interpretation.

Each phase includes detailed recommendations to optimize scan reliability, reduce artifacts, and ensure accurate correlation between structural and vascular findings. Emphasis is placed on proper patient preparation, equipment calibration, scan protocol selection, motion tracking, and segmentation validation, as well as on the integration of both qualitative and quantitative data for robust clinical interpretation. This structured methodology promotes reproducibility, improves diagnostic confidence, and supports effective longitudinal monitoring in both clinical and research settings. A flowchart summarizing the Step-by-Step SOP for OCT-A Acquisition and Analysis is provided in Figure 80.

9.1. Preparation

In preparation for high-quality OCT-A image acquisition using the CIRRUS OCT, it is essential to ensure that both the operator and equipment meet the highest standards of performance and accuracy. All operators must undergo comprehensive training in the use of OCT/OCT-A technology and image analysis. Additionally, they should have prior experience in diagnosing ocular diseases or be exclusively engaged in research settings to guarantee precise and reliable image acquisition.

The equipment and examination environment require meticulous verification before initiating any imaging procedure. Regular safety inspections must be conducted to maintain the integrity and accuracy of the system. All components, including lenses and accessories, should be examined for damage, and the instructional manual must be readily available. Proper cleaning protocols should be followed to prevent coating degradation of optical components. Furthermore, adequate lighting and ventilation must be ensured within the examination room to minimize external interference that could compromise image quality.

Patient identification and data verification are critical steps in preventing errors. Before proceeding with the scan, the operator must confirm that the correct patient record has been selected.

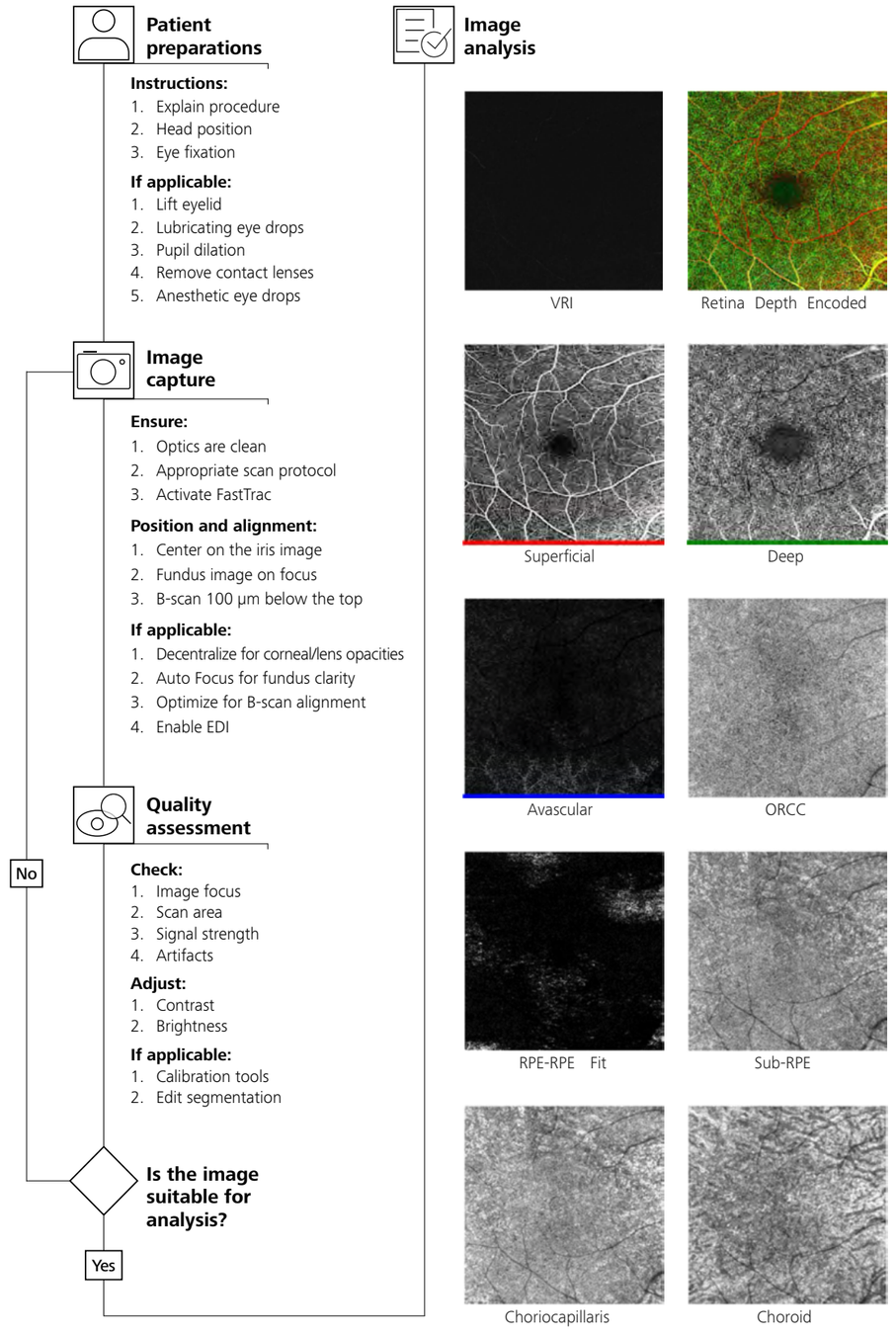

Figure 80: Flowchart of the Step-by-Step SOP for OCT-A Acquisition and Analysis

Section 9: Step-by-step SOP for OCT-A acquisition and analysis

Proper patient preparation is paramount to achieving optimal scan quality. Although pupil dilation is not mandatory, a minimum pupil size of 2 mm is recommended. If dilation is performed for the initial scan, it should be consistently maintained in follow-up examinations to ensure comparability. The CIRRUS OCT system automatically corrects for refractive error; however, manual adjustments may be required in certain cases to optimize image clarity. Patients wearing contact lenses should be instructed to remove them before the procedure to prevent artifacts. Clear communication is essential, and the operator must explain the procedure thoroughly, emphasizing the importance of maintaining a stable head position and steady fixation throughout the scan. If necessary, the upper eyelid should be gently elevated to prevent obstruction of the imaging field. Additionally, lubricating eye drops may be administered to enhance patient comfort and minimize excessive blinking, which can contribute to motion artifacts. In cases where blinking remains problematic despite lubrication, the use of mild topical anesthetics may be considered to further reduce involuntary eye movements, ensuring optimal scan stability and image quality.

9.2. Acquisition

During the image acquisition phase of OCT-A using the CIRRUS OCT system, meticulous attention must be given to scan configuration, patient positioning, image optimization, and acquisition protocols to ensure high-quality results. The selection of the appropriate scan protocol should align with the clinical objective. Available scan sizes include 3×3 mm, 6×6 mm, HD 6×6 mm, 8×8 mm, HD 8×8 mm, and 12×12 mm. For broader retinal evaluations, extended field scans using montage techniques should be employed, as they provide a more comprehensive view without compromising resolution.

Proper patient positioning is essential for achieving accurate and repeatable imaging. The patient must be correctly seated with their chin and forehead resting against the support to ensure stability. The iris image should be aligned appropriately to facilitate optimal scan acquisition. In cases of corneal or crystalline lens opacities, slight adjustments should be made by focusing slightly off-center from the pupil to enhance image clarity. The system's automatic brightness and contrast adjustments should be leveraged to optimize visualization of the fundus and ensure even illumination across the scan area.

Ocular tracking and stabilization play a crucial role in minimizing motion artifacts. Activating FastTrac, the automatic eye-tracking system, helps to maintain scan alignment and reduce distortions caused by involuntary eye movements. Once FastTrac is enabled, manual adjustments should be avoided, as they may interfere with tracking precision. If modifications are necessary, FastTrac must be temporarily deactivated, adjustments should be made, and then the tracking function should be reactivated.

In addition to motion stabilization, optimizing image depth is essential for accurately assessing deeper retinal and choroidal structures. To achieve this, the EDI mode should be utilized in cases requiring evaluation of structures posterior to the RPE, such as in AMD and CSC.

Image focus and adjustment are key components of high-quality OCT-A acquisition. The Auto Focus function should be utilized to bring the fundus into sharp focus, while Auto Fine Focus further refines the alignment and enhances the sharpness of B-scans. The B-scan should be accurately positioned within the image window, maintaining a placement approximately 100 µm below the top of the scan window to ensure a standardized and reproducible acquisition.

During the image capture process, the patient should be instructed to blink before the scan begins and to keep their eyes open throughout the procedure to minimize blinking artifacts. Environmental factors must also be considered to avoid potential interference; aerosols or liquids should not be used or placed near the device to prevent contamination or imaging distortions. Once all parameters are optimized, the operator should initiate the scan by selecting the Capture function, ensuring that all acquisition settings are properly executed for optimal imaging results.

Section 9: Step-by-step SOP for OCT-A acquisition and analysis

9.3. Analysis: Quality assessment

Following OCT-A image acquisition, a rigorous post-capture review and optimization process is essential to ensure diagnostic accuracy and image quality. The initial quality assessment involves verifying that the fixation target is correctly centered on the pupil, as improper alignment may introduce artifacts and compromise scan reliability. The signal strength should be assessed, with a minimum threshold of ≥6 to ensure sufficient image clarity and diagnostic utility. Additionally, the overall image should be examined for uniform illumination and the clear visualization of blood vessels, as uneven lighting or shadowing can obscure fine vascular details.

Artifact identification and minimization are crucial steps in enhancing image reliability. Motion artifacts, often caused by saccadic eye movements during scanning, should be detected and corrected through realignment when necessary. Segmentation artifacts, which may arise due to automated layer misclassification in B-scans, must be manually reviewed and adjusted to prevent inaccuracies in vascular layer interpretation. Projection artifacts, which can cause superficial retinal vessels to appear as ghost images in deeper layers, should be differentiated from true vascular structures by comparing en face images with corresponding structural B-scans.

Image optimization techniques further refine visualization and measurement accuracy. Adjusting contrast and brightness enhances the visualization of microvascular structures, particularly in regions with low perfusion. Calibration tools should be employed for precise measurement of vascular alterations, ensuring consistency in quantitative analysis.

Segmentation and image quality verification are critical for ensuring that vascular signals are correctly attributed to their respective anatomical layers. Any segmentation errors should be reviewed and manually corrected to maintain the integrity of layer-specific vascular assessments. The presence or absence of flow within the layers of interest should be verified to confirm accurate perfusion mapping. Additionally, the retinal position within the scan must be evaluated to ensure it is not too low, as incorrect positioning may lead to contrast loss and suboptimal image interpretation.

9.4. Analysis: Interpretation and report

The analysis of OCT-A data and the generation of diagnostic reports require a structured approach that integrates both qualitative and quantitative assessments. A qualitative review involves examining the vascular patterns of each en face segmentation map, from the innermost layer (VRI) to the outermost (choroid), identifying deviations from the normal pattern. Additionally, the flow overlay analysis on B-scans should be qualitatively assessed to detect subtle vascular alterations that may not be apparent in individual segmentation maps.

Building upon the qualitative evaluation, the integration of objective metrics enhances the precision of the analysis. The AngioPlex Metrix system provides quantitative parameters, including vessel density, perfusion density, and FAZ metrics. These parameters should be systematically assessed to detect deviations from normative values and to facilitate disease monitoring over time.

To ensure meaningful longitudinal comparisons, sequential scans must be accurately aligned. Proper alignment is crucial for detecting subtle vascular changes over time, preventing misinterpretations due to patient positioning variations or segmentation shifts. In this context, angiographic difference maps serve as valuable tools for identifying capillary alterations, such as vessel loss, remodeling, or reperfusion, which may indicate disease progression or treatment response.

Given the complexity of vascular pathologies, a multimodal imaging approach should be implemented whenever possible. By integrating multiple imaging modalities, clinicians can obtain a more comprehensive understanding of both vascular and structural abnormalities, reducing the likelihood of misinterpretation inherent to OCT-A findings alone. This approach enhances diagnostic confidence and refines clinical decision-making.

Once the imaging analysis is complete, the final step is the generation of standardized reports to ensure consistency in the interpretation and communication of findings. Reports should include relevant details regarding image acquisition (e.g., pupil dilation, patient cooperation, and any challenges encountered during the examination), examination methodology (e.g., scan protocol, use of FastTrac, EDI), and reliability criteria (e.g., image quality and artifacts). The findings section should present both qualitative observations and quantitative metrics, ensuring a comprehensive assessment.

To further support clinical decision-making, the report should conclude with a summary of key pathological findings and clinical impressions. Additionally, any limitations in the ability to interpret the examination—such as motion artifacts, segmentation errors, or optical interference—should be explicitly documented to provide context regarding the reliability of the results.

Section 10

Flowchart for rapid OCT-A interpretation

Ensuring that the examination adheres to best practices and meets all reliability criteria is fundamental for accurate interpretation. To streamline the analysis process and enhance efficiency, it is essential to establish a structured approach based on key diagnostic questions. By following a logical flow of inquiry, clinicians can optimize their assessments, improve diagnostic accuracy, and save time.

A foundational aspect of this approach is recognizing that vascular alterations can occur at three distinct anatomical planes: (1) Preretinal, as seen in proliferative retinopathies; (2) Intraretinal, which involves retinal circulation abnormalities; and (3) Subretinal, associated with choroidal circulation disorders. Additionally, conditions such as Type 3 MNV may involve direct communication between the retinal and choroidal circulations. Figure 81 presents a schematic flowchart for rapid OCT-A interpretation.

Building upon this anatomical framework, the OCT-A analysis should begin by addressing four fundamental questions before proceeding to a detailed case-specific evaluation:

1. Is there proliferative retinopathy (i.e., vessels on the retinal surface/ONH extending toward the vitreous cavity)?
2. Are there abnormalities in the retinal circulation?
3. Are there abnormalities in the choroidal circulation?
4. Is there communication between the retinal and choroidal circulations?

These guiding questions help clinicians establish a logical diagnostic framework, facilitating the differentiation of underlying pathologies and directing the analysis toward the most relevant imaging features.

OCT-A quick interpretation flowchart

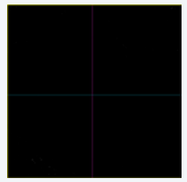

Step 1
Check VRI map for proliferative retinopathy (vessels on the retinal surface/ONH extending toward the vitreous cavity).

Step 2
Check depth encoded and retina maps for abnormalities in the retinal circulation. If there are no abnormalities, skip Step 3.

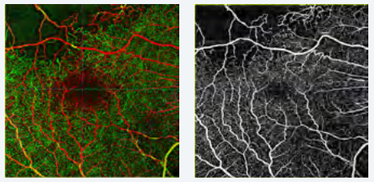

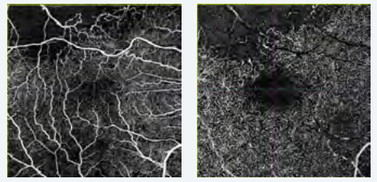

Step 3
Check superficial and deep maps to identify the topographic location of the lesion

Step 4
Check avascular map for abnormalities (it should be marked black)

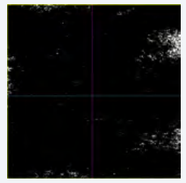

Step 5
Check RPE-RPE fit map for abnormalities (they should be marked black).

Step 6
Check ORCC, Sub-RPE and Choriocapillaris maps for similarity (they should be similar).

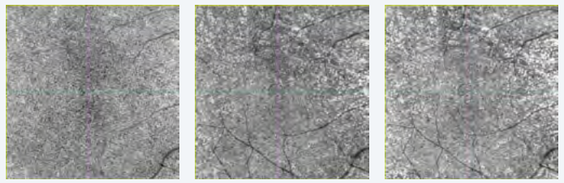

Step 7
Check for quantitative analysis, if available.

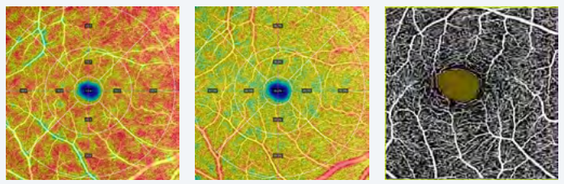

Section 10: Flowchart for rapid OCT-A interpretation

To accurately distinguish these vascular alterations, different en face angiographic maps serve specific diagnostic purposes:

- Preretinal proliferations, extending toward the vitreous, are best visualized in the VRI map.
- Intraretinal vascular alterations appear in the Superficial, Deep, Depth-Encoded, and Retina maps.
- Choroidal circulation abnormalities are identified using the RPE-RPE fit, Sub-RPE, ORCC, Choriocapillaris, and Choroid maps.
- The avascular segmentation provides a key reference point for differentiating abnormalities originating from either the retinal or choroidal circulation, serving as a marker for a comprehensive layer-by-layer assessment.

To ensure an intuitive and time-efficient interpretation, the following optimized workflow is proposed for OCT-A analysis:

1. **Is the VRI map abnormal?**
   - **Yes** ⟶ Check the B-scan to differentiate artifacts from true proliferative changes.
   - **No** ⟶ NO PROLIFERATIVE RETINOPATHY. Proceed to the next step.
2. **Is the Depth-Encoded map normal?**
   - **Yes** ⟶ Skip to the RPE-RPE fit map.
   - **No** ⟶ Examine the Superficial, Deep, and Avascular layers separately to determine the nature of the abnormality.
3. **Is the avascular zone normal?**
   - **Yes** ⟶ Consider normal findings.
   - **No** ⟶ Check segmentation accuracy, exclude artifacts, and proceed with a detailed choroidal circulation analysis (NEXT STEPS).
4. **Is the RPE-RPE fit map entirely black?**
   - **Yes** ⟶ Consider normal findings.
   - **No** ⟶ Check the B-scan for projection artifacts and consider a Type 1 MNV.
5. **Are the ORCC, Sub-RPE, and Choriocapillaris maps similar?**
   - **Yes** ⟶ Consider normal findings.
   - **No** ⟶ Evaluate each map individually for distinct abnormalities.
6. **Perform quantitative analyses and follow-up assessments, if available.**

By following this structured workflow, clinicians can minimize interpretation variability, reduce time spent on OCT-A evaluation, and improve diagnostic precision. The combination of qualitative assessments and targeted quantitative analyses ensures a systematic and reproducible approach to OCT-A interpretation.

Section 11

Training checklists

Pre-capture: Patient and equipment preparation	Yes	No
1. Is the equipment clean and free of artifacts?		
2. Is the environment adequate, e.g., low lighting, no direct airflow?		
3. Has the patient's data been confirmed?		
4. Was pupil dilation assessed and performed if necessary?		
5. Did the patient remove contact lenses?		
6. Did the patient receive clear instructions about the exam?		
7. Was eyelid positioning adjusted to avoid obstructions?		
8. Were lubricating eye drops used if necessary?		

Capture: OCT-A image acquisition	Yes	No
9. Was the scanning protocol selected according to the clinical objective?		
10. Is the patient correctly positioned on the chin and forehead support?		
11. Was iris alignment adjusted for proper focus?		
12. Was decentralization performed in case of corneal or lens opacities?		
13. Were brightness and contrast properly adjusted?		
14. Was ocular tracking (FastTrac) activated?		
15. Was EDI activated when necessary?		
16. Were Auto Focus and Auto Fine Focus used for clarity?		
17. Was the B-scan positioning correctly adjusted (100 µm below the top)?		
18. Did the patient blink before capture to prevent dry eye?		
19. Was the image captured without interference?		

Post-capture: Image review and optimization	Yes	No
20. Is the fixation target correctly centered?		
21. Is the signal strength ≥ 6?		
22. Is the illumination uniform and are the blood vessels visible?		
23. Were motion artifacts reviewed and realigned when necessary?		
24. Was segmentation reviewed and corrected if necessary?		
25. Were projection artifacts evaluated and differentiated from real findings?		
26. Were contrast and brightness adjusted to optimize visualization?		
27. Were calibration tools used for precise vascular measurements?		
28. Was EDI applied for better choroid analysis when necessary?		
29. Were vascular signals correctly assigned to corresponding anatomical layers?		
30. Is the retina not too low in the image, preventing contrast loss?		

Section 12

Case studies and practical examples

12.1. Diabetic Macular Edema

Sex/Age: Male, 52yo

- True-color imaging **(A)** reveals microaneurysms and exudates in the macular region, which are better visualized in the red-free image **(B)**.
- The retinal thickness map **(C)** highlights areas of increased macular thickness, indicated in red.
- The en face mid-retinal segmentation **(D)** clearly demonstrates regions of fluid accumulation (hyporeflective areas), exudates (marked hyperreflective spots), and microaneurysms (hyperreflective borders with hyporeflective centers). OCT-A images, captured using the AngioPlex HD 6x6 mm scan, illustrate irregularities in the FAZ and diffuse structural alterations in capillaries, particularly evident in retina segmentation **(E)** and depth-encoded segmentation **(F)**.
- The latter enables simultaneous analysis of superficial retinal layer **(SRL, G)** and deep retinal layer **(DRL, H)** segmentations.

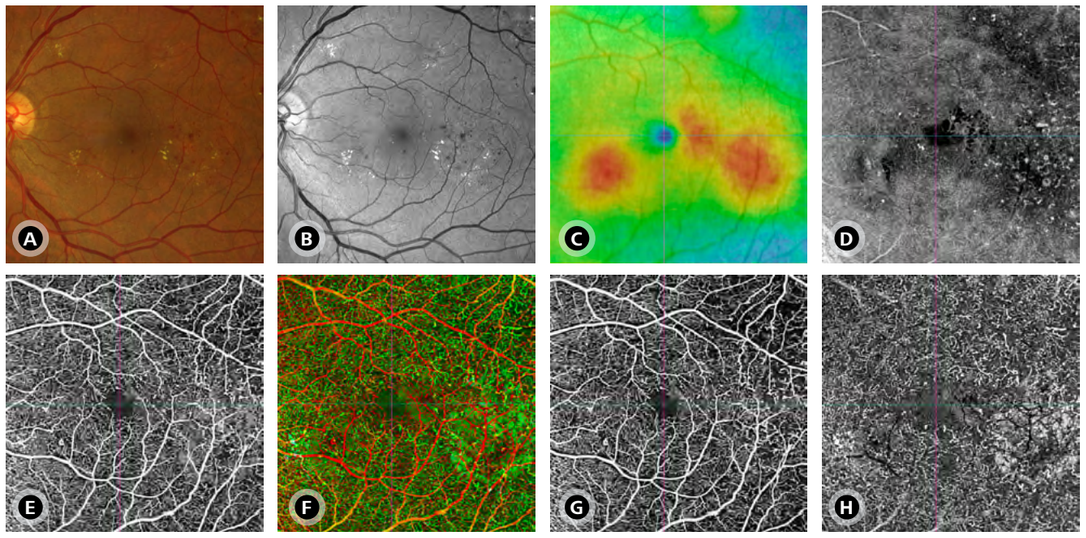

12.2. Diabetic Retinopathy – FAZ Abnormality

Sex/Age: Male, 42yo

Clinical and OCT angiographic characteristics of focal ischemic maculopathy in a patient with diabetic retinopathy.

- **A)** True-color image and **B)** Green-light reflectance (green channel)
- **C)** AngioPlex HD 8x8 mm scan with retina segmentation demonstrating microvascular changes in the midperiphery and irregularity in the FAZ.
- **D)** AngioPlex 3x3 mm scan (quantitative FAZ analysis) highlights the FAZ area in yellow, clearly illustrating the loss of circularity (0.47 in this case) due to focal ischemia in the inferonasal quadrant.
- **E–F)** Quantitative analysis from AngioPlex 6x6 mm scans showing vessel density **(E)** and perfusion density maps **(F)**, emphasizing the reduction of perfusion in the temporal region.

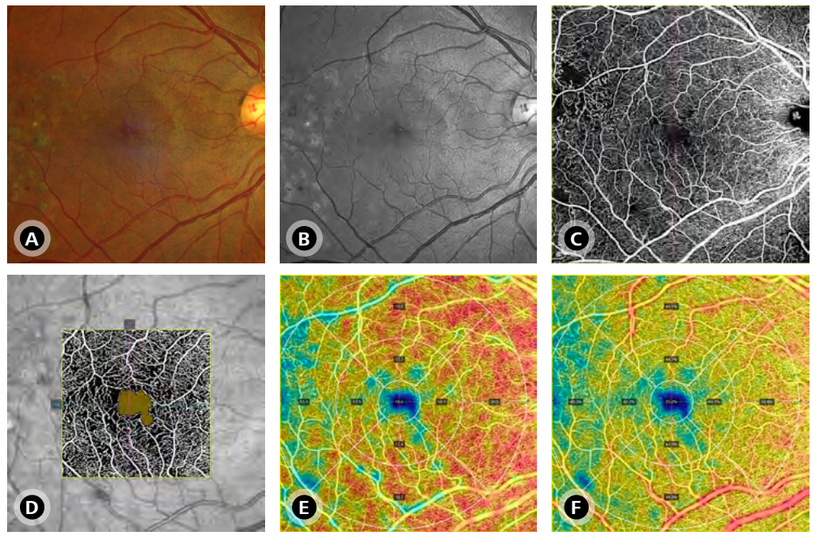

Section 12: Case studies and practical examples

12.3. Diabetic Ischemic Maculopathy – Deep Capillary Plexus Ischemia

Sex/Age: Male, 52yo

- **A)** True-color image and **B)** Green-light reflectance (red-free)
- **C)** OCT B-scan (100x HD, 12 mm line) revealing irregularities in the deeper layers of the inner retina at the levels of intermediate and deep capillary plexuses.
- **D-G)** AngioPlex HD 6x6 mm en face angiographic map and B-scan (with flow overlay and segmentation boundaries) of retina segmentation **(D)**, depth-encoded **(E)**, superficial retinal layer **(SRL, F)**, and deep retinal layer **(DRL, G)**. Predominant involvement of the deep capillary plexus is evident in depth-encoded images **(E)** and DRL analysis **(G)**.

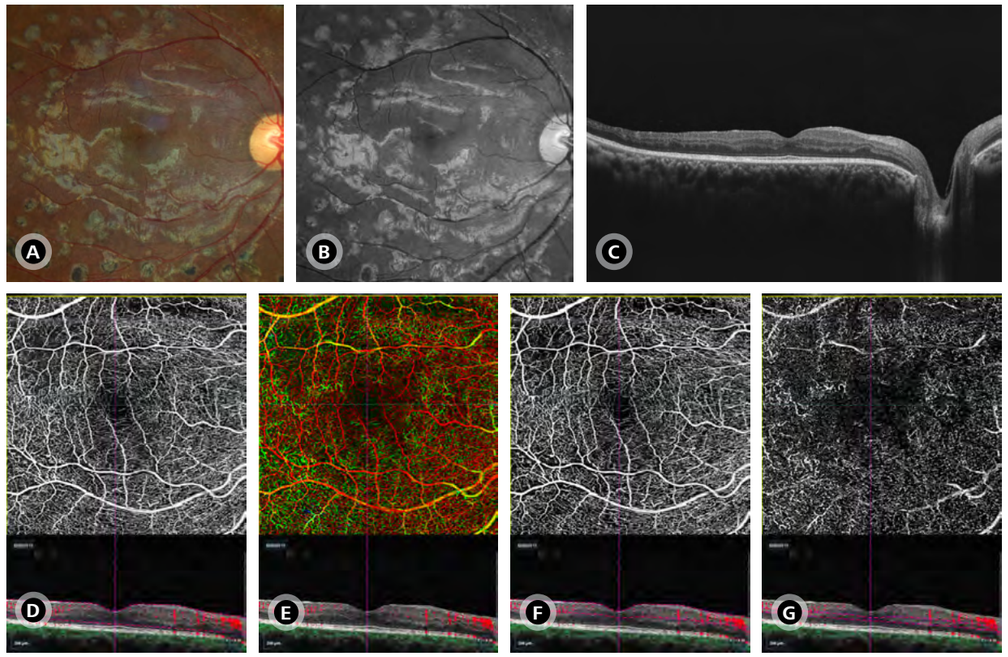

12.4. Refractory Proliferative Diabetic Retinopathy

Sex/Age: Male, 42yo

- **A)** True-color image and **B)** Green-light reflectance (red-free).
- **C)** AngioPlex 12x12 mm scan (retina segmentation) demonstrates a suspected area of neovascularization.
- **D)** AngioPlex 12x12 mm scan (VRI segmentation) provides en face angiographic and structural views, alongside a B-scan with segmentation lines highlighting the examined region and clearly showing macular neovascularization.
- **E-G)** Images depict the neovascularization in greater detail via red-free imaging **(E)**, en face angiographic retina segmentation **(F)**, and VRI segmentation **(G)**.

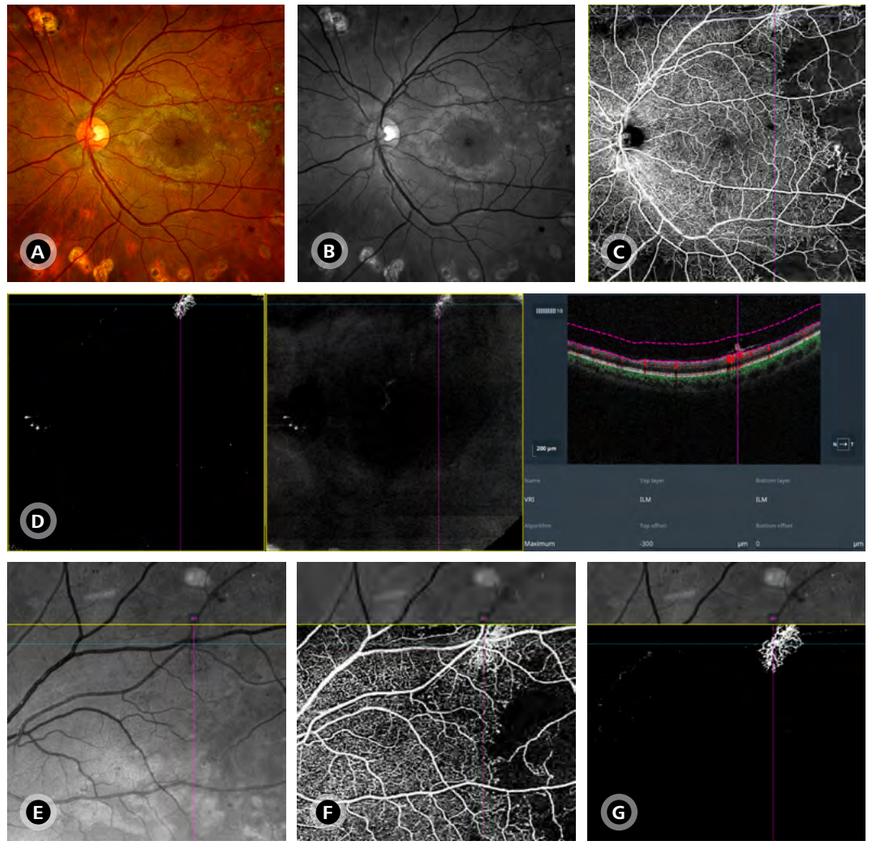

Section 12: Case studies and practical examples

12.5. Advanced Proliferative Diabetic Retinopathy

Sex/Age: Female, 32yo

- **A)** Wide-field true-color image showing tractional retinal detachment in the mid-periphery, associated with extensive fibrovascular proliferation involving the posterior pole, best visualized in the higher-magnification color image **(B)** and in the red-free green-light reflectance image **(C)**.
- **D-F)** AngioPlex 12x12 mm scans in depth-encoded **(D)**, retina **(E)**, and VRI **(F)** segmentations. Neovascular vessels appear prominently in the depth-encoded map, predominantly in red, and are visible as anomalous vessels in the retina segmentation. The VRI segmentation highlights vessels elevated above the retinal plane in both the structural en face map and the B-scan with segmentation lines.

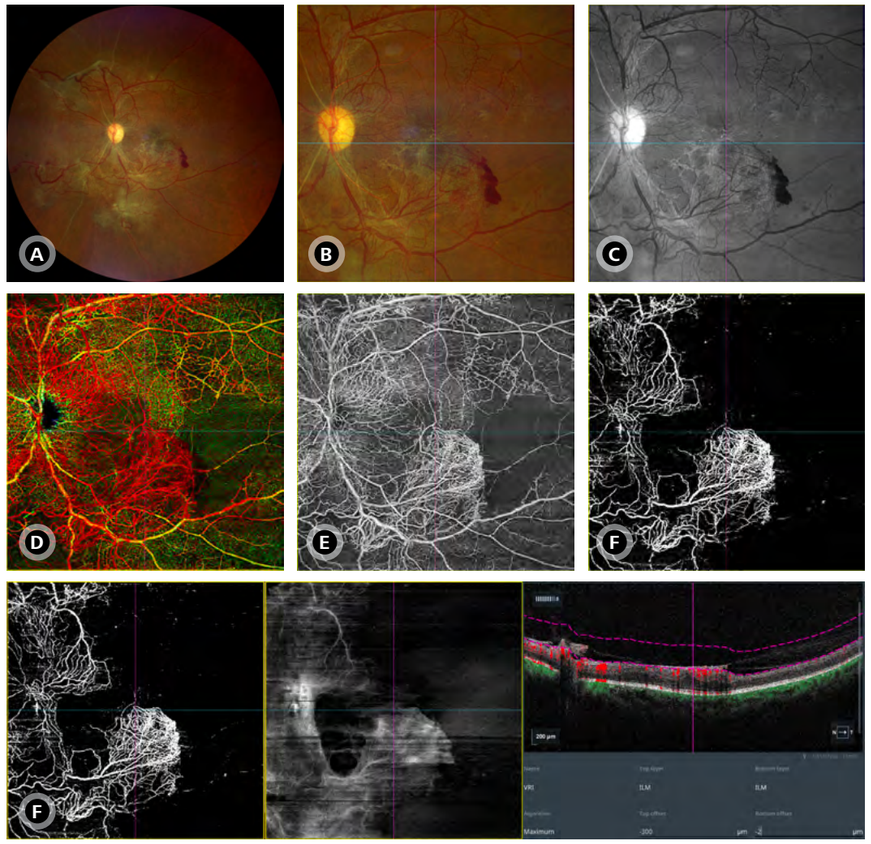

12.6. Non-ischemic Branch Retinal Vein Occlusion

Sex/Age: Female, 69yo

- Fundus image **(A)** illustrating an inferotemporal non-ischemic BRVO involving the inferior temporal arcade.
- Follow-up appearance 6 months after the occlusive event **(B)**. En face angiographic images demonstrate the macular involvement in this inferotemporal BRVO case. AngioPlex HD 6x6 mm scans highlight vascular abnormalities in the inferior hemisphere vessels of the macula, without significant flow voids in either the superficial **(C)** or deep capillary plexus **(D)**. The depth-encoded image **(E)** shows reduced green coloration in the affected area, indicating greater involvement of the deep plexus.

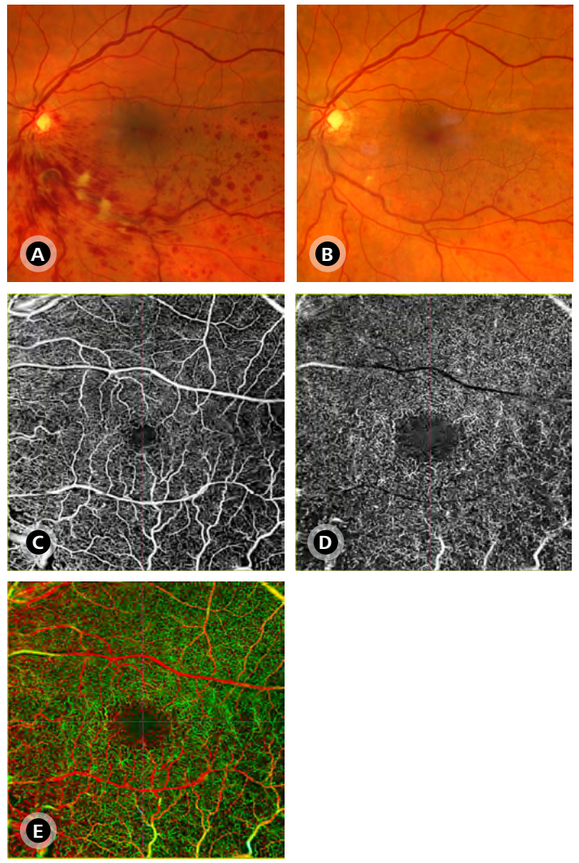

Section 12: Case studies and practical examples

12.7. Ischemic Branch Retinal Vein Occlusion

Sex/Age: Male, 63yo
A case of superior temporal ischemic BRVO associated with vitreous hemorrhage.

- **A)** Fundus photograph showing intraretinal hemorrhages in the affected area and the presence of vitreous opacities.
- **B)** Wide-field FA highlighting areas of nonperfusion in the affected region.
- **C–D)** AngioPlex 12x12 mm scans using retina and depth-encoded segmentations, respectively, reveal flow voids in the superficial and deep capillary plexuses within the affected area.
- **E–H)** AngioPlex HD 6x6 mm scans with retina, depth-encoded, SRL, and DRL segmentations (respectively) provide detailed visualization of macular involvement and demonstrate preservation of the foveal and parafoveal regions. These findings assist in safely determining the posterior boundary for laser photocoagulation **(I)**.
- **J)** Fundus autofluorescence imaging performed one month post-laser treatment shows hyperautofluorescent spots over the treated area.

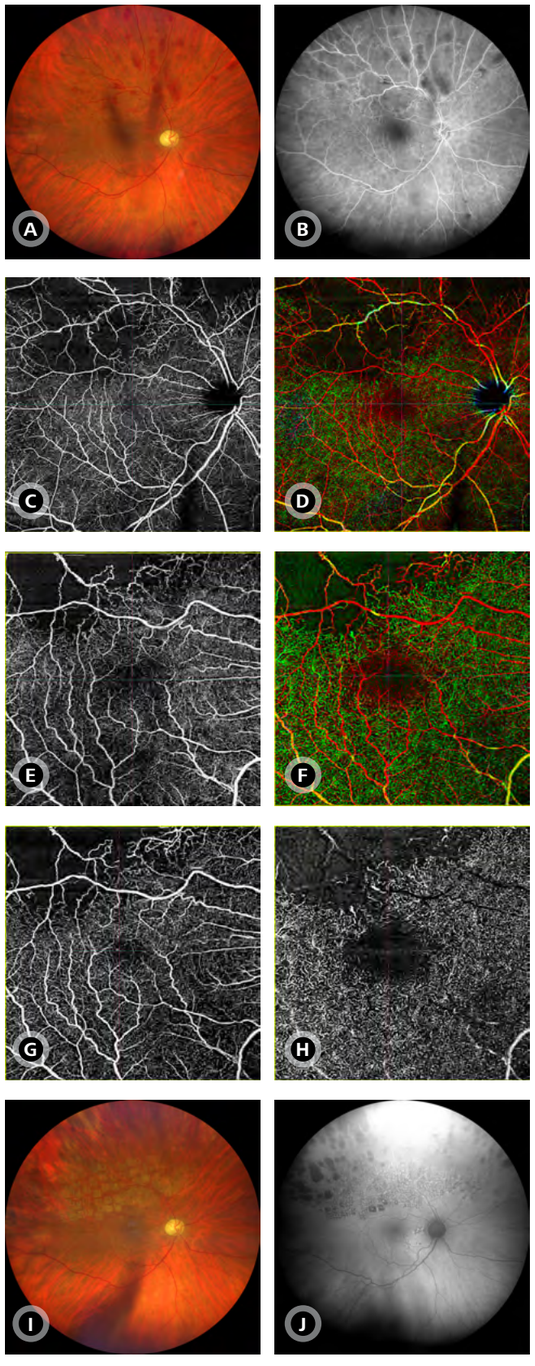

12.8. Non-ischemic Central Retinal Vein Occlusion

Sex/Age: Male, 62yo

- **A)** True-color fundus image obtained during the acute phase of CRVO, showing intraretinal hemorrhages, cotton-wool spots, and optic disc edema in all four quadrants.
- **B)** Macular OCT (B-scan 100x HD) reveals macular edema with both intraretinal and subretinal fluid.
- **C–E)** AngioPlex HD 6x6 mm scans paired with structural B-scans and segmentation boundaries for the retina, superficial retinal layer (SRL), and deep retinal layer (DRL), respectively. Retinal perfusion is preserved, although small areas of flow void are observed in the retina segmentation. This image provides the most clinically relevant information for this case, as segmentation artifacts are present in the SRL and DRL layers due to anatomical distortion from macular edema. These artifacts particularly affect the visualization of the deep plexus in the SRL image and may falsely suggest absence of flow in the DRL segmentation.

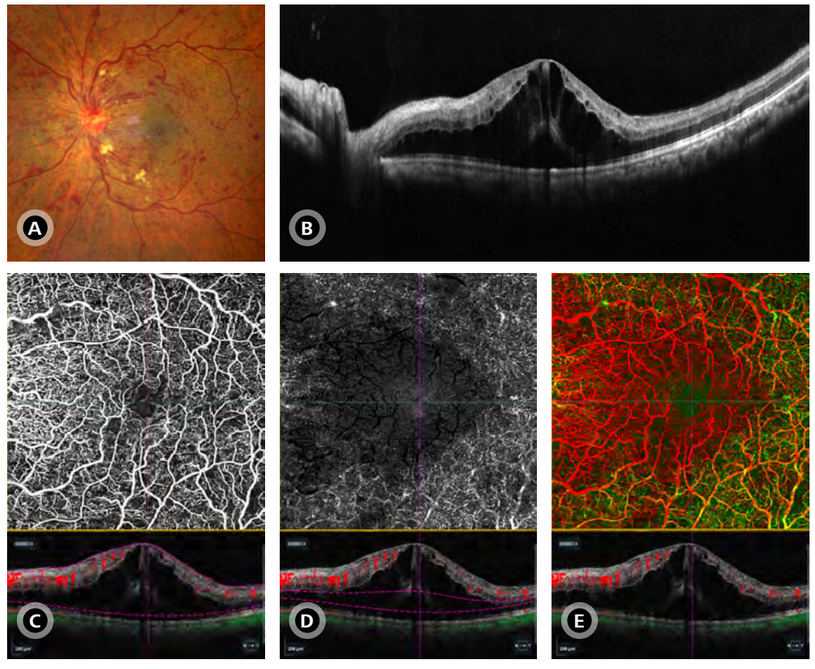

Section 12: Case studies and practical examples

12.9. AMD – Drusen

Sex/Age: Male, 74yo

- **A)** True-color image showing multiple soft drusen in the macular region, better visualized in the red-free image **(B)**.
- **C)** Mid-phase fluorescein angiography demonstrates hyperfluorescence of the drusen.
- FAF green imaging reveals a target-like pattern for most drusen, with a hypoautofluorescent center and a hyperautofluorescent border, corresponding to an epithelial defect at the center of the drusen. This appears as hyperreflective lesions in the en face structural image using customized choroidal segmentation **(E)**. OCT-A images acquired with the AngioPlex HD 6x6 mm scan show multiple projection artifacts in the RPE-RPE fit map, overlying the drusen topography. These artifacts are evident in the corresponding en face structural image with RPE-RPE fit segmentation **(G)**, which shows the projection areas as hyporeflective, and in the en face angiographic image with sub-RPE segmentation **(H)**, which highlights the absence of flow in these regions. Using a customized segmentation **(I)**, it is also possible to identify a quiescent Type 1 MNV at the edge of the inferonasal quadrant, near the optic disc. This finding is confirmed by the combined analysis of angiographic and structural en face maps.

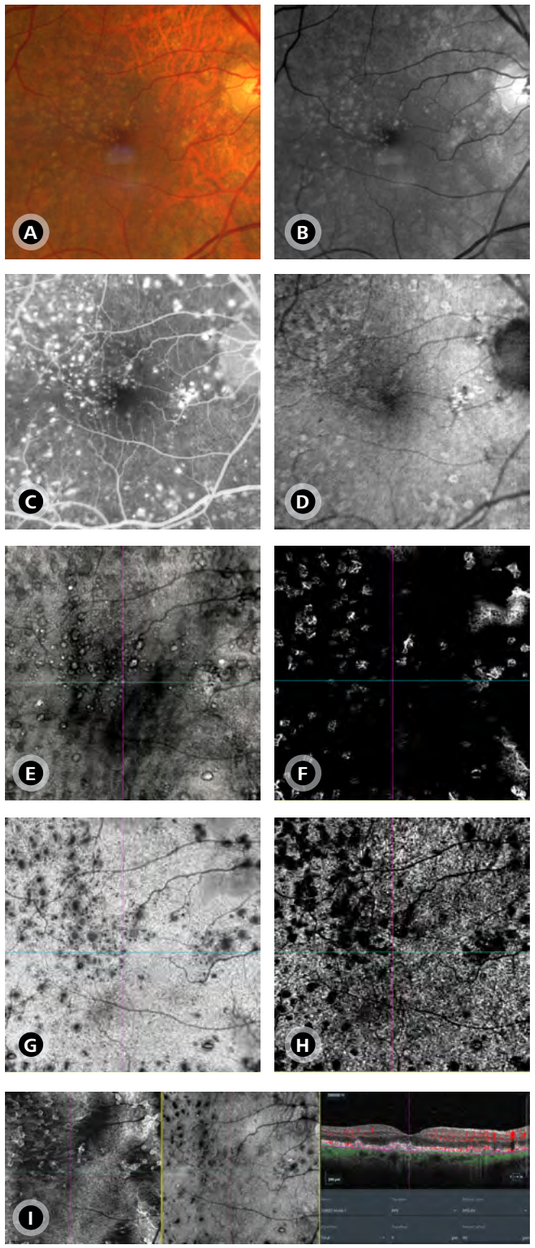

12.10. AMD – GA

Sex/Age: Female, 69yo

- True-color image **(A)** showing multiple confluent soft drusen and pigment mobilization surrounding an extensive area of geographic atrophy.
- FAF green image **(B)** demonstrates a large hypoautofluorescent area corresponding to the region of geographic atrophy. The mottled pattern of hyper- and hypoautofluorescence surrounding the atrophic zone reflects the various evolutionary stages of soft drusen.
- En face structural imaging **(C)** with customized choroidal segmentation allows identification of the atrophic area as hyperreflective. The absence of the RPE in the region of geographic atrophy produces an unmasking effect, leading OCT-A images acquired with the AngioPlex HD 6x6 mm scan to reveal posterior structures with enhanced reflectivity. This is evident in the whole eye segmentation **(D)** and becomes even clearer when comparing the normal retina segmentation **(E)** with the choroid segmentation **(F)**, which shows deeper choroidal vessels with greater intensity in areas lacking RPE.
- In this case, analysis of the RPE-RPE fit segmentation **(G)**, which contains multiple projection artifacts, and the sub-RPE segmentation **(H)** confirms the absence of macular neovascularization.

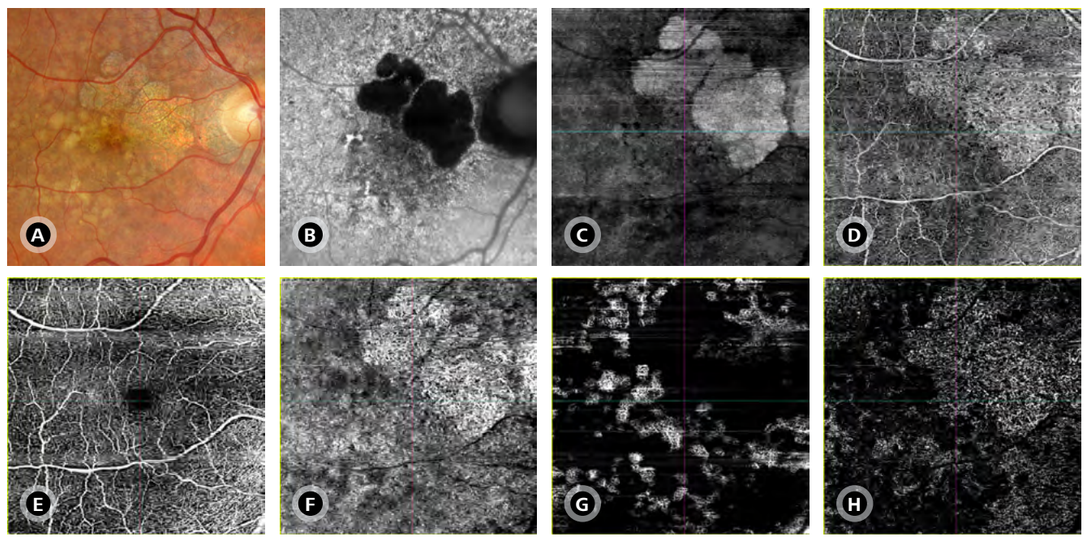

Section 12: Case studies and practical examples

12.11. AMD – Type 1 MNV + Quiescent

Sex/Age: Male, 79yo

- **A)** True-color image showing no significant findings in the posterior pole or macular region. However, OCT-A imaging performed with the AngioPlex HD 6x6 mm scan **(B–E)** clearly reveals a quiescent Type 1 MNV.
- The ORCC **(B)**, RPE-RPE fit **(C)**, and sub-RPE **(D)** maps show subtle signs suggestive of neovascularization. When customizing the RPE-RPE fit segmentation with a top offset of +29 and a bottom offset of +49 **(E)**, the neovascular complex becomes clearly and richly detailed.

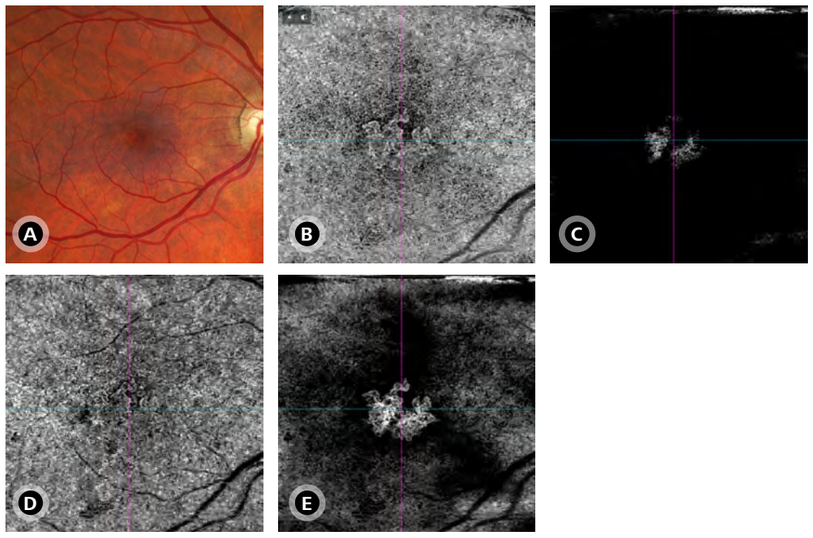

12.12. AMD - Type 1 MNV + Fluid

Sex/Age: Male, 81yo

- **A)** True-color image reveals pigment mobilization and a few drusen in the macular region.
- **B)** FAF green image shows a mottled pattern of hyper- and hypoautofluorescence in the macula, with a hyperautofluorescent area extending inferiorly due to gravitational effect.
- **C)** Structural OCT B-scan demonstrates subretinal fluid and fibrovascular PED. The spatial distribution of subretinal fluid is better visualized in the en face images using IS/OS-ellipsoid **(D)** and minimum intensity **(E)** segmentations.
- **F)** Customized RPE-RPE fit segmentation on OCT-A performed with the AngioPlex HD 6x6 mm scan enables precise identification and excellent characterization of the macular neovascularization.

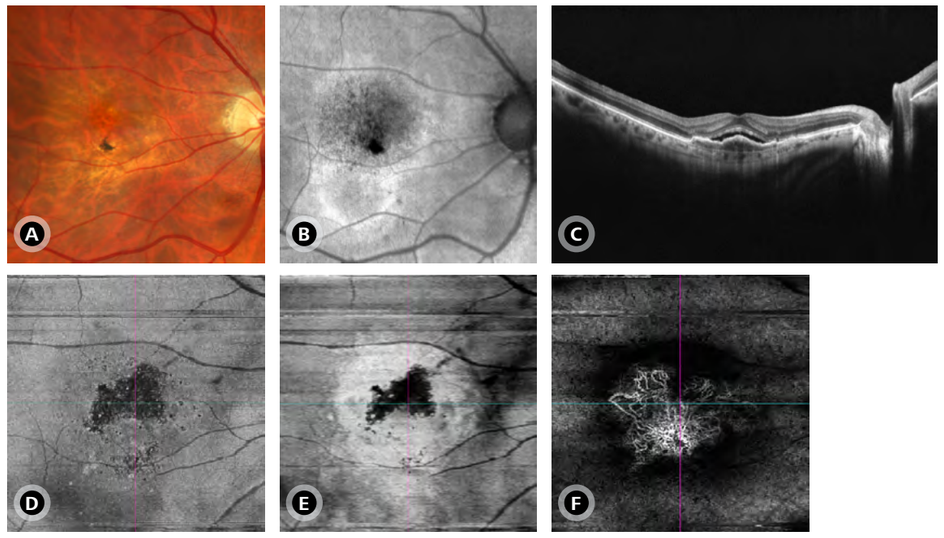

Section 12: Case studies and practical examples

12.13. AMD – Macular Neovascularization and RPE Tear

Sex/Age: Female, 78yo

- **A)** True-color image showing subtle drusen in the macular region, along with an area of RPE loss in the inferior portion of the macula resulting from an RPE tear.
- **B)** FAF green image reveals marked hypoautofluorescence corresponding to the tear.
- **C)** OCT B-scan shows fibrovascular PED with a small amount of subretinal fluid.
- **D)** The extent of subretinal fluid is better appreciated in the en face structural image with IS/OS-ellipsoid segmentation, where it appears as a hyporeflective area.
- **E-F)** En face images with OCT fundus **(E)** and choroid **(F)** segmentations highlight the RPE-deficient area as hyperreflective.
- **G-I)** OCT-A images acquired with an AngioPlex 12x12 mm scan encompass the entire lesion, allowing for structural analysis of the full neovascular complex via RPE-RPE fit segmentation **(G)** and visualization of the unmasking effect caused by RPE loss at the tear site using the sub-RPE **(H)** and whole eye **(I)** segmentations.

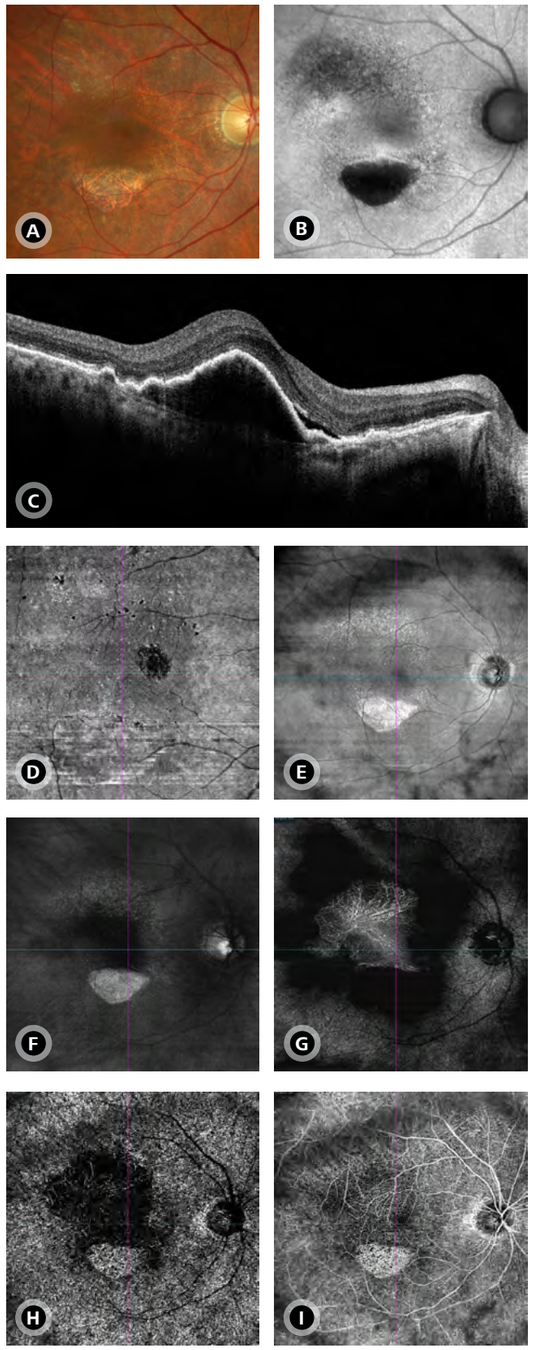

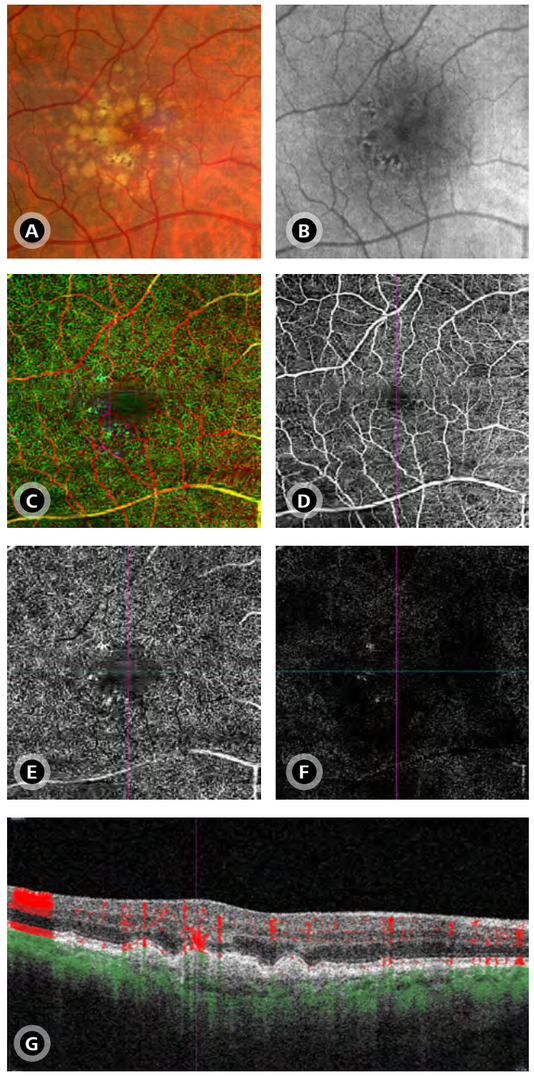

12.14. AMD – Type 3 MNV

Sex/Age: Male, 74yo

- **A)** True-color image reveals multiple confluent soft drusen associated with pigment mobilization.
- **B)** FAF green image displays a mottled pattern of hyper- and hypoautofluorescence.
- **C-G)** OCT-A images, acquired with the AngioPlex HD 6x6 mm scan, demonstrate the presence of Type 3 MNV, easily identified in the depth-encoded map **(C)** as cooler-colored areas (blue).
- **D-F)** Segmented analysis of the superficial plexus **(D)**, deep plexus **(E)**, and avascular zone **(F)** confirms the lesion, with the latter showing flow signals in this case.
- **G)** Flow overlay on the B-scan clearly demonstrates communication between the retinal and choroidal circulation, a hallmark of this neovascularization type, with retinal flow highlighted in red and choroidal flow in green.

Section 12: Case studies and practical examples

12.15. Polypoidal Choroidal Vasculopathy

Sex/Age: Male, 85yo

- **A)** True-color image reveals aneurysm-like lesions in the macular region, not contiguous with the retinal circulation, accompanied by mild adjacent exudation.
- **B)** The en face map with IS/OS-ellipsoid segmentation shows subretinal fluid in the affected area, visualized as a hyporeflective region.
- **C–E)** OCT-A images obtained using the AngioPlex HD 6x6 mm scan demonstrate macular neovascularization.
- **C)** Whole eye segmentation reveals an anomalous vascular structure in the macular area.
- **D)** ORCC segmentation provides enhanced visualization of the larger neovascular vessels.
- **E)** Customized RPE-RPE fit segmentation offers an excellent view of the full extent of the neovascular complex, including detailed morphology of the polypoidal lesions.

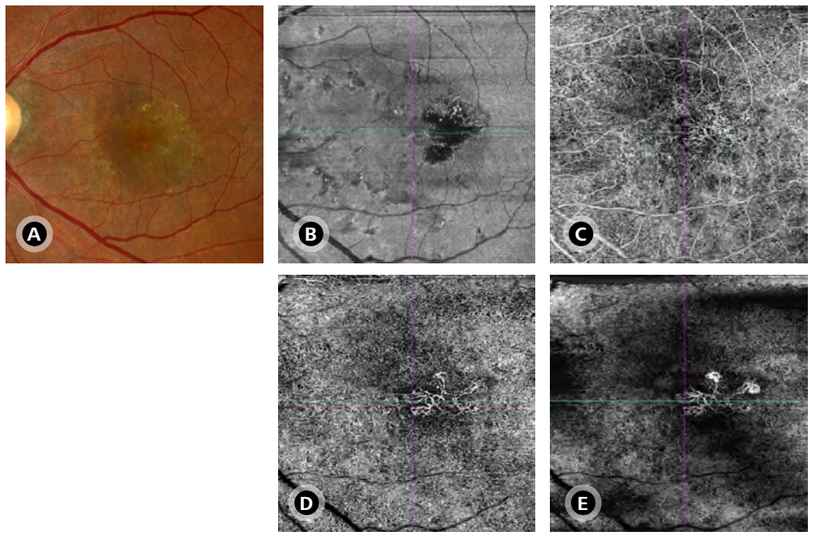

12.16. MacTel Type 1

Sex/Age: Male, 79yo

A patient with a presumed diagnosis of MacTel Type 1, with a history of exudation and anti-VEGF therapy.

- **A)** True-color image and **B)** red-free image show vascular abnormalities in the foveal avascular zone.
- **C–F)** OCT-A performed with the AngioPlex HD 6x6 mm scan reveals detailed vascular alterations and a flow void area on the depth-encoded **(C)**, SRL **(D)**, and DRL **(E)** maps. The avascular map **(F)** appears normal.

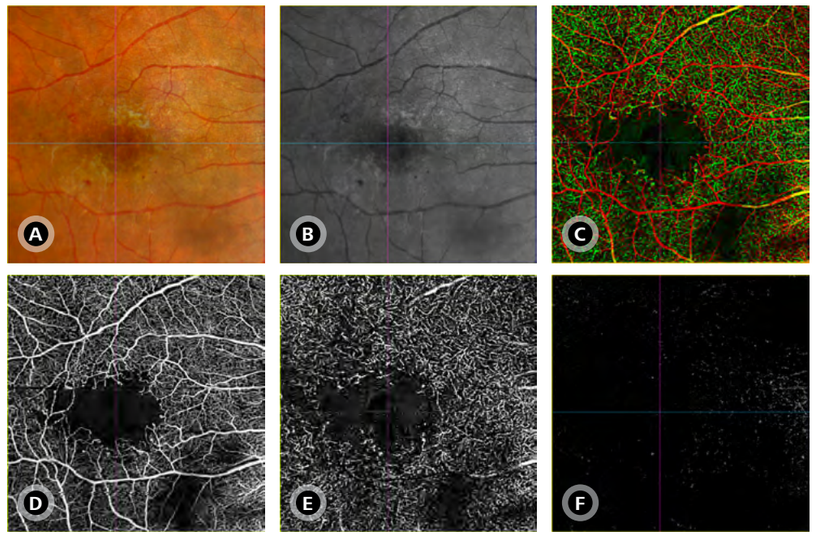

Section 12: Case studies and practical examples

12.17. MacTel Type 2

Sex/Age: Female, 54yo

- **A)** True-color image shows a pale area temporal to the fovea with pigment mobilization.
- B) Green-light reflectance (red-free) highlights vascular changes in the temporal region of the FAZ.
- **C)** Blue-light reflectance reveals a hyperreflective area in the temporal fovea, corresponding to the location of vascular abnormalities.
- **D–G)** AngioPlex HD 6x6 mm scans highlight vascular alterations and deep layer involvement.
- **D)** Depth-encoded map displays cooler colors in the affected region.
- **E–G)** SRL **(E)**, DRL **(F)**, and avascular **(G)** maps further illustrate these changes, with the avascular map notably showing vascular structures in a region that should be vessel-free.

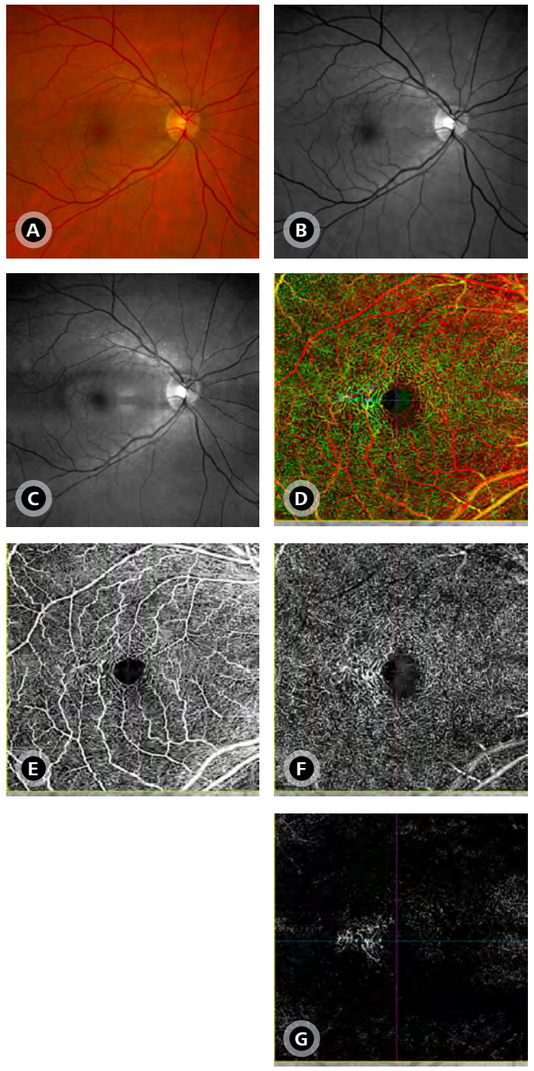

12.18. Central Serous Chorioretinopathy

Sex/Age: Male, 41yo

- **A)** True-color image shows a subtle pigmentary change in the inferotemporal quadrant of the macula.
- **B)** FAF green image highlights this area as hyperautofluorescent, corresponding to residual subretinal fluid. Additionally, focal hypoautofluorescent lesions are observed along the papillomacular bundle, marking the leakage site from a previous CSC episode.
- **C–I)** AngioPlex HD 6x6 mm OCT-A images reveal segmentation artifacts, evident in the depth-encoded map **(C)** as cooler tones in areas of residual subretinal fluid.
- **D–F)** ORCC **(D)**, choriocapillaris **(E)**, and sub-RPE **(F)** maps should ideally appear similar but instead show darker regions suggestive of choriocapillaris hypoperfusion, especially at the leakage point. The RPE-RPE fit map shows a projection artifact over this area, consistent with the location of the serous RPE detachment.
- **H–I)** Choroid **(H)** and whole eye **(I)** segmentations confirm decreased perfusion in this region.

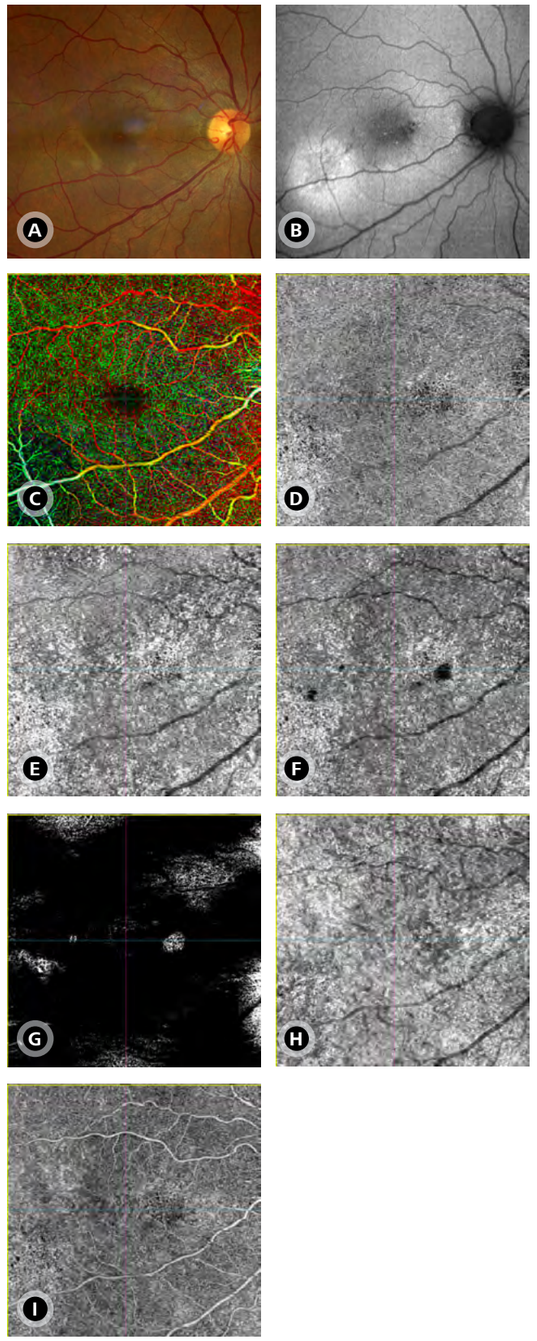

Section 12: Case studies and practical examples

12.19. Sickle Cell Ischemic Maculopathy

Sex/Age: Female, 15yo

- **A)** True-color image shows subtle, darker areas of discoloration in the temporal retina near the horizontal raphe.
- **B)** Blue-light reflectance highlights these areas as hyporeflective, with no corresponding abnormalities on mid-phase fluorescein angiography **(C)**.
- **D–F)** AngioPlex HD 8x8 mm OCT-A images clearly reveal a flow void in the corresponding region.
- **D)** Depth-encoded map shows this most prominently, with milder changes in the SRL **(E)** and more pronounced flow loss in the DRL **(F)**.

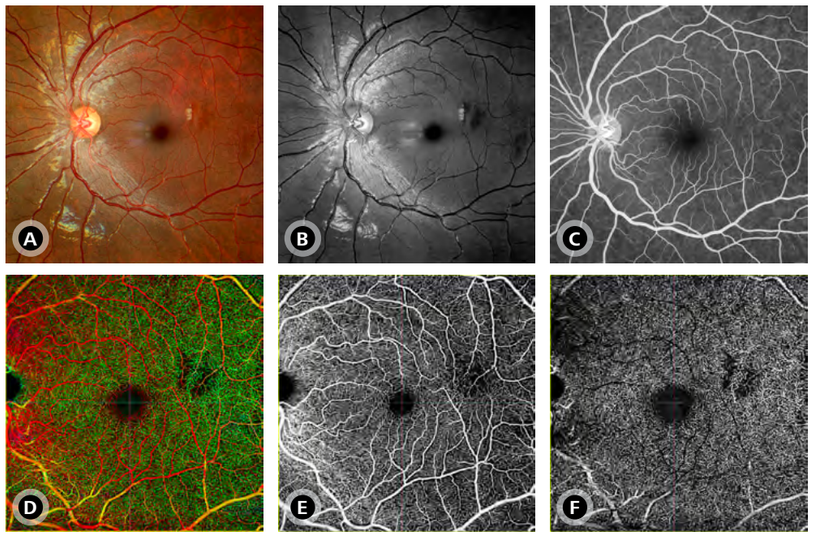

12.20. Foveal Hypoplasia

Sex/Age: Female, 33yo

- **A)** True-color and **B)** near-infrared reflectance images appear normal in the macular region.
- **C)** Structural OCT B-scan shows persistence of inner retinal layers in the foveal area.
- **D–F)** AngioPlex HD 6x6 mm OCT-A images demonstrate persistence of inner retinal vessels at the fovea, visible in the retina **(D)** and SRL **(E)** maps, while the DRL **(F)** map shows an apparently normal configuration of the deep capillary plexus.

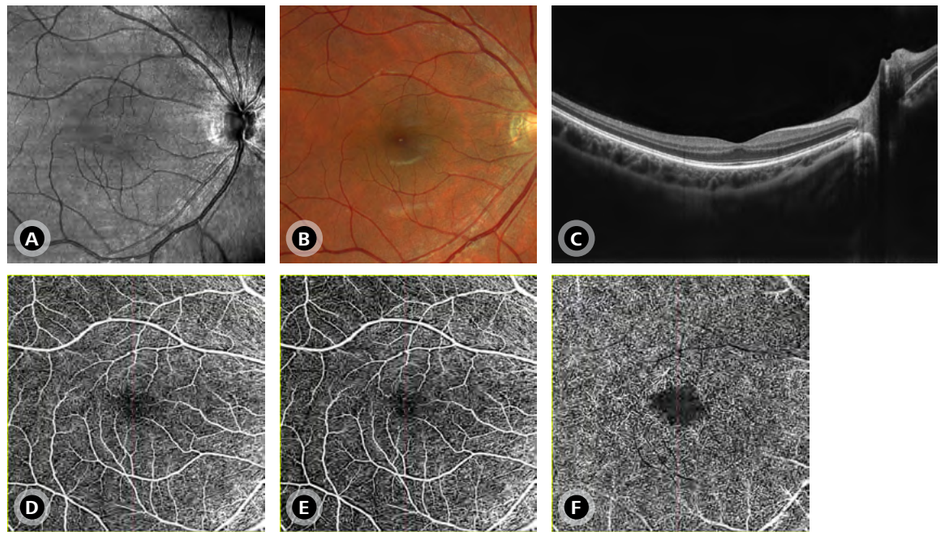

12.21. References

Alibhai A, Moult E, Shahzad R, Rebhun C, Moreira-Neto C, McGowan M, et al. Quantifying microvascular changes using OCT angiography in diabetic eyes without clinical evidence of retinopathy. *Ophthalmol Retina*. 2017;2(5):418–27. https://doi.org/10.1016/j.oret.2017.09.011

Arrigo A, Aragona E, Battaglia Parodi M, Bandello F. Quantitative approaches in multimodal fundus imaging: state of the art and future perspectives. *Prog Retin Eye Res*. 2023;92:101111.

Arya M, Rebhun CB, Cole ED, Sabrosa AS, Arcos-Villegas G, Louzada RN, et al. Visualization of choroidal neovascularization using two commercially available spectral domain optical coherence tomography angiography devices. *Retina*. 2019;39(9):1682–92. https://doi.org/10.1097/IAE.0000000000002241

Bicas L, Penha FM, Paques M, Leitão Guerra RL. Branch retinal vein occlusion. In: Chhablani J, editor. Retinal and choroidal vascular diseases of the eye. 1st ed. Burlington (MA): Academic Press; 2024. p. 179–98.

Borrelli E, Sarraf D, Freund KB, Sadda SR. OCT angiography and evaluation of the choroid and choroidal vascular disorders. *Prog Retin Eye Res*. 2018;64:1–55.

Chua J, Tan B, Wong D, Garhöfer G, Liew XW, Popa-Cherecheanu A, et al. Optical coherence tomography angiography of the retina and choroid in systemic diseases. *Prog Retin Eye Res*. 2024;103:101292. https://doi.org/10.1016/j.preteyeres.2024.101292

Coscas F, Sellam A, Glacet-Bernard A, Jung C, Goudot M, Miere A, et al. Normative data for vascular density in superficial and deep capillary plexuses of healthy adults assessed by optical coherence tomography angiography. *Invest Ophthalmol Vis Sci*. 2016;57(9):OCT211–23. https://doi.org/10.1167/iovs.15-18793

Guo J, She X, Liu X, Sun X. Repeatability and reproducibility of foveal avascular zone area measurements using AngioPlex spectral domain optical coherence tomography angiography in healthy subjects. *Ophthalmologica*. 2017;237:21–8. https://doi.org/10.1159/000453112

Hsu S, Ngo H, Stinnett S, Cheung N, House R, Kelly M, et al. Assessment of macular microvasculature in healthy eyes of infants and children using OCT angiography. *Ophthalmology*. 2019. https://doi.org/10.1016/J.OPHTHA.2019.06.028

Laíns I, Wang JC, Cui Y, Katz R, Vingopoulos F, Staurenghi G, et al. Retinal applications of swept source optical coherence tomography (OCT) and optical coherence tomography angiography (OCTA). *Prog Retin Eye Res*. 2021;84:100951. https://doi.org/10.1016/j.preteyeres.2021.100951

Lafeta M, Huemer JC, Novais EA, Leitão Guerra RL. Optical coherence tomography angiography in diabetic macular edema. In: Diabetic macular edema. 1st ed. Singapore: Springer; 2022. p. 37–47. https://doi.org/10.1007/978-981-19-7307-9

Leitão Guerra R, Barbosa GCS, Leitão Guerra C, Badaro E, Roisman L, Lucatto LF, et al. Blue light reflectance imaging in non-perfusion areas detection: insights from multimodal analysis. *Int J Retina Vitreous*. 2024;10(1):84. https://doi.org/10.1186/s40942-024-00602-z

Leitão Guerra RL, Leitão Guerra CL, Bastos MG, de Oliveira AHP, Salles C. Sickle cell retinopathy: what we now understand using optical coherence tomography angiography. A systematic review. *Blood Rev*. 2019;35:32–42. https://doi.org/10.1016/j.blre.2019.03.001

Leitão Guerra RL, Leitão Guerra CL, Meirelles MGB, Barbosa GCS, Novais EA, Badaró E, et al. Exploring retinal conditions through blue light reflectance imaging. *Prog Retin Eye Res*. 2025;105:101326. https://doi.org/10.1016/j.preteyeres.2024.101326

Linderman R, Salmon A, Strampe M, Russillo M, Khan J, Carroll J. Assessing the accuracy of foveal avascular zone measurements using optical coherence tomography angiography: segmentation and scaling. *Transl Vis Sci Technol*. 2017;6. https://doi.org/10.1167/tvst.6.3.16

Louzada RN, de Carlo TE, Adhi M, Novais EA, Durbin MK, Cole E, et al. Optical coherence tomography angiography artifacts in retinal pigment epithelial detachment. *Can J Ophthalmol*. 2017;52(4):419–24. https://doi.org/10.1016/j.jcjo.2016.12.012

Moein HR, Novais EA, Rebhun CB, Cole ED, Louzada RN, Witkin AJ, et al. Optical coherence tomography angiography to detect macular capillary ischemia in patients with inner retinal changes after resolved diabetic macular edema. *Retina*. 2018;38(12):2277–84. https://doi.org/10.1097/IAE.0000000000001902

Novais EA, Roisman L, de Oliveira PR, Louzada RN, Cole ED, Lane M, et al. Optical coherence tomography angiography of chorioretinal diseases. *Ophthalmic Surg Lasers Imaging Retina*. 2016;47(9):848–61. https://doi.org/10.3928/23258160-20160901-09

Novais EA, Waheed NK. Optical coherence tomography angiography of retinal vein occlusion. *Dev Ophthalmol*. 2016;56:132–8. https://doi.org/10.1159/000442805

Rio JA, Barbosa GCS, Guerra RLL. Long-term follow-up in macular telangiectasia type 1: clinical image. *Oman J Ophthalmol*. 2024;17(1):137–9. https://doi.org/10.4103/ojo.ojo_205_22

Roisman L, Goldhardt R. OCT angiography: an upcoming non-invasive tool for diagnosis of age-related macular degeneration. *Curr Ophthalmol Rep*. 2017;5(2):136–40. https://doi.org/10.1007/s40135-017-0131-6

Roisman L, Rosenfeld PJ. Optical coherence tomography angiography of macular telangiectasia type 2. *Dev Ophthalmol*. 2016;56:146–58. https://doi.org/10.1159/000442807

Roisman L, Zhang Q, Wang RK, Gregori G, Zhang A, Chen CL, et al. Optical coherence tomography angiography of asymptomatic neovascularization in intermediate age-related macular degeneration. *Ophthalmology*. 2016;123(6):1309–19. https://doi.org/10.1016/j.ophtha.2016.01.044

Spaide RF, Fujimoto JG, Waheed NK, Sadda SR, Staurenghi G. Optical coherence tomography angiography. *Prog Retin Eye Res*. 2018;64:1–55. https://doi.org/10.1016/j.preteyeres.2017.11.003

Waheed NK, Rosen RB, Jia Y, Munk MR, Huang D, Fawzi A, Chong V, Nguyen QD, Sepah Y, Pearce E. Optical coherence tomography angiography in diabetic retinopathy. *Prog Retin Eye Res*. 2023 Nov;97:101206. doi: 10.1016/j.preteyeres.2023.101206. Epub 2023 Jul 26. PMID: 37499857; PMCID: PMC11268430.

Yannuzzi NA, Gregori NZ, Roisman L, Gupta N, Goldhagen BE, Goldhardt R. Fluorescein angiography versus optical coherence tomography angiography in macular telangiectasia type I treated with bevacizumab therapy. *Ophthalmic Surg Lasers Imaging Retina*. 2017;48(3):263–6. https://doi.org/10.3928/23258160-20170301-12

Zhang Q, Zhang A, Lee CS, Lee AY, Rezaei KA, Roisman L, et al. Projection artifact removal improves visualization and quantitation of macular neovascularization imaged by optical coherence tomography angiography. *Ophthalmol Retina*. 2017;1(2):124–36. https://doi.org/10.1016/j.oret.2016.08.005

Dr. Ricardo Luz Leitao Guerra is an accomplished ophthalmologist specializing in surgical retina and cataract surgery. With over 50 scientific publications, his research has focused on advancing retinal imaging, including blue-light reflectance, fundus autofluorescence, and OCT technologies.

Drawing on his dual expertise as a clinician and researcher, Dr. Guerra is dedicated to applying optical principles to everyday practice and developing strategies that improve patient care. His insights directly shape the practical, step-by-step, approach presented in this guide, helping clinicians worldwide adopt OCT-A with confidence and clarity.

This book was authored by Ricardo Luz Leitão Guerra, MD, MSc, FICO, in collaboration with ZEISS, with the goal of providing ophthalmologists with a simplified, practice -oriented guide to OCT-A. We want to extend our gratitude to Dr. Guerra and colleagues and peers whose clinical experience continues to inspire progress in the field.

en-OUS_31_010_0145II CZ X/2025 International edition: Only for sale in selected countries.
The contents of the brochure may differ from the current status of approval of the product or service offering in your country. Please contact our regional representatives for more information. Subject to changes in design and scope of delivery and due to ongoing technical development. CIRRUS, FastTrac, AngioPlex, and FORUM are either trademarks or registered trademarks of Carl Zeiss Meditec AG or other companies of the ZEISS Group in Germany and other countries.

Carl Zeiss Meditec, Inc.
5300 Central Parkway
Dublin, CA 94568
USA
www.zeiss.com/cirrus6000
www.zeiss.com/med/contacts

Carl Zeiss Meditec AG
Goeschwitzer Strasse 52
07745 Jena
Germany
www.zeiss.com/cirrus6000
www.zeiss.com/med/contacts